High Resolution Quantification of Eastern Arabian Sea Climate Change during Quaternary based On IODP Expedition 355

Thesis to be submitted to Goa University for the degree of Doctor of Philosophy in the School of Earth, Ocean and Atmospheric Sciences

Shubham Tripathi

Reg. No. 201409087

Research Guide

Dr. Manish Tiwari

Scientist-E & Incharge (Paleoceanography)

National Centre for Polar and Ocean Research

Headland Sada, Vasco-da-Gama

403804, Goa, India

October 2020

Statement

As required under the University Ordinance 0.19.8 (VI), I state that the present thesis entitled “High Resolution Quantification of Eastern Arabian Sea Climate Change during Quaternary based On IODP Expedition 355”, is original contribution and the same has not been submitted on any previous occasion. To the best of my knowledge, the present study is the first comprehensive work of its kind for the area mentioned. The literature related to the problem investigated has been cited.

Certificate

This is to certify that the thesis entitled "High Resolution Quantification of Eastern Arabian Sea Climate Change of Eastern Arabian Sea Climate Change during Quaternary based On IODP Expedition 355", submitted by Mr. Shubham Tripathi for the award of the degree of Doctor of Philosophy in Marine Sciences is based on original studies carried out by him under my supervision. The thesis or any part thereof has not been previously submitted for any other degree or diploma in any universities or institutions.

Dr. Manish Tiwari ***(Supervisor)***
Scientist-E and Incharge (Paleoceanography Section)
National Centre for Pacific and Ocean Research
Vasco da Gama, Goa, India

October 21, 2020

List of figures

Figure 2.9 Classification of SOM based on atomic C/N ratios and organic □^{13}C values of marine, lacustrine algae, C-3, C-4 plants and Marine biomass (Source: Meyers, 1994).

Figure 2.10 Electron microscope image of *G. sacculifer* from Site U1457 sediment sample.

Figure 3.1 Locations of the IODP Expedition 355 Site U1456 in the Eastern Arabian Sea (3640 m of water depth, 16°37.28′N, 68°50.33′E) denoted by pink star. The red circles represent ODP and IODP sites in the Arabian Sea Bay of Bengal and South China Sea which have been discussed in the present study. The white patch represents Potwar plateau. The thin dotted curves in the Arabian Sea and the Bay of Bengal show modern anoxia based on WOA 2005 climatology. The thick black dotted curve in the Arabian Sea represents the approximate extent of denitrification zone (Figure created using GeoMapApp3.6.0, www. geomapapp.org).

Figure 3.2 Record of denitrification, surface water productivity, and provenance of the Sedimentary Organic Matter (SOM) in the Eastern Arabian Sea since Late Miocene. (a) Lithostratigraphy of site U1456, (b) denitrification variability (δ^{15}N of SOM), (c,d) paleoproductivity variability (weight percent total organic carbon [TOC] and total nitrogen [TN] of SOM), (e,f) SOM provenance indicators (δ^{13}C and C/N ratio). The coloured, rectangular boxes show the intensified OMZ coupled with surface water productivity when denitrification occurred in the basin. The horizontal dotted lines indicate the position of the hiatuses. The vertical dashed line over panel ‘b’ show denitrification threshold and horizontal brown lines separates different lithological units. The age data (in Ma) at Site U1456, shown by the Indo-Arabic numerals in ‘panel b’, are based on calcareous nannofossil and planktonic foraminifera biostratigraphy, together with magnetostratigraphy.

Figure 3.3 Comparative records of the South Asian Monsoon and East Asian Monsoon since Mid-Miocene.(**a**) $\delta^{15}N$ and total organic carbon (TOC) from IODP site U1456, (**b**) Magnetic susceptibility record[37] of Chinese loess plateau and Hm/Gt (40 point moving average) from the South China Sea ODP site 1143, (**c**) Chemical Index of Weathering (CIA) from the Indus river fan, (**d**) Mn/Ca record from the Maldives inner Sea (**e**) Magnetic susceptibility record of the southern Bay of Bengal ODP site 758, (**f**) *G. bulloides* abundance from ODP site 722, (**g**) *G. bulloides* abundance from ODP site 722, and (**h**) $\delta^{13}C$ of calcretes from the Potwar Plateau. The green arrows represent the strengthening of monsoon and the purple indicate the weakening of monsoon. The yellow band marks the arid period when many of the studies including the present study show the weakened monsoon while the green bands indicate the periods of strengthened monsoon.

Figure 4.1 Location Map and schematic diagram of the Arabian Sea. (a) and (b) shows southwest and northeast monsoon wind (black arrows) and intermediate water flow (blue arrows) during glacial and interglacial periods, respectively. Thicker arrows reflect stronger winds/circulation. The present study site (U1457) is shown by yellow star. Denitrification gradient during the glacial and interglacial period is shown in grey colour (darker colour indicates stronger denitrification).

Figure 4.2 Denitrification record from the Eastern Arabian Sea since the Late Miocene. (a) denitrification variability ($\delta^{15}N$ of SOM); (b, c) past productivity variability (weight percent of total organic carbon and total nitrogen of SOM); (d, e) Provenance indicators ($\delta^{13}C$ and C/N ratio of SOM). The vertical broken lines indicate the position of the hiatuses. The horizontal dashed line over panel ‘a’ show denitrification threshold (*Tripathi et al*., 2017). The age data (in million years ago, Ma) at Site U1456 is shown by the Indo-Arabic numerals in ‘panel a.

Figure 4.3 High-resolution denitrification variability from the Eastern Arabian Sea (present study; Site 1457A; panel 'a') and its comparison with denitrification in the Western Arabian Sea (Altabet et al., 1999; Site 722B; panel 'c'). Panel (b) represents TN concentration of core 1457A related to productivity; (d) and (e) represent $\delta^{13}C$ and $\delta^{18}O$ variability from Site 722B related to ventilation and global ice volume, respectively (*Clemens et al*., 1996); panel (f) shows the LR04 stack (*Lisiecki and Raymo*, 2005) representing the glacial-interglacial cycles (the grey bands show the interglacial periods with corresponding MIS numbers).

Figure 4.4 Comparison among denitrification variability from the Western and Eastern Arabian Sea, Northern Hemisphere temperature, and productivity from the western Arabian Sea. (a) The Greenland ice core $\delta^{18}O$ record GSIP 2 (*Groot and Stuiver*., 1997). (b) $\delta^{18}O$ and (c) $\delta^{13}C$ of benthic foraminifera (*C. kullenbergi*) of core NIOP 905 (*Jung et al., 2009*). (d) $\delta^{15}N$ of core MD- 04 2876 from North Arabian Sea (*Pichevin et al., 2007*) (e) $\delta^{15}N$ of core RC 27-14 from Oman margin (*Altabet et al*., 2002) (f) $\delta^{15}N$ (g) organic carbon percentage and (h) Ba/Al ratio of core 905P (*Ivanochko et al*., 2005). Grey bands represent colder periods (Henrich events, H1 to H6); dark orange bar indicates the Bølling-Allerød warm period; YD denotes Younger Dryas.

Figure 5.1. The Span of MPT. Benthic foraminiferal $\delta^{18}O$ record (greenish grey curve), the mid-Pleistocene Transition (blue box) is characterized by increasingly more extreme $\delta^{18}O$ maxima (Marine Isotope Stages (MIS), are mentioned in the upper graph; Lisiecki and Raymo, 2005). MIS 24-21 are considered the mid-point of the MPT (Mudelsee and Schulz, 1997). The light pink band in the upper graph outlines our study interval (~0.1–1.0 Ma).

Figure 5.2. Comparison with LR-04 stack (bottom panel) and oxygen isotope curve from the present study (top panel). The original data points are shown by grey colour while the dark blue lines represent the 3-point running average. The red lines marks the tie-points at peak interglacials and purple lines shows the tie-lines connecting maximum $\delta^{18}O$ values, which represents the glacial periods.

Figure 5.3. Age-depth model and sedimentation rate of the site 1457 based on new stratigraphic tie points.

Figure 5.4. Cross-plot between $\delta^{15}N$ and total nitrogen (TN); $\delta^{13}C$ and total organic carbon (TOC) concentration to test the effect of digenesis on the sedimentary organic matter.

Figure 5.5. Provenance of SOM of U1457 based on atomic C/N ratios and organic $\delta^{13}C$ values of marine, lacustrine algae, C-3, C-4 plants and Marine biomass.

Figure 5.6. High-resolution denitrification and productivity variability during MPT from the Eastern Arabian Sea. Panel (a) represents the $\delta^{18}O$ of G *sacculifer* (present study), the lower values represents the warmer condition and higher values represents cooler condition (b) represents down core variability of $\delta^{15}N$ of SOM from Site U1457A, which shows the denitrification during MPT (present study) (c), (d) represent TOC and TN variability from present study both representing productivity, (f) shows $\delta^{15}N$ variability of ODP site 722, which represents the denitrification variability from the WAS (Altabet et al., 1999), (g) shows the TN variability from WAS (Altabet et al., 1999), and (h) shows the benthic $\delta^{13}C$ variability showing the ventilation during MPT in WAS (Clemens et al., 1996). The light green bands show the periods with high productivity, high denitrification and strong monsoon.

Figure 5.7. Annual variability of SST and SSS near the Site U1457. The minimum SST is noticed during the summer monsoon period (shown by August) indicating the effect of moderate upwelling during that period. The SSS is high during the summer monsoon period and lower during the pre-monsoon. This figure is based on the World Ocean Database 2009 (Boyer et al., 2009).

Figure 5.8. (a) LR04 Benthic $\delta^{18}O$ stacks (Lisiecki and Raymo, 2005). (b) $\delta^{18}O_{sac}$ variability from the present study, the dark green curve is the 3-point average. (c) represents the *G. sacculifer* Mg/Ca based mixed layer temperature (MLT) variability, (d) represents the ice volume corrected salinity variability, (e) and (f) represents the chemical index of alteration and K/Al as chemical weathering index from Site U1456 (Cai, et al., 2019). The yellow bands represents the comparatively warm period. The blocks over panel (c) and (d) show three different slices for discussion of MLT variability. The Indo-Arabic numerals in purple indicate the MIS numbers.

Figure 5.9. (a) $\delta^{18}O_{sac}$ variability from the present study, the dark green curve is the 3-point average, (b) represents the *G. sacculifer* Mg/Ca based mixed layer temperature (MLT) variability, (c) and (e) represent the Precession, and Insolation at 15˚S.

Figure 5.10. Spectral analysis including (a) the CWT and (b) the redfit graph of the $\delta^{18}O_{sac}$.

List of Tables

Acknowledgements

Acknowledgement provides a chance to express our token of appreciation to people who encouraged and helped us unconditionally in every possible way they could for completion of my research work.

I would like to express my deep gratitude to Dr. Manish Tiwari my PhD supervisor who has given me opportunity to work with him and for his patient guidance, enthusiastic encouragement during my Ph.D in National Centre for Polar and Ocean Research (NCPOR). He gave me absolute freedom to express myself and discuss ideas. He applied his best possible effort and given critiques on this research work and brought out the best in me.

I acknowledge National centre for Polar and Ocean Research (NCPOR) for providing me Junior and Senior Research fellowship. In the same breath, I would like to express great appreciation to acknowledge the support of the Director NCPOR Dr. M. Ravichandran who encouraged and permitted me to work in this esteemed institute. I want to thank NCPOR again for providing me funding and opportunity to attending different national conferences.

I am immensely thankful to my departmental research committee members Prof. G.N Nayak, and Dr. P Divaker Naidu for interesting, informative discussions. Their enthusiastic and useful comments during DRC meetings have improved the thesis in great way.

I am thankful to all the members of Paleoceanography section for their help and support during my research work. I express my deep gratitude to the summer interns and dissertation students Saumya, Vaishnavi, Elcome, Simran, Prajeeth, Karishma, Ruchi, Naveen, Vishal and Kaushiki for their sincere contribution; they all are always the integral part of my PhD.

I would like to place on record the valuable help rendered by Viola Rodrigues. Her constant support and willingness to help during the stable isotope analysis is always appreciated. I thank Padmasini Behera for co-authoring a publication with me. I want to thank Mr. Vikash Kumar and Dr. Siddesh Nagoji with whom I started my PhD journey.

The valuable discussions with Vikash Kumar and the work during ICP-OES calibration is much appreciated. Dr Nagoji helped me in understanding the basics of IRMS in the early days of my research work. I would like to thank Dr. Sarthchandra Prasad for valuable suggestion on interpretation and trace metal analysis. I want to appreciate Mr. Tejaswar Das for his curiosity and asking questions during and after lab hours.

I love to thank and appreciate my best friend Mr Parijaat Mukherjee for encouragement and indulging me in great discussions on finance, business analysis, climate, and statistics. I am very thankful to my friend dear Dr. Anuj Shukla for fact based discussions on various aspects of research. His research work on cognitive science helped me a lot during the bad phases of my life.

I thank Md Tarique, for corel draw lesson in the beginning of my research; we have unforgettable companionship. I will never forget the road trips I made with Dr Abhilash Nair to various places in Goa. The discussions and chats with Abhilash have always enriched my brain. I can't forget the help and support by Dr. Mahesh Badnal during the adverse time in my personal and professional life.

Dr Shramik Patil always forced me to work on weekends and continually motivated me through his experience. I also appreciate the effort of Nibedita Sahoo for her friendship and tying the rakhshabandhan every year, she provided food and tea whenever I asked her.

My special thanks to my BHU friends Dr. Rakesh Mishra, Mr Utkarsh Mishra and Mr Chitrasen Singh for a great friendship. A very special thanks to University of Hyderabad friends Feba, Abhishek, Ashish, Rita for making me feel special and encouraging me by saying you can do it!!

A special mention to my Prof. A.K. Misra (BHU) who taught me mathematics and being humble during my graduation days, Prof. Misra is one of the major forcing factors for my research. I will never forget to thank Prof A.C. Narayana who introduced me to the field of paleoclimatology. His saying of being the flag bearer of the Earth and Space Science Centre in University of Hyderabad always bring fire in my belly to excel in the research.

I want to thank administration section of NCPOR, for their help and suggestion at different stages. I want to mention Ms. Rupali Rane and Ms. Shushma Chodanker for their immense support and timely providing the necessary documents.

I am grateful to my school friends Ashish, Abhijeet, Sanket, Vivek, for showing their confidence in me and being in touch for such a long periods. Thank you for not giving up on me.

I want to mention the support of my younger brother Shivam Tripathi who took the entire burden his shoulders during my absence in house. Thanks to Papa who always created a gradient for knowledge in me my giving examples of great and visionary philosophers and scientists. My mother Late Smt. Shanti Tripathi always wanted me to be studious, and gain and acquire big position in life but left me a little early before I do it. But I will try!!

At last I thank My Grandfather Sri Satya Narayana Tripathi who was my first professor. He introduced me to nature and natural phenomenon like rainbows, constellation, the pole star, shapes of clouds, seasons, cold and warm ocean currents, winds, types of soils, and types of interactions in ecology. He told me literally everything a growing brain need to know much early during my childhood.

Contents

Chapter 1

1. Introduction

The climate of the eastern Arabian Sea is affected by the reversal of the southwest monsoon (SW Monsoon) (June–August) and northeast monsoon (NE Monsoon) (December–February) winds and associated oceanic circulation. The two monsoon regime generates distinct biological responses. The Arabian Sea experiences calm, stratified, oligotrophic condition during the different intermonsoon periods (March–April and October–November) to eutrophic conditions due to strong winds and nutrient-rich upwelled waters during the SW monsoon and NE monsoon (Smith et al., 1998). The strong winds blowing from the southwest induces an offshore Ekman transport. This promotes intense coastal upwelling near Somalia, Yemen and Oman coast. This nutrient-rich upwelled water feeds the euphotic zone (Morrison et al., 1999). High aeolian dust flux with nutrient-rich water leads to high primary production (~1.5 $gCm^{-2}d^{-1}$; Lee et al., 1998; Barber et al., 2001). On the other hand, during the NE monsoon, cold and dry winds from the northeast result in convective mixing over the Northeastern Arabian Sea that ultimately results in nutrient pumping to the surface. This sustains relatively high primary production (1–2 $gCm^{-2}d^{-1}$), in the Northeastern Arabian Sea (Barber et al., 2001).

The monsoon induced productivity creates high O_2 demand at intermediate depth and is one of the two crucial factors responsible for causing suboxic to anoxic conditions and making the Arabian Sea oxygen minimum zone (OMZ) (Olson et al., 1993). The other factor which influences the extent of OMZ is the ventilation of the intermediate-depth water from the oxygenated Indian Central Water (ICW) at intermediate depths (Olson et al., 1993; Shenoy et al., 2020). The Arabian Sea is one of the largest among three OMZs (the other two being the

eastern tropical North and South Pacific). It contributes significantly to global water column denitrification (Naqvi and Shailaja, 1993; Codispoti et al., 2001). Furthermore, the Arabian Sea is characterized by seasonally reversing currents, extreme differences in sea surface salinity, localized intense upwelling and so on (Centurioni et al., 2017). Thus, it offers excellent opportunity to study past climatic variability as it undergoes intense biogeochemical changes during the monsoons which get recorded in different paleoclimate archives like sediments, foraminifera, corals and so on.

The Earth, over the past several million years, has experienced a series of cold and warm periods. These alternate cold and warm periods are known as glacial-interglacial cycles with periodicities of 100 kyr (thousand years) and of 41 kyr prior to Mid-Pleistocene Transition (MPT). It matches with the obliquity (41 kyr) and eccentricity (100 kyr) cycles of the Earth's axial tilt and orbit around Sun, respectively (Hays et al., 1976). The MPT is one such period that initiated after ~1.2 Ma (million years ago). It is characterized by the extension and intensification of glacial-interglacial climate cycles. During MPT, low-amplitude 41 kyr climate cycles of the early Pleistocene were gradually replaced in the late Pleistocene by high-amplitude quasi 100 kyr cycles (Pisias and Moore, 1980; Lisiecki and Raymo, 2005; Raymo et al., 2006). This climate transitions, especially the increasing severity and duration of cold stages, had an intense effect on the monsoon, oceanic productivity, and denitrification. In the Arabian Sea, not many studies have been carried out with a focus on understanding the MPT. Therefore, it is crucial to study the monsoon, denitrification, oceanic productivity, and temperature variability during MPT to understand climate change in the Arabian Sea during this important transition.

1. 1 The Arabian Sea and the South Asian Monsoon

The South Asian Monsoon (SAsM) represents the most dynamic ocean-atmosphere-terrestrial interaction processes. The SAsM greatly influence the climate of South Asia. The Indian subcontinent is one of the highly populated agrarian economies the world. The primary source of income of the people in this region is Agriculture. The agriculture in Indian subcontinent depends on the monsoonal rainfall and, accounts for almost half of the total production (Gadgil et al., 1999). The heating over Tibetan Plateau and northwestern Indian subcontinent leads to formation of low pressure area, which causes an atmospheric pressure gradient with the southern Indian Ocean. In response, the Intertropical Convergence Zone (ITCZ) moves northward during northern hemisphere summers causing the onset of SAsM (Webster, 1987). During the SW Monsoon wind blows from the southwest towards the northeast during summers (June-October) and the NE Monsoon brings the wind from the opposite direction during the winters (December-April) (Schott & McCreary 2001). The monsoonal winds act as a forcing for the boundary currents in the northern Indian Ocean and reverse seasonally. It drives upwelling circulations during the SW Monsoon and downwelling circulations during the NE Monsoon respectively (Schott & McCreary 2001; Shankar et al., 2002). The Northeast Monsoon current (NMC) during NEM flows westward and brings lower salinity water (< 33 ppt) from the Bay of Bengal towards Arabian Sea (Schott & McCreary 2001). The East Indian Coastal Current (EICC) flows southward and coalesce with the NMC (Schott et al., 1994). The currents then flow around the clockwise Lakshadweep eddy and from south to north along the western Indian coastline as the WICC (Schott & McCreary 2001; Vos et al., 2013).

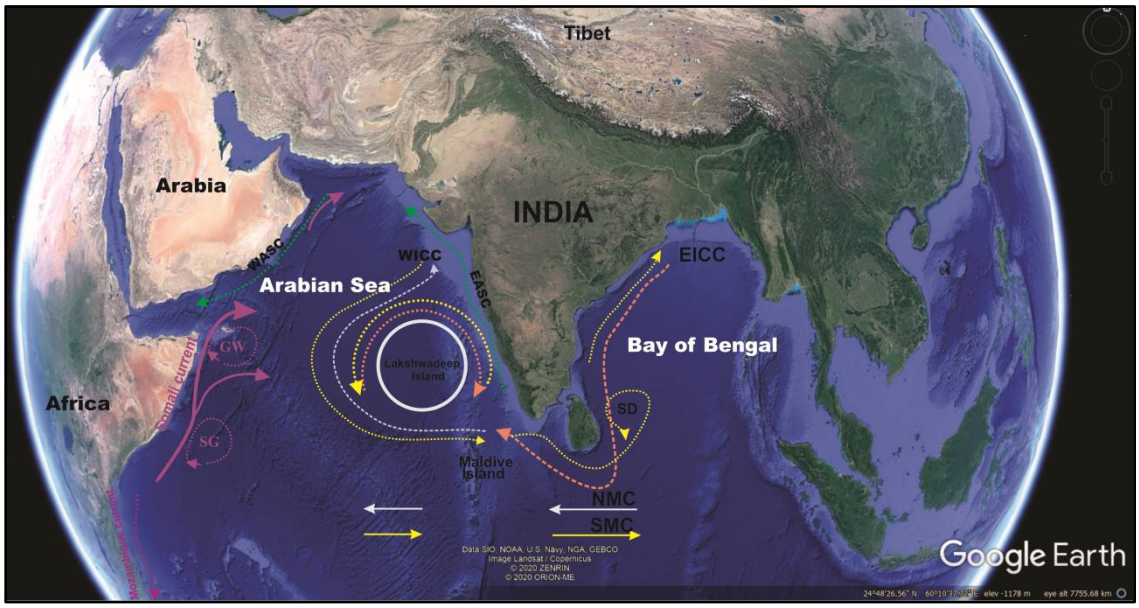

Figure (1.1) Schematic showing different ocean currents in the Arabian Sea and Bay of Bengal. Northeast Monsoon current (NMC), East Indian Coastal Current (EICC), the western Indian coastline current (WICC), Southwest Monsoon Current (SwMC), Somali current, Somali gyre (SG), Western Arabian Sea current (WASC), (Based on Smith et al., 1998, Schott & McCreary 2001,)

Conversely, during the SW Monsoon, the Southwest Monsoon Current (SwMC) flows from west to east, transporting more saline water (~36.5 ppt) from the Arabian Sea to eastward (Schott et al., 1994; Schott & McCreary 2001). The WICC in the Arabian Sea flows southwards along the West Indian coastline to join the eastward flowing SwMC (Schott & McCreary 2001). Passing the Sri Lanka coastlines, an anti-clockwise eddy known as the Sri Lanka Dome is formed (83˚E, 7˚N) (Vinayachandran & Yamagata 1998). A southward current is driven by the western arm of this eddy along the eastern coast of Sri Lanka while the remaining flows towards North along the eastern Indian coast and continues as the EICC (Vinayachandran & Yamagata., 1998; Schott et al., 1994). The broad picture regarding the

paleomonsoon variation is that SW Monsoon was stronger during interglacials and weaker during glacial periods with the NE Monsoon exhibiting the opposite behaviour. The high-resolution qualitative changes in the past monsoon on centennial to sub-centennial timescale have been reconstructed from both the Arabian Sea and Bay of Bengal (Schulz et al., 1998; Kudrass et al., 2001, Tiwari et al., 2015). There are evidences for the same from the terrestrial records from the Indian subcontinent (Ramesh et al., 1985; Sinha et al., 2005). Some records have centennial resolution and spans over a part of the last glacial period as well as the full termination I (Saher et al., 2007; Saraswat et al., 2013). Several studies on various timescale have been made to study monsoon variability, surface water productivity, sea surface salinity (SSS), oceanic temperature, in the Arabian Sea (Nair et al., 1989, Agnihotri et al., 2003, Gupta et al 2005, Saher et al., 2009, Tiwari et al., 2016, Naik et al., 2017). It has been observed that, the trend and intensity of the SAsM, which accounts for ~80% of the rainfall in South Asian region, have varied greatly during the last several million years (Tada et al., 2016; Tripathi et al., 2017). This suggests a considerable change in the pattern of chemical weathering/erosion of the rocks in the Himalayan region and adjacent flood plains. A significant variation is also observed in the surface water circulation systems of the Arabian Sea, which ultimately control the transport and deposition of sediments (Schott & McCreary, 2001; Clift et al., 2010; Pandey et al., 2016; Tiwari et al., 2013; Joussain et al., 2017).

Clemens et al., 1991 used SPECMAP $\delta^{18}O$ record (Imbrie et al., 1984) as a proxy and assuming that changes in global ice volume represent the changes in the vicinity of Himalayan and Tibetan Plateau; he concluded that maximum global ice volume corresponds to maximum albedo. And increased albedo reduces effective sensible heating. Thus periods corresponding to the global ice maxima show weakened monsoon circulation. Various tracers of monsoon strength with independent pathway have been studied to examine the monsoon

variability on a glacial-interglacial timescale (Clemens et al., 1991). The Planktic foraminifera *G. bulloides* found in high abundance in the upwelling region characterised by cold and nutrient-rich water (Prell 1984a, 1984b; Cullen, 1984; Hutson, 1980; Peterson et al., 1991). High opal flux (silica productivity) is related to high productivity in the modern oceans (De Master, 1981; Leinen, 1986). Thus it can be linked to monsoon induced upwelling (Nair et al., 1989; Murray, 1991). The grain size of the lithogenic fragments is also related to the strength of monsoon winds, larger lithogenic particles show the stronger winds transport Clemens et al., 1990).

The $\delta^{13}C$ of pedogenic carbonates from the Potwar plateau shifted considerably at ~7 Ma, which has been attributed to the fundamental ecological change from C-3 to C-4 biomass in the Himalayan foreland (Quade et al., 1989). An et al., 2001 suggested that the Himalaya–Tibet rise at ~9–8 Ma caused arid conditions in the interior of the Asian continent causing prevalence of C-4 plants during late Miocene. The output from the modern climate models show that monsoon intensification is related more to the surface heat flux than to the elevated terrains (Boos and Kuang, 2010). However, the decline of atmospheric CO_2 between 8 and 6 Ma led to the abrupt changes in vegetation to C-4 land plants (Cerling et al., 1997). Herbert et al., 2016 noted that the temperature and ecosystems changed during the Late Miocene, which supports Cerling et al., 1997. Further, drop down of atmospheric CO_2 level did not support the observation of low (~280 ppm) atmospheric pCO_2 level and slight changes between 10 and 5 Ma (Pearson and Palmer, 2000).

1.1.1 The sea surface productivity variability in the Arabian Sea

The marine productivity is responsible for fixing large amount of atmospheric CO_2 into the organic matter. This organic matter produced at the surface reaches the ocean bottom and

constitutes the sediment. The marine productivity in the oceans can sequester the atmospheric CO_2 and influence the global climate. The productivity depends on physicochemical factors such as the nutrients availability and light in the euphotic zone. The Arabian Sea experiences very high productivity during the monsoon (Qasim, 1977; Lévy et al., 2007). During the monsoon season, the carbonate flux constitutes ~50–60% of the total flux to the seafloor. Calcification increases many-fold during the monsoon season as compared to non-monsoon seasons (Nair et al., 1989; Balch et al., 2001). Other evidence of increased productivity is high chlorophyll concentrations towards the end of the northeast (February) and southwest (August–September) monsoon (Banse, 1987; Marra and Barber, 2005). Huge regional variability is observed in the sea surface productivity during different seasons in different parts of the Arabian Sea (Wiggert et al., 2005, Nair et al., 1989).

Further, the marine productivity is found to be maximum in the western Arabian Sea during summer, when intense coastal and open ocean upwelling occurs off Somalia and Oman regions (Banse, 1987; Prell et al. 1990). The northeastern Arabian Sea records high biological productivity during NEM linked to cool wind-induced convective churning of the surface water leading to the deepening of the mixed layer to a depth of 100–125m, which injects deeper layer nutrients to the surface (Madhupratap et al., 1996).

An earlier study found high (low) marine productivity during the glacial (interglacial) periods (Rostek et al., 1997). During glacial periods, the NE Monsoon is proposed to be stronger (Sarkar et al., 1990; Rostek et al., 1997; Tiwari et al., 2005). The subsequent increase in wind stress breaks the stratification causing the deeper waters with more nutrients to come in to the euphotic zone that increases the productivity (Rostek et al., 1997). The productivity in the western Arabian Sea is 2.0, 1.0 and 0.5 g C/m^2/day during the SW monsoon, NE monsoon and the inter monsoon periods, respectively (Codispoti 1991; Barber et al., 2001). The eastern

Arabian Sea experiences productivity values are 0.6, 0.3 and 0.2 g C/m^2/day for the SW monsoon, NE monsoon and the inter monsoon periods, respectively (Bhattathiri et al., 1996). However, high variability is recorded in regional productivity during the last glacial-interglacial transition (Jaccard et al., 2013). Similarly, a multiproxy study concludes that the interglacials (Marine isotope stages (MIS)-1, 3 & 5) experienced higher paleoproductivity than the glacials (MIS-2, 4 & 6), and the terrestrial input was high during the glacial periods (Pattan et al., 2003; 2005).

1.1.2 Oxygen minima zone in the Arabian Sea

Perennial oxygen minimum zones (OMZs) exist in the Arabian Sea and Bay of Bengal due to high productivity and weak ventilation (Wyrtki, 1971; Naqvi, 1987). Because of the high biological productivity, a large quantity of organic matter is delivered to the deeper layers (Nair et al., 1989), which ultimately uses the ambient oxygen leading to its depletion. In suboxic conditions, the nitrate acts as an oxidizing agent and is reduced to oxides of nitrogen and nitrogen gas. This phenomenon is known as denitrification. This not only produces a strong greenhouse gas (N_2O) but also depletes a major nutrient (nitrate) that influences the marine productivity (Naqvi et al., 2010; Olson et al., 1993; You and Tomczak 1993). Therefore, OMZs play an important role in controlling the marine nitrogen and carbon cycles and ultimately the climate (Codispoti & Christensen, 1985; Thamdrup, 2011; Ward, 2013).

Characterizing oxygen minima zones (OMZ)

Schmidt, et al., 1925 used Winkler's titration and found the Panama west coast water is practically anoxic at the intermediate waters (400-500m). Winkler, 1888 introduced the titration method for determining the dissolved oxygen concentration, which remains the

standard method. The limit of detection of this method is about 1 μM. The 1 μM concentration is adequate to distinguish between the areas of anaerobic metabolism and aerobic metabolism. Recently, a switchable trace oxygen (STOX) amperometric microsensor (Revsbech et al., 2009) is developed for measuring very low concentrations of dissolved oxygen in the water column.

STOX measurements along more than 1600 km in the Eastern Tropical South Pacific show that the observations made off Peru and in the coast of Iquique, Chile show that when oxygen concentration becomes less than 50 μM, the nitrite is formed (>0.5 μM) (Thamdrup, et al., 2012). Based on this information, Thamdrup, et al., 2012 suggested that the OMZ occupies a volume of at least 2.4×10^{13} m^3 in the Eastern Tropical South Pacific. The STOX sensors have been used for detecting dissolved oxygen-free and nitrite rich waters of the Arabian Sea (Jensen, et al., 2011). These experiments established that an extensive amount of nitrite-rich water (OMZs) occurs in the ETSP and the Arabian Sea.

Thus the entire characterization of the most intense OMZs (O_2< 20 μM reaching 1 μM in the core) is based on the CRIO (CRIterion on O_2) criterion from the eastern South Pacific OMZ and including a large range of O_2 concentrations (Paulmier, et al., 2006, 2009, Revsbech, et al. 2009, Jensen, et al., 2011, Schmidt, et al., 1925). Another study synthesizes the existing hypoxia to draw biologically meaningful thresholds (Hofmann et al., 2011). According to the CRIO criterion, mild hypoxia starts at a concentration of O_2 <2.45 ml L^{-1} and the species sensitive to oxygen concentration start escaping. Intermediate hypoxia (O_2 <1.4 ml L^{-1}) is the limit where organisms that can adapt to low oxygen are found. Acute hypoxia (O_2<0.5ml L^{-1}) is the limit beyond which only organisms with highly specialized adaptions survives (Hofmann et al., 2011).

Based on the studies described above, the schematic diagram (Fig 1.2) shows the evolution of different oceanic conditions based on the interplay different parameters. These parameters include the supply of oxygen, the rate nitrogen fixation and primary production. The open ocean OMZ has low primary productivity and high nitrogen fixation with abundant oxygen availability and much of the world ocean belongs to this type.

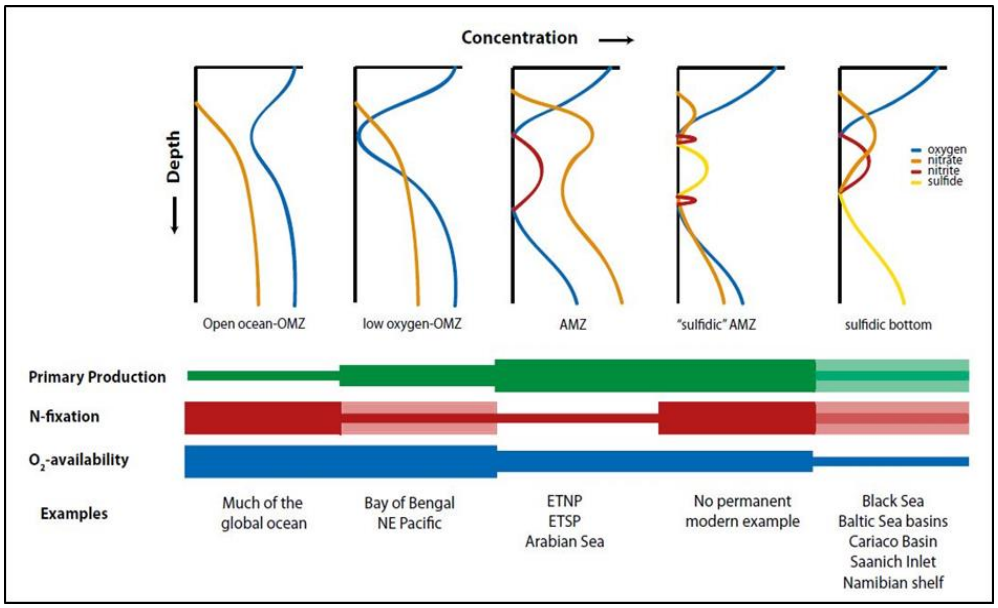

Figure (1.2) Schematic of classification of OMZs in the world ocean; see text for details (Modified from Ulloa et al., 2012)

Low oxygen OMZ has relatively higher primary productivity and nitrogen fixation is moderately less. The recent measurements show that the accumulation of nitrates occurs when O_2 concentration falls below 50 µM. Anoxic Marine Zones occurs when the oxygen concentration falls below about 50 µM and accumulation of nitrite takes place. Such AMZ experiences high primary productivity and lower oxygen concentrations, however, the N fixation are the lowest of the OMZ types. The Eastern tropical pacific and the Arabian Sea

develop similar OMZ condition. The sulfidic AMZ witnesses similar oceanic condition as AMZ but it has higher N fixation. The geographical setting of the Arabian Sea greatly controls the circulation in the basin and biological productivity (Morrison et al., 1999; Naqvi et al., 2003) consequently, developing the oxygen deficient conditions (Codispoti et al., 2005).

1.1.3 The denitrification in the Arabian Sea

Very low concentration of oxygen (< 2 μM) causes denitrification to takes place in the subsurface depths (250 - 1250 m) of Arabian Sea (Naqvi, 1987; Olson et al., 1993; Paulmier and Ruiz-Pino., 2009). Around half of the total nitrogen lost from the oceans takes place due to denitrification in the oceans (Deuser et al., 1978; Ganeshram et al., 1995). The three most prominent areas for the global denitrification are eastern equatorial north and south Pacific, and the Arabian Sea. During denitrification, kinetic fractionation causes the uptake of lighter isotope (^{14}N) that leads to increase of ^{15}N in remaining NO^{3-}. The upwelling takes the enriched nitrate to the surface which is consumed by the organisms resulting in particulate organic matter with higher $\delta^{15}N$ that gets deposited in the sediment. Thus, past water-column denitrification variations can be reconstructed using $\delta^{15}N$ of organic matter from sediments (Altabet et al., 1995; 1999; Ganeshram et al., 1995). The factors responsible for the development of OMZ and denitrification are ventilation and the monsoon induced productivity (Schulz et al, 1998; Ganeshram et al, 2002). Thus the variability and intensity of OMZ and denitrification can be linked to monsoon strength (Reichart et al, 1997; Altabet et al, 2002; Ganeshram et al, 2002). The longest record of denitrification in the Arabian Sea spanned only the last 1 Myr (Altabet et al., 1995) before the denitrification record generated

from International Ocean Discovery Program (IODP) Expedition 355 was reconstructed extended it to 10 Ma.

1.2 Mid-Pleistocene Transition and the Arabian Sea Climate

The Mid-Pleistocene Transition (MPT, ~600 to1200 ka), earlier described as Mid-Pleistocene Revolution (Clark et al., 2006; Head et al., 2008), is one of the recent major events during the climatic evolution of the earth. During the MPT, the 41 kyr periodicity of glacial-interglacial cycles changes to a quasi-100 kyr periodicity (Shakleton and Opdyke., 1976; Imbrie et al., 1992, 1993; Raymo and Nisancioglu, 2003, Clark et al., 2006). The low frequency climate change is caused by changes in parameters of Earth's orbit like eccentricity, obliquity, and precession (Hays et al., 1976). These parameters change with the cyclic interval that modifies the energy budget of the earth (Hays et al., 1976; Zachos et al., 2001; Ruddiman, 2006).

During these cycles, most of the changes in glacial ice have happened in Northern Hemisphere (CLIMAP project group). This is because the Northern Hemisphere has more landmass and more ice growth capacity. The southern hemisphere has lesser ice growth because of its lesser landmass and Antarctica is close to its ice storage saturation (Maslin et al., 2010). This record of change in cyclicity is most clearly shown by oxygen isotope ratios found in the marine sediment core. The beginning of high-amplitude glacial variability with quasi-100 kyr cycles instead of regular 41 kyr cycles – is a challenging question in paleoclimatology (Pisias and Moore., 1980; Raymo et al., 2006, Lisiecki and Raymo., 2005). Several mechanisms have been proposed as causes for the MPT but the debate is not settled (Clark et al., 2006; Siddall et al., 2010; Ganopolski and Calov, 2011; Huybers, 2011; McClymont et al., 2013). Most of the mechanisms attribute it to various climate boundaries

conditions like the decline in atmospheric CO_2 concentration, ice sheet dynamics variations, the formation of large ice sheets and reorganization of the thermohaline circulation (Berger et al., 1994; Clark et al., 2016; and McClymont et al., 2013). However, many questions need to be addressed about how the change in orbital cycles and the insolation caused the change from the 41 kyr to quasi-100 kyr cycle during MPT. This is especially intriguing considering the 100-kyr eccentricity cycle feebly influence the seasonal or mean annual insolation. In contrast, the obliquity (41 kyr) and the precession (23 kyr) governs the changes in the insolation. Many studies have proposed that 100-kyr glacial cycles are a response to the eccentricity-driven modulation of precession (Raymo, 1997; Lisiecki, 2010), multiple obliquity cycles (Huybers and Wunsch, 2005; Liu et al., 2008), or by combination of internal oscillations (Saltzman et al., 1984; Gildor and Tziperman, 2000; Toggweiler., 2008). Two different patterns of climate change were obtained from the North Atlantic (DSDP Site 607) and South Atlantic ODP site 1123 (Ford et al., 2016). Mg/Ca-based bottom water temperature record reveals a ~2-3 ˚C cooling from ~1500 to 500 ka across the MPT. However, it is hypothesised that during the MIS-24 thermohaline reorganization took place which intensified near MIS-22 (Ford et al., 2016). This led to a sudden increase in ice-volume during ~900 ka. Thus, thermohaline circulation and ice-volume also have a huge impact on the MPT.

Ziegler et al., 2010 is the only study that investigates the paleoceanographic conditions during Mid Pleistocene Transition in the northern Arabian Sea. This multiproxy record from the Arabian Sea shows that the paleoproductivity record varies with 100 kyr glacial-interglacial cyclicity. High productivity is observed during interglacials. There are glacial

periods in which OMZ extent has increased vertically, this may be linked to deep-water ventilation (Ziegler et al., 2010).

1.3 Significance and Objectives of the Study

A few paleoclimate studies from the Arabian Sea span millions of years that study the monsoon, denitrification, productivity etc. but are qualitative in nature. They also do not focus specifically on MPT - a climatically important period. Especially, from the eastern Arabian Sea, we don't have any record that examines the climate during MPT. The present study is first to quantify the climate variability during MPT from the Eastern Arabian Sea in terms of oceanic temperature and salinity. Furthermore, this study, for the first time, presents a 10 Ma long record of the denitrification (longest denitrification record from the Arabian Sea) and SAsM variability using squeezed cake sediment samples from the IODP Expedition 355 Site U1456 in the EAS.

Thus, it is evident from the survey of existing knowledge that there is a great lacuna in the understanding of climate change from the EAS especially on a long time scale and during the Mid-Pleistocene Transition. To address these gaps, the following objectives were chosen:

I. To determine high-resolution (millennial) South Asian Monsoon variability in the Eastern Arabian Sea (EAS) during the Quaternary and beyond.

II. To quantify the temperature and salinity changes at high-resolution (millennial) to study the South Asian Monsoon induced changes in the EAS since Mid Pleistocene Transition.

III. To understand the impact of monsoon intensification on the denitrification in the Oxygen Minima Zone.

IV. To explore the relationship between the various forcing factors and the climate variability of the EAS.

1.4 International Ocean Discovery Program (IODP) Expedition 355

To achieve the above objectives, we need to go past in time spanning several millions of years for which we need very long sediment cores. Scientific Drilling in the ocean allows us to explore the change in past in the various climate states. These drilling can retrieve sediment samples that have large distribution and high resolution to understand the impacts of climate change of the past several million years. Using various proxy methods that reveal a lot of useful paleoclimate information, we can reconstruct the mixed layer and deep ocean temperatures, ocean circulation, distribution of nutrients, and ocean productivity. Reconstructions of the past climate challenge and provide assistance to the climate modelling community to improve the physics and chemistry represented in numerical simulations. Deep Ocean drilling is generating highly resolved temporal and spatial sets of data, revealing our planet's dynamic climate history over a range of climate states and periods. IODP is one such program which is responsible for Deep Ocean drilling and gathering past information in the world ocean from almost all the latitudes.

1.4.1 Expedition 355

International Ocean Discovery Program Expedition 355 drilled two sites (U1456 and U1457) in Laxmi Basin in the eastern Arabian Sea to decipher the evolution of mountain building, weathering, erosion, and climate on different timescales. IODP Expedition 355 has recovered sediment from the Sites U1456 and U1457 in Laxmi Basin, penetrating 1109.4 and

1108.6 m below seafloor (mbsf), respectively (Pandey et al., 2016). The drilled sediment reached to 13.5–17.7 Ma age (late early to early middle Miocene) at Site U1456, although with a large hiatus between the lowermost sediment and overlying deposits dated at <10.9 Ma. A long hiatus is found near the base of the cored section at Site U1457, spanning from ~10.9 to ~62 Ma. Two hiatuses from ~8.2–9.2 and ~3.6–5.6 Ma exist at the Site U1456 and U1457. A condensed section is also encountered spans from ~2.0-2.6 Ma. However, the chronology for each hiatus is different for the sites. The recovered sediments found to be derived from the Indus River and consist of the minerals unique to the Indus Suture Zone. The minerals like glaucophane and hypersthene found to be originated from the structural base of the Kohistan arc (i.e., within the Indus Suture Zone). More distal facies are found in Site U1457, and it reflects the more marginal setting. Thus, Laxmi Basin was not affected by any active lobe since the late early Pleistocene (~1.2–1.5 Ma) (Pandey et al., 2016). Based on the paleoceanographic research carried out on IODP 355 samples using the multiproxy approach, noteworthy contributions are being made on the monsoon evolution especially during the Quaternary period and its impact on the eastern Arabian Sea oceanography (Tripathi, et al., 2017; Khim, et al., 2019; Kim et al., 2018; Satpathy, et al., 2019). The new results also provided insights into our current understanding on tectonics and climatic interactions.

1.5 Thesis Structure

The background and introduction to the Arabian Sea climate, climate events like Mid-Pleistocene transition (MPT) and the previous studies along with the objectives of the thesis are discussed in chapter 1. The methodology and the materials used in this research work is explained in chapter 2, while the scientific outcomes are described in chapters 3-5. The thesis is structured as follows:

Chapter 1: Introduces the current understanding of both the Eastern Arabian Sea climate and the proxies that are the focus of this study. The objectives are also listed in this chapter.

Chapter 2: Explains the methodology and material used in the study. It also discusses the proxies used to generate the records.

Chapter 3: Explains the variability of monsoon and denitrification from the sediment samples spanning up to ~10 Ma. A comprehensive comparison of the new results to previously published records is also carried out.

Chapter 4: Describes the variability of denitrification from 40 kyr to 600 kyr at a high-resolution and comparison to previously published records is carried out.

Chapter 5: The findings from the new MPT records produced is explained in this study. The wavelet analysis is carried out to find out the influence of external/internal forcing effects on South Asian Monsoon.

Chapter 6: Concludes the main findings from the new records produced during this study. Their significance within the context of palaeoclimate research is discussed. Potential further work, resulting from the conclusions of this thesis is also discussed.

Chapter 2

2. Materials and Methods

This chapter describes the different materials/samples used and the experimental techniques used for the research. Brief discussions of regional settings with locations of the sediment cores are discussed. The on-board generated age-depth model and sampling procedure is also mentioned. Various proxies used in the research with the measurement techniques are also described in this chapter.

2.1 Regional setting and location of the Sites

The Arabian Sea occupies approximately an area of 3 million 863 thousand sq. km and is located between 7° N and 25° N latitudes and 54° E and 75° E longitudes (Fig 2.1). The basin is surrounded by the Arabian Peninsula and Africa in the west and the Indian subcontinent in the north and the east. The Arabian Sea has the world's second-largest submarine fan known as the “Indus Fan”. The sediments brought by the Indus River draining the Himalayas form the Indus Fan. The fan is bound by the Indian continental margin and Laccadive Ridge in the east, the Owen-Murray Ridge in the west, and the Mid-Indian Ridge in the south.

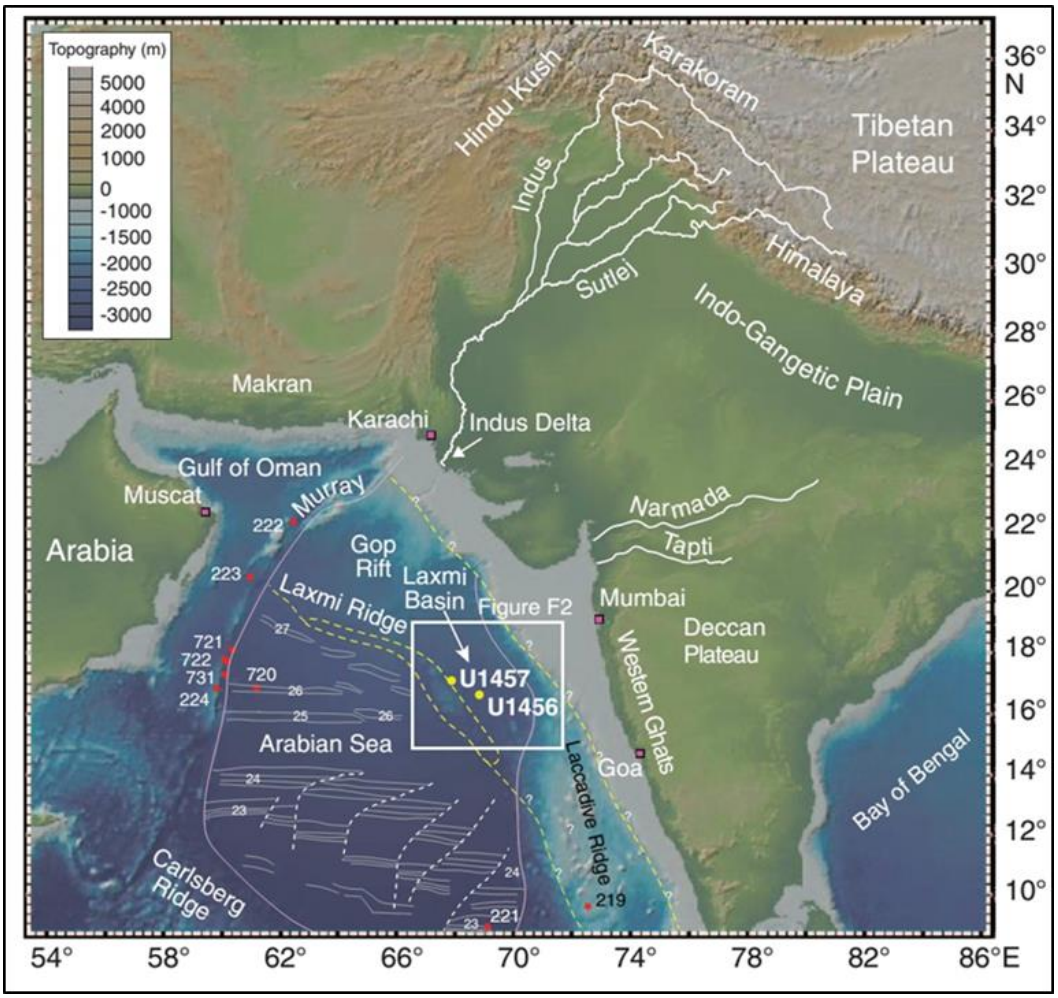

Figure 2.1. Location of the IODP Expedition 355; major rivers shown by white curves; Indus, Narmada and Tapti drain in the Arabian Sea (Pandey et al., 2016)

Sediment samples were collected for the present study on-board JOIDES *Resolution* during IODP Expedition 355 from March 2015 to May 2015 in the Laxmi Basin of Eastern Arabian Sea. The details of the Sites drilled during IODP Expedition 355 are given in Table 2.1 below. Both the Sites are above the modern lysocline in the Arabian Sea (~4000 m). Fig 2.1 shows the location of the Sites, which is ~475 km from the Indian coast and ~820 km from the modern mouth of the Indus River (Pandey et al., 2016).

Table 2.1. Details of the IODP Sites used in the present work

Site	Latitude	Longitude	Water depth
U1456	16°37.28’ N	68°50.33’ E	3640 m
U1457	17°09.95’N	67°55.80’E	3534 m

2.2 Sampling Procedure

The samples were collected during the IODP Expedition 355. Each core (9.5 m long) is divided into six sections of around 150 cm each. Then each section is sliced into working-half and archive-half. The working-half are used for further geochemical and geological analysis. Archive-half is sent to different repositories of IODP for archiving the cores for future use. The IODP adopts a unique nomenclature system, which provides complete information about a selected sample. The core arrives from a very deep ocean floor so it may suffer expansion or loss due to slumping inside the corer. Thus, ends of cores do not match to the beginnings of the core below because of missing section between each core. This problem was first identified during DSDP Leg 85.

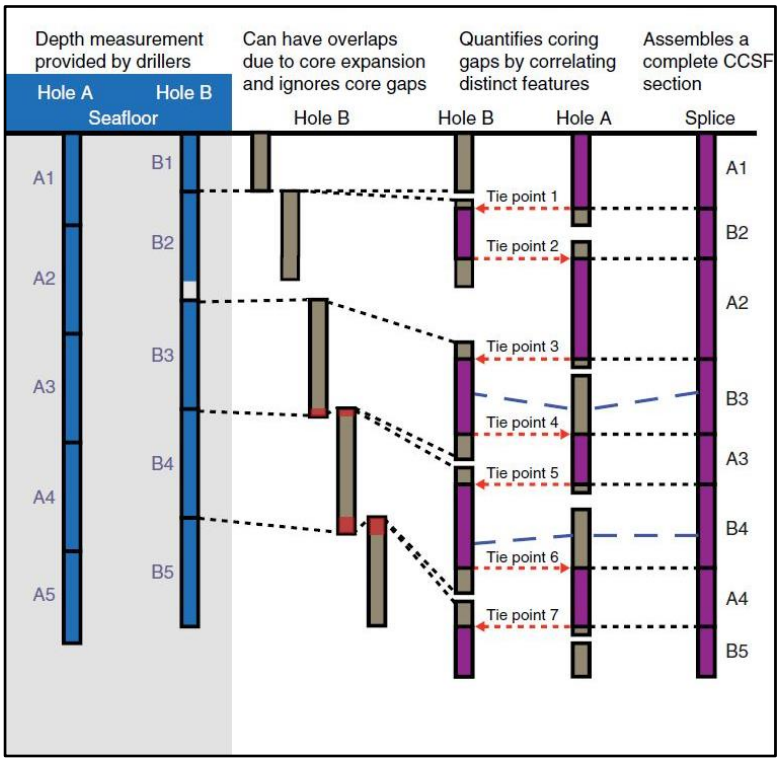

Figure 2.2. Schematic of different cores and tie points for splicing

For compensating this loss IODP use a very special technique known as splicing as shown in Fig. 2.2 and 2.3. The splicing uses the lithology and physical properties like natural gamma-ray and magnetic susceptibility of the sediments from different sections for filling the gaps in the sediment cores. The following represents a sample description from IODP Expedition 355.

355 U1456C-2H-5W, 80-85 cm

The nomenclature is explained below:

- The number 355 represents the Expedition number.
- The "U" indicates the hole was drilled by the United States Implementing Organization (USIO) platform, the *JOIDES Resolution* (JOIDES stands for Joint

Oceanographic Institutions for Deep Earth Sampling). If the other IODP scientific drilling vessel D/V *Chikyu* operated by Centre for Deep Earth Exploration (CDEX) under Japan Agency for Marine-Earth Science and Technology (JAMSTEC) is used, then the prefix "C" is used before the site number. If European Consortium for Ocean Research Drilling (ECORD) Science Operator (ESO) mission-specific platforms are used for drilling in specialized regions, the prefix "M" is used.

- The number 1456 represents the Site of the drilling. Drilling sites follow a continuous numbering scheme since the first site drilled by the D/V *Glomar Challenger* in 1968.
- The "A" represents the Hole at that particular Site. There can be several Holes called A, B, C and so forth at a Site.
- 2H is the core number; H is the type of corer used in the drilling operation ["H" indicates Advanced Piston Corer (APC) used for soft sediments and is 9.5 m long]. Other types of corers used are Half-Length Advanced Piston Corer (HLAPC; 4.7 m long; used to recover high-quality cores from short intervals of soft sediment between hard layers), Extended Core Barrel (XCB; used in firm sediments), and Rotary Core Barrel (RCB; used in medium to hard crystalline sediments) denoted by letters "F", "X", and "R", respectively.
- 1W shows the 1st 150 cm long section in that particular core while the "W" denotes the working-half.
- 80-85 cm is the sample interval in that particular Section i.e., taken between 80 and 85 cm below the top of the Section

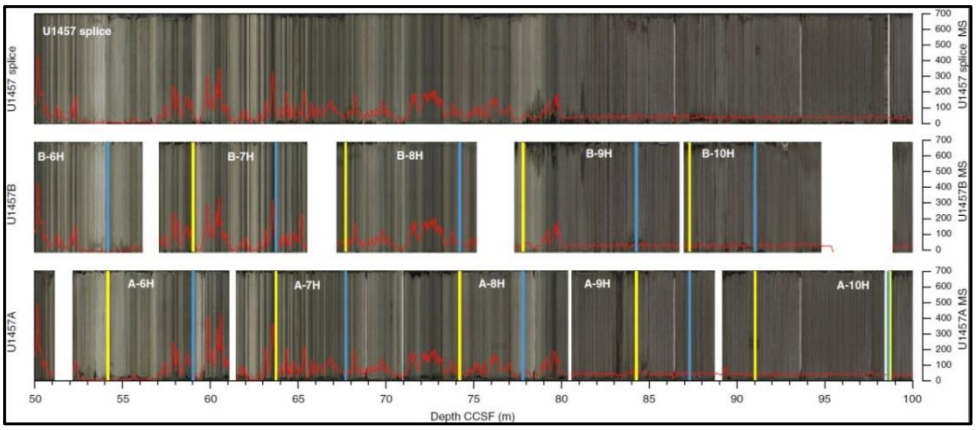

Figure 2.3. A splice made by combining two different cores (Pandey et al., 2016)

The subsampling was done in sampling party organized by IODP. The sediments were scooped and sealed in plastic packets. The scoops have different volume and samples were allotted according to the requirement of analysis. We have been allotted 10cc to 20cc based on the availability of sediments.

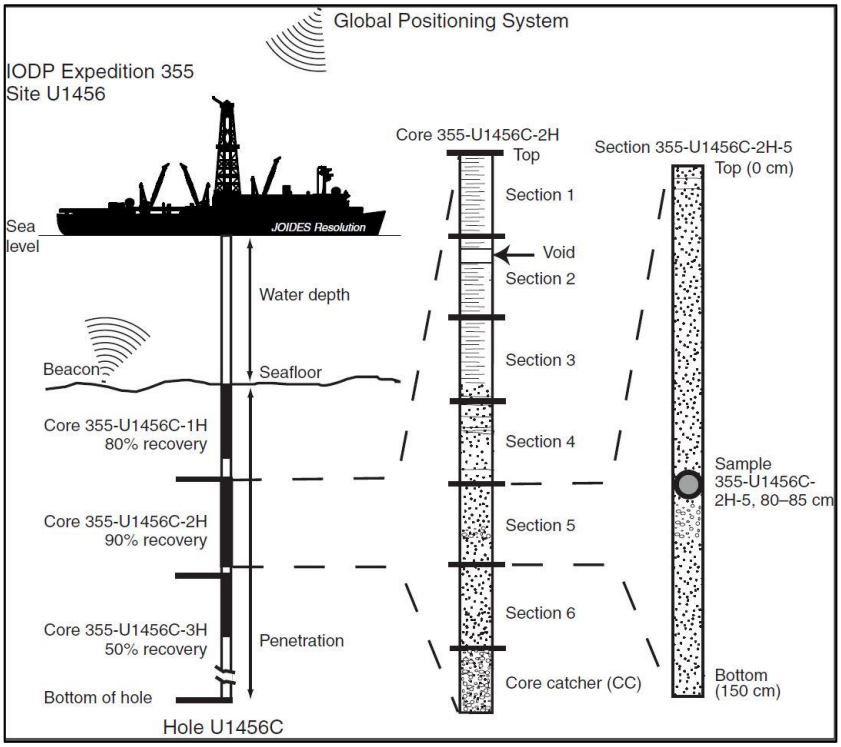

Figure 2.4. Schematic showing the coring procedure and a standard complete core during an IODP Expeditions (Source: IODP website)

2.2.1 Lithology of the sediment core recovered during IODP Expedition 355

Site U1456, the first site drilled during Expedition 355, is located ~475 km west of the Indian coast and ~820 km south from the modern mouth of the Indus River. The Indus river is supposed to be the primary contributor of sediment to this area (Clift et al., 2001, Pandey et al., 2016). Based on the presence of various minerals, fossils, nannofossils and heavy minerals assemblages the cored sections at Site U1456 and at Site U1457 are divided into different lithological units as shown in Fig. 2.5. The Site U1456 is divided into four units. Unit I consists of a ~121 m thick sedimentary sequence. This unit is light brown to light greenish nannofossil ooze and foraminifer-rich nannofossil ooze interbedded with clay, silt, and sand. Quartz, feldspar, and mica are common minerals in this unit. The heavy minerals are rare in abundance. Unit II is ~240 m thick and mainly made of massive dark grayish to blackish sand and silt interbedded with thinly bedded nannofossil-rich clay. Unit III is ~370 m thick and mainly consists of semi-indurated to indurated light brown to dark green clay/claystone, light brown to dark gray sand/sandstone, light greenish nannofossil chalk, and light to dark greenish gray nannofossil-rich claystone. Clay/claystone and sand/sandstone cycles of sedimentation are separated by intervals dominated by nannofossil chalk and nannofossil-rich claystone. Unit IV is about 380 m thick made of interbedded lithologies dominated by dark gray massive claystone, light greenish massive calcarenite and calcilutite, and conglomerate/breccia, with minor amounts of limestone. Quartz and mica are the common minerals in this unit. Presence of a 2 m thick sandstone and claystone in the base of this unit suggests an active Indus submarine fan at that time.

Site U1457 is the second drill site of Expedition site is located ~490 km west of the Indian coast and ~760 km south from the present-day Indus River mouth quite close to the Site 1456. Similar compilation through the Holes U1457A to U1457E is shown in figure 2.5 the cored sections at the site is divided into five sections. Unit I is made of ~74 m sequence consists of brown to light greenish nannofossil ooze including foraminifer-rich nannofossil ooze and nannofossil-rich clay, interbedded with silty clay and silty sand. Unit I of Site U1457is very similar to Unit I at Site U1456 both are mostly muddy and carbonate-rich. Quartz, feldspar, and mica grains are common in Unit I, whereas heavy minerals (hornblende, clinopyroxene, epidote, garnet, and augite) are rare. Unit II is ~311 m thick and consists mainly of light brownish gray to dark gray silty clay and dark gray sandy silt. Silty clay layers are typically massive and interbedded with very thin gray sandy silt layers. Unit II of Site U1457 and Unit II of Site U1456 are similar in age, but the sediment is finer-grained in U1457. Unit III is ~450 m thick and consists of semi-indurated to indurated light brown to dark green silty claystone, light brown to dark gray silty sandstone, light greenish nannofossil chalk, and light to dark greenish gray nannofossil-rich claystone. Nannofossil chalk and nannofossil-rich claystone cycles of sedimentation are separated by intervals dominated by clay/claystone and sand/sandstone deposition. The silty sandstone and silty claystone of Unit III occasionally have very thin (<1 cm) wood-rich layers, as well as large numbers of tiny wood particles. Unit III contains abundant light minerals with variable amounts of heavy minerals.

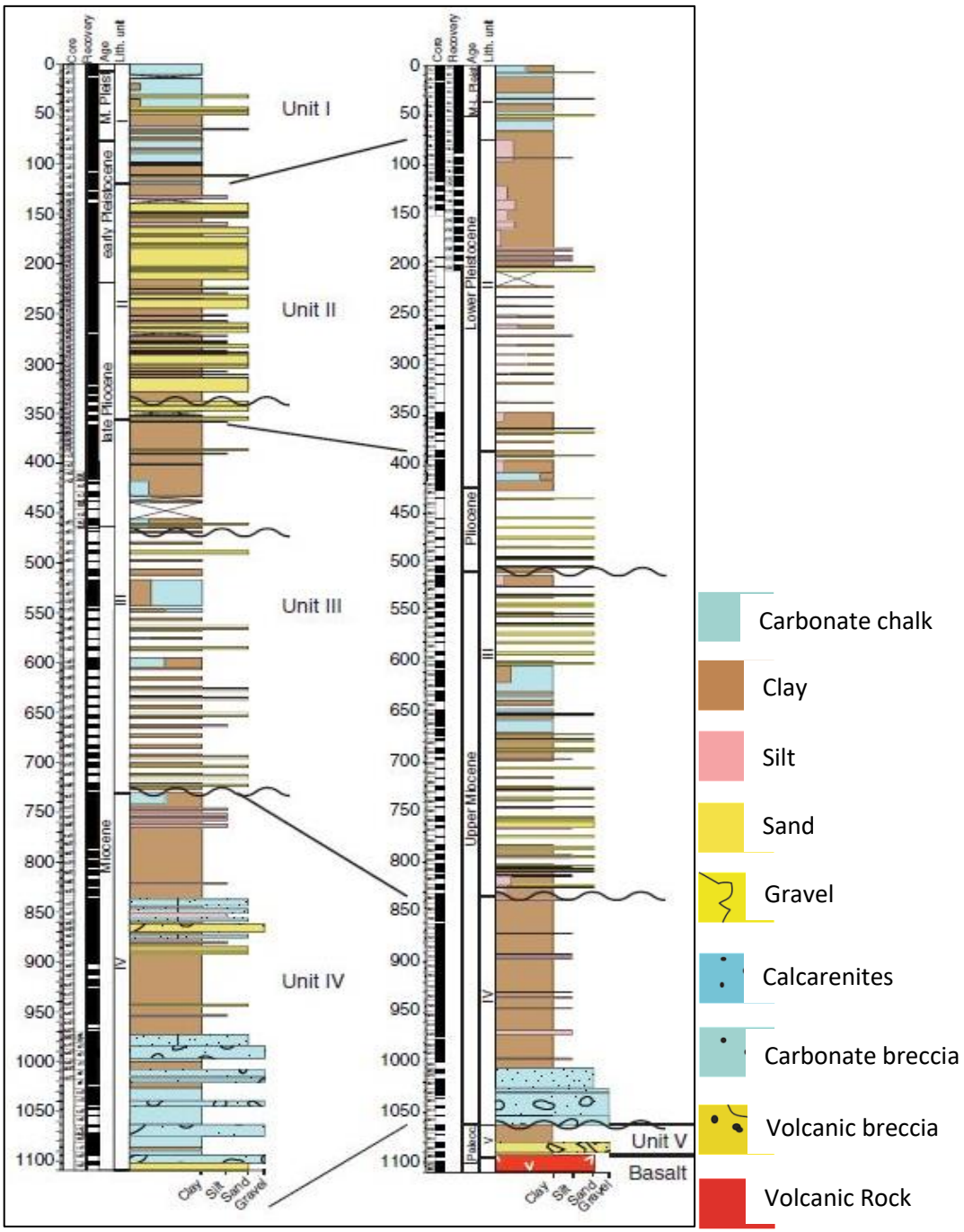

Figure 2.5. The lithostratigraphy of Site U1456 and U1457 with different units and the dominant lithology of the sediment cores (Pandey et al., 2016)

Unit IV is ~225 m thick and consists of dark gray to greenish gray massive claystone, light greenish massive calcarenite and calcilutite, breccia, and limestone,

particularly toward the base of the unit. Light minerals are abundant in Unit IV, whereas heavy minerals are only present in trace amounts. The ~30 m thick Unit V consists mostly of dark brown to dark greenish gray claystone and dark gray to black volcano clastic sediment that overlies the basaltic basement. The dark brown massive claystone shows very small amounts of interbedded dark greenish gray silty claystone. The thick dark greenish gray claystone contains black, discontinuous manganese layers and nodules, as well as small (1 to 3 cm) gray inclusions and rare parallel bands that are identified as carbonate-cemented nodules. Unit V contains abundant glass particles, trace amounts of light minerals, and no heavy minerals.

2.2.2 The squeezed cake samples of IODP Expedition 355

For interstitial water analyses during the Expedition, the cores from Sites U1456 and U1457 interstitial water was extracted from 5 to 15 cm long whole-round sections that were cut and capped immediately after core retrieval on deck. Whole-round sections at a frequency of one sample from each core were taken when. Sediments were removed from the whole-round sections of the core liner. The outer surfaces were carefully scraped with spatulas to minimize potential contamination by the coring process. The sediments then placed into the titanium and steel squeezing device (shown in Fig. 2.6; Manheim and Sayles, 1974) and squeezed at ambient temperature.

Fig 2.6. Titanium and Steel Squeezing Device Onboard *JOIDES Resolution*

The interstitial water collected was subsequently filtered through a 0.45 µm polysulfone disposable filter into separate clean vials for shipboard routine analyses and different shore-based analysis requests. Following interstitial water removal, squeeze cakes were removed from the squeezing device, placed in sterile bags, and were further used for different shipboard and shore-based analysis.

2.2.3 Onboard Age-Depth Model Reconstruction

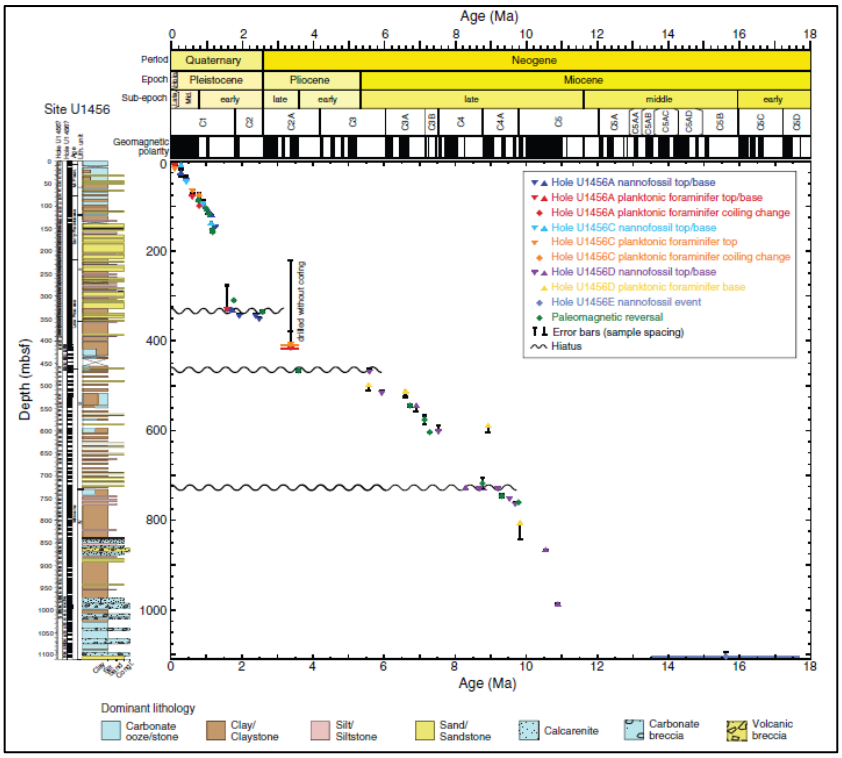

Figure 2.7. The Age-Depth Model of Site U1456 based on planktic foraminifera, nannofossils biostratigraphy and paleomagnetic reversals (Pandey et al., 2016).

The preliminary age models for Site U1456 and Site U1457 were determined on-board during the expedition. It is based on the biostratigraphy of planktic foraminifera and calcareous nannofossil, together with magnetostratigraphy (Fig. 2.7 and Fig. 2.8). The first and last appearance of the nannofossils and microfossils like *Pseudoemiliania lacunose, Reticulofenestra asanoi, G ruber, G tosaensis* is used. The change in the coiling pattern of the planktic foraminifera *Pulleniatina* is also used in the biostratigraphy. The microfossil bioevents are calibrated from Gradstein et al. (2012) geological time scale unless otherwise indicated (Pandey et al., 2016). The sedimentary sequence at Site U1457 spans the lower Paleocene through Holocene, despite a very long hiatus (~50 Ma from the lower Paleocene to the upper

Miocene) at ~1062 metres below seafloor (mbsf) (Pandey et al., 2016). It is also punctuated by three unconformities of ~0.8 Myr duration at ~8 Ma, ~2 Myr between the Miocene/Pliocene boundary and the lower Pliocene, and ~0.45 Myr during the lower Pleistocene (Fig 2.8). The sedimentation rate was ~17 to ~10 cm kyr^{-1} during late Miocene. A lower sedimentation rate (~4 cm kyr^{-1}) was measured between ~7.4 and 6.0 Ma and between late Pliocene and early Pleistocene times, although the sedimentation rate was very high (~58 cm kyr^{-1}) during an interval of early Pleistocene time. Since then and into the Holocene period, it decreased to ~7 cm ka^{-1}.

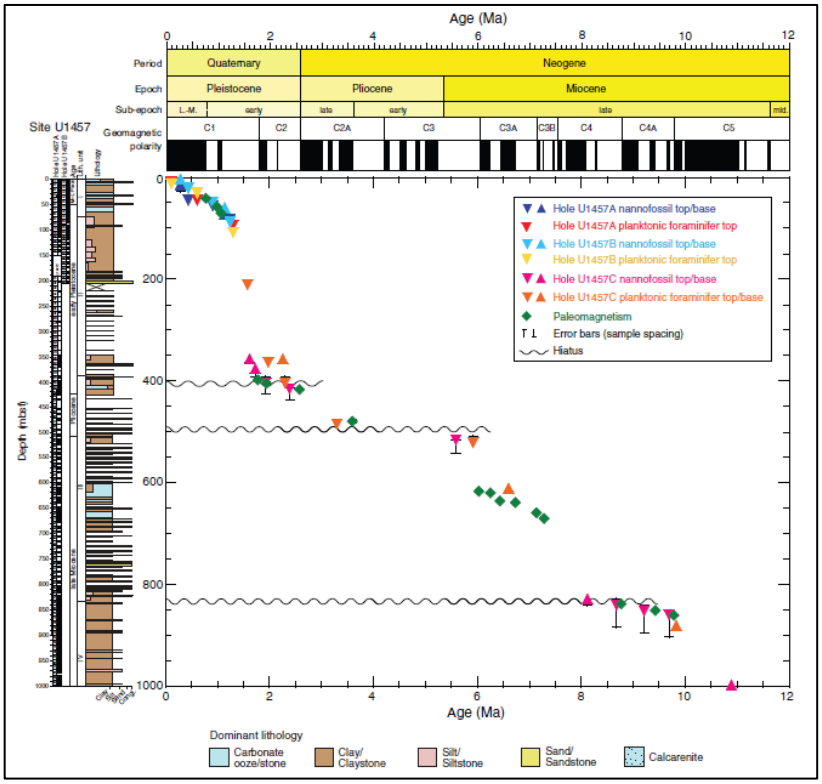

Figure 2.8. The age-depth model of Site U1457. It is based on planktic foraminifera, nannofossils biostratigraphy and paleomagnetic reversals (Pandey et al., 2016).

2.3 Proxies used in the study

The sediments from the ocean document the amplitude, frequency and timing of climate variability, which span timescales from centuries to millions of years and provide a measure of the ocean sensitivity to natural forcing. The geological proxies provide insights into processes that are not captured by short shipboard measurements and instrumental records. In the present study, (i) stable isotope ratio of nitrogen and carbon of sedimentary organic matter, (ii) stable isotopes ratio of carbon and oxygen of foraminifera (*Globigerinoides sacculifer*), (iii) trace metal ratio (Mg/Ca) of foraminifera (*G. sacculifer*), and (iv) organic carbon and total nitrogen concentration of sediment is used to investigate the past climate change. The systematics and application of these proxies are explained below.

2.3.1 Stable Isotope Systematics

Isotopes are atoms of an element that possess the same atomic number but a different mass number i.e. number of neutrons are different. The isotopes are specified in the form ${}^{m}_{n}Z$, where "m" is the mass number and "n" is the atomic number of an element "Z". Many of these isotopes are radioactive and decay spontaneously with half-lives ranging from seconds to millions of years. On the other hand, there are stable isotopes that do not decay or have half-lives comparable to the age of the earth and so are stable for all practical purposes. For example, nitrogen has 14 radioactive isotopes with very short half-lives out of which ${}^{13}_{7}\mathrm{N}$ has the longest half-life of ~10 minutes. It also has two stable isotopes - ${}^{15}_{7}\mathrm{N}$ and ${}^{14}_{7}\mathrm{N}$, which have seven protons each, and seven and eight neutrons in their nuclei, respectively. Usually, the heavier isotope is less abundant. For example, in the case of nitrogen, ${}^{15}\mathrm{N}$ is the less

abundant isotope constituting only 0.365% of the global nitrogen pool while the ^{14}N makes up the rest (99.635 %) (Ostrom, et al., 1998). Because of the very low abundance of heavier isotopes, it is very tough to measure their absolute abundance accurately. Therefore, the ratio of the heavier to the lighter isotope is measured. Isotope Ratio Mass Spectrometers (IRMS) are used to measure these isotope ratios. IRMS cannot measure the isotopic ratio of a single substance with high precision but can measure the difference between the isotopic ratios of two different substances with very high precision as both substances experience similar conditions. Therefore, isotopic ratios are expressed in terms of "delta" (δ) value, which is the relative difference between isotope abundance ratios between a sample and a standard (Coplen, 2011).

$$\delta^{15}N = [(^{15}N/^{14}N)_{spl} / (^{15}N/^{14}N)_{std}] - 1 \qquad (2.1)$$

The δ-value is a dimensionless quantity as it is the ratio of the two quantities of the same kind. Since δ-value is a small quantity, so it is multiplied by extraneous numerical factors like 1000 and expressed in "per mil" (‰) for the sake of readability. These extraneous factors do not form a part of the definition of the delta value and hence it is recommended to avoid its usage in the formula (Coplen, 2011). The international reference standards used are VPDB (Vienna Pee-Dee-Belemnite) for carbon and oxygen isotopes of carbonate, VSMOW (Vienna Standard Mean Ocean Water) for hydrogen and oxygen isotopes of water, Air-N_2 for nitrogen isotopes, VCDT (Vienna Canyon Diablo Troilite) for sulphur isotopes etc.

2.3.2 Nitrogen isotopes in the marine sediment

The two stable isotopes of Nitrogen are ^{14}N and ^{15}N with abundances of 99.64% and 0.36%, respectively. The availability of nitrogen is an important control on primary productivity. Nitrogen gets into the biological system by the process of Nitrogen Fixation. It involves the reduction of N_2 to ammonia (NH_3) by the nitrogen-fixing microorganisms and by lightning strikes. Most of the Nitrogen Fixation is done by bacteria known as diazotrophs such as Rhizobium. There is a genus of algae - *Trichodesmium* - that can fix atmospheric nitrogen as well. "Nitrification" is defined as the conversion of the NH_3 and NH_4^+ to nitrite (NO_2^-) and nitrite to nitrate (NO_3^-) by the nitrifying microbes *Nitrosomonas* and *Nitrobacter*, respectively. In the world oceans, three regions support most of the perennial anaerobic conditions in the water depths of ~200 m to ~1000 m called as oxygen minima zone (OMZ) with oxygen concentration falling below 0.5 ml/l. Due to lack of oxygen in OMZ, the anaerobic bacteria utilize NO_3^- as an oxidizing agent for the decomposition of organic matter and reduce it to gaseous compounds like NO, NO_2, and N_2 - a process called as "denitrification". During this process, microbes preferentially use NO_3- with a lighter isotope (^{14}N), thus enriching the residual nitrate in the heavier isotope (^{15}N), which gets upwelled to the sea surface and is taken up by the organisms as a nutrient. This enriched $\delta^{15}N$ signature is preserved when the organic matter settles down and get preserved in sea sediments (Saino and Hattori, 1987). Thus, a high $\delta^{15}N$ can be related to increased denitrification, which in turn is controlled by the climate-induced productivity and/or ventilation changes (Ganeshram et al., 1995). Further discussion on the

application of $\delta^{15}N$ as denitrification indicator in the Arabian Sea is provided in Chapter 4.

2.3.3 Organic matter and its Carbon Isotopes in the Marine Sediment

The composition and preservation of sedimentary organic matter depend upon many factors. Some of the factors are overhead primary productivity, sedimentation rate, oxygen exposure times, organic carbon to mineral surface area ratio, amount of refractory and non-refractory carbon (Muller and Suess., 1979; Calvert and Pederson., 1992; Schulz et al, 1998; Canfield et al., 1993; Mayer et al., 1994; Keil et al., 1994, 1997, 1999; Nagoji et al., 2017). Around ~5% of the organic carbon fixed by photosynthesis in the euphotic zone is exported to the deep waters where it undergoes further degradation and only 10% reaches the seafloor. In addition to this, because of the degradation of organic matter in the diagenetically active sediment less than 10% of the organic matter flux reaching the sediment bed gets ultimately preserved. However, the preservation of organic carbon is better in the OMZ dominated regions where reducing conditions prevail at the sediment-water interface. A high sedimentation rate supports enhanced preservation as it rapidly removes the organic matter from the diagenetically active zone and the exposure to the oxidizing agents is minimum (Heinrichs, 1993). Marine sedimentary organic matter is derived from the marine as well as from the terrestrial sources. For proper interpretation of marine productivity, it is necessary to ascertain the source of the organic matter. TOC/TN ratios have been widely used as a proxy to identify the origin of organic matter (Prahl et al., 1980, 1994, Ishiwatari and Uzaki, 1987, Meyers et al., 1996, Ujiie et al., 2001, Farquhar et al., 1989). The source distinction is based on the generalization that fresh algal organic

matter typically has atomic TOC/TN ratios between 5 and 8, whereas that from vascular land plants has TOC/TN ratios of 20 and greater (Emerson and Hedges, 1988; Meyers, 1994). The TOC/TN ratio of modern sediments comprising marine organic matter has a value of 8 to 10 whereas the ancient sediments have a value of 12-15 (Mackenzie, 1980). This difference in elemental compositions arises principally from (a) The lack of cellulose in algae and cellulose-richness in higher plants, and (b) the nitrogen-rich proteins present in algal organic matter (Premuzic et al, 1982; Meyers, 1994). Organic matter derived from land plants have some compounds exclusive to terrestrial biota such as lignin, chitin etc. has C/N values between 20 and 100 (Premuzic et al, 1982; Meyers, 1994). There are evidence, which show selective degradation of sedimentary organic matter during diagenesis has altered the original TOC/TN ratios of the sedimentary organic matter. A decrease in TOC/TN ratios over time of burial below the seafloor is reported in open ocean settings (Muller, 1977; Waples and Sloan, 1980; Meyers et al., 1996).

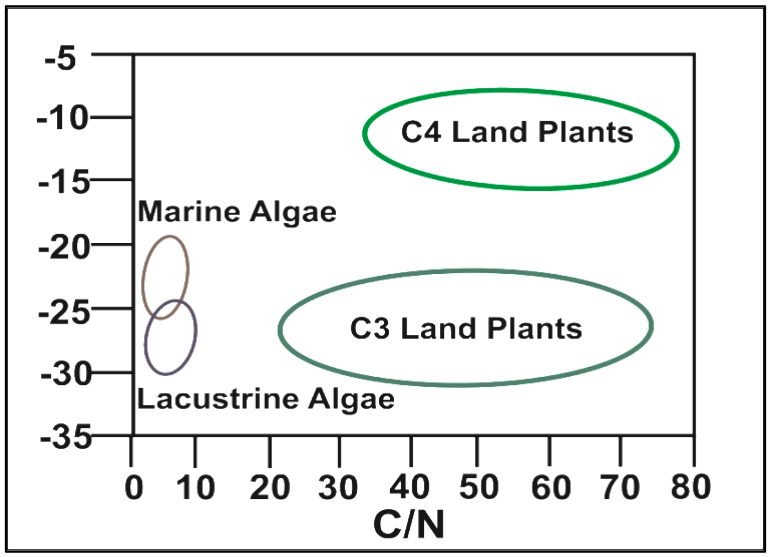

Figure 2.9. Classification of SOM based on atomic C/N ratios and organic $\delta^{13}C$ values of marine, lacustrine algae, C-3, C-4 plants and Marine biomass (Source: Meyers, 1994).

In general, $\delta^{13}C$ values of organic matter are different among terrestrial C3 plants (−30 to −23‰; Smith & Epstein, 1971), C4 plants (−17 to −9‰; Smith & Epstein, 1971) and marine phytoplankton (−22 to −19‰; Fry & Sherr, 1984). In this study, mean $\delta^{13}C$ values of C3 plants (−26 ‰), C4 plants (−13 ‰) and marine phytoplankton (−21 ‰) were assumed as end-members from previous literature (Fontugne & Duplessy, 1986; Calvert et al. 1995; Cowie et al. 2014). In the present study (Fig 2.9), we used $\delta^{13}C$ together with TOC/TN to decipher the provenance of sedimentary organic matter.

2. 4 Foraminifera

Foraminifera are a group of unicellular organisms that belongs to the phylum Protozoa. It is a widely used proxy in past climate studies. They secrete calcium carbonate shells (called tests) of various shapes and structural complexity, which get preserved in sea sediments as fossils. The tests can be composed of calcium carbonate (calcareous foraminifera) or composed of a variety of grains (agglutinated foraminifera) cemented together. The different species of foraminifera are identified based on their morphology (Kemle-von Mücke and Hemleben, 1999). Every species live in a specific ecological condition and have a lifespan of 2-4 weeks (Bé and Tolderlund, 1971; Johannessen et al., 1994, Farmer et al., 2001). This depth and ecological preference of foraminifera allow reconstruction of a variety of the past climate conditions, like oceanic temperature, thermocline dynamics, oceanic salinity etc. Foraminifera are further divided on the presence of spines on their surface. “Spinose” forms bear spines and “Non-Spinose” forms don’t possess spines. The size of the foraminifera ranges from 0.01 mm (10 μ) to 10 mm. The shells of foraminifera are divided into different

chambers. The wall separating one chamber from another is called the **septum**. The opening through which protoplasm extends is known as **aperture**. The highest diversity of foraminifera occurs in tropical regions. They are found in almost all the latitudes; however, with increasing latitude the species diversity decreases to a single species in the polar waters.

On the basis of depth habitat, the foraminifera are classified into planktic and benthic. Benthic foraminifera are the bottom-dwelling form and have lived in the ocean since the Cambrian time (~570 Ma). They live in all depths ranging from the continental shelf to abyssal plain. Planktonic foraminifera are the floaters i.e., found floating in the upper water column. They are more recent in origin and have existed since Jurassic (~200 Ma). Most of the planktonic foraminifera exist in the upper 200 m of the water column (mixed layer dwelling). Some of the species can inhabit deep into 600 m (thermocline dwelling). Planktonic foraminifera can be further classified into three categories viz. “Shallow-water dwelling”, “Intermediate-water dwelling” and “Deep-water dwelling” species. Foraminifera living predominantly in the upper 50 m of the water column are Shallow-water species. Intermediate-water species thrive in the upper 100 m. Deep-water species live in the euphotic zone as the juveniles and migrates below 100 m as adults.

The actual concentration of foraminifera tests in sediments, either modern or ancient, depends largely upon the rate at which non-biogenic (inorganic) sediments have accumulated. For example, the sediment supply near the mouth of a major river is so high that for getting a single foraminifera shell; we have to look in large quantities of sediment. Conversely, some deep-sea sediment (far removed from the

source of most non-biogenic sediments) may be almost purely made up of foraminiferal tests called as “Calcareous Ooze”.

In the present study, *G. sacculifer* is selected which is a spinose mixed-layer dwelling planktic foraminifer (Hemleben et al., 1989). It is one of the most abundant species in the sediments of the Eastern Arabian Sea. In general, its highest relative abundances (>30%) occur in the northern part with lower abundances (20-30%) in the southern region (Be, 1977, Naidu et al., 1993). *G. sacculifer* calcifies in the mixed layer of the ocean (25–40 m) (Farmer et al., 2007). *G. sacculifer* is resistant to dissolution compared to other planktic foraminifera (Delaney et al., 1985; Dekens et al., 2002) and thus becomes one of the ideal species for paleoceanographic study.

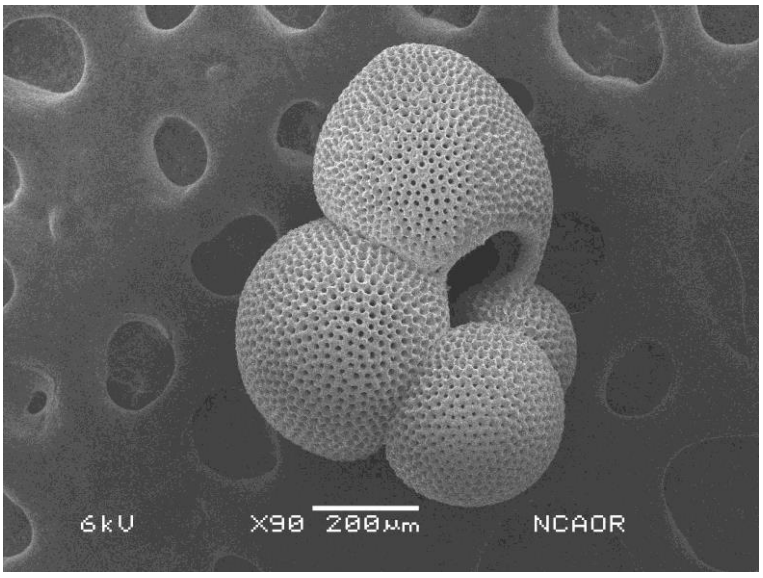

Figure 2.10. Electron microscope image of *G. sacculifer* from Site U1457 sediment sample

2.4.1 Oxygen isotopes of planktic foraminifera

The uptake of different trace elements and isotopes in the shells from surface seawater reflects the seawater composition and the physiochemical conditions during calcification. Oxygen isotope values recorded in planktic shells are primarily controlled by the temperature and oxygen isotope ratio of the ambient seawater, which is related to salinity and the amount of ice stored in continents (ice-volume effect) (Spielhagen and Erlenkeuser, 1994). The three stable isotopes of oxygen ^{16}O, ^{17}O and ^{18}O have 99.763%, 0.0375% and 0.1995% abundances, respectively. The two international standards PDB and SMOW are used for oxygen isotope study are provided by international atomic energy agency (IAEA).

PDB is a carbonate obtained from *Belemnitella americana*, was the lab standard used by Horald Urey's group in the University of Chicago during 1950s for developing the initial paleotemperature calibration equation (McCrea, 1950). *Belemnitella americana* is a belemnite from the Pee dee formation in South Carolina, USA. This standard is used in the low-temperature carbonate studies. PDB. The original PDB standard has been exhausted and not available now. IAEA has introduced new standard Vienna-PDB (VPDB) with values nearly identical to PDB. It is defined by its relationship to carbonate reference materials NBS-19 and IAEA-603. NBS-19 is calcium carbonate from a marble of a geological origin with $\delta^{18}O$ and $\delta^{13}C$ values of –2.20 ‰ and +1.95 ‰ respectively with respect to VPDB. IAEA-603 is a (Calcite, $CaCO_3$) primary reference material provided by IAEA with $\delta^{18}O$ and $\delta^{13}C$ values of -2.37 and +2.46 ‰ respectively with respect to VPDB.

SMOW is a hypothetical standard with $\delta^{18}O$ value close to the modern mean seawater value. The $\delta^{18}O$ value of SMOW with respect to an existing water standard NBS-1 (distilled Potomac River water) is –7.94 ‰ (Craig, 1961). The SMOW does not exist as a real water sample so it can't be distributed for laboratory measurements. IAEA distributes an international standard VSMOW with values identical to SMOW. VSMOW is prepared by mixing distilled ocean water collected from the Pacific Ocean, 0° lat., 180°long, in July 1967 (Gonfiantini, 1981). It has $\delta^{18}O$ value of 0 ‰ with respect to SMOW (by definition). This scale has been used for oxygen isotope analyses involving waters, silicates, phosphates, high-temperature carbonate etc.

The conversion equations based on Coplen et al., 1983 for $\delta^{18}O_{(PDB)}$ to $\delta^{18}O_{(SMOW)}$ and vice-versa are given below

$$\delta^{18}O_{(SMOW)} = 1.03091\ \delta^{18}O_{(PDB)} + 30.91 \qquad \textbf{(2.2)}$$

$$\delta^{18}O_{(PDB)} = 0.97002\ \delta^{18}O_{(SMOW)} - 29.98 \qquad \textbf{(2.3)}$$

Erez and Luz (1983) determined the following empirical temperature equation by comparing the isotopic composition of the planktonic foraminifera *Globigerinoides sacculifer* with the actual growth temperature:

$$T(°C) = 17.0 - 4.52\ (\delta^{18}Oc - \delta^{18}Ow) + 0.03\ (\delta^{18}Oc + \delta^{18}Ow)^2 \qquad \textbf{(2.4)}$$

The estimated temperature (T) is in °C. $\delta^{18}O_{sample}$, $\delta^{18}O_{seawater}$ are the isotopic composition of the shell carbonate and the seawater respectively.

To apply this paleotemperature equation we must know the $\delta^{18}O$ value of the seawater which complicates and inhibits its widespread application. However, it is tough to establish the isotopic composition of seawater. The salinity depends on the amount of ice stored on the continents, which gives rise to the "ice volume effect". Evaporation over the surface of the ocean forms water vapour relatively enriched in lighter isotope, as the vapour pressure of $H_2{}^{16}O$ is more than $H_2{}^{18}O$. Kinetic fractionation also complicates the process by further relatively enriching the vapour phase in lighter isotope. The isotopically lighter water vapour produced during the evaporation gets locked in the form of continental ice sheets, the remaining ocean water gets more and more enriched in the heavier isotope. During the Last Glacial Maximum (LGM) the average seawater $\delta^{18}O$ was 1.2 ‰ heavier than the present (Labeyrie et al, 1987, Fairbanks et al, 1989). The depletion of the heavier isotope in freshwater leads to the correlation of salinity with $\delta^{18}O$, salinity and $\delta^{18}O$ of the seawater increases with increasing evaporation. It is found that in the Arabian Sea, 1‰ increase in salinity causes a 0.33 ‰ increase in $\delta^{18}O$ of water (Duplessy et al, 1981, Sarkar et al, 2000). Analysis of planktic and benthic foraminifera calcite from the same location can resolve the ice volume effect. The $\delta^{18}O$ values of the planktics reflects the changes in both the temperature as well as the $\delta^{18}O$ of water. The bottom water is more or less at constant temperature and thus the benthic foraminifera records only the change in the isotopic composition of seawater.

There are several effects associated with the biology of foraminifera that causes deviation from the equilibrium. This deviation may be either due to metabolic effect or due to the kinetic effect (McConnaughey, 1989a, b). These effects, include respiration, ontogeny, and secretion of gametogenic calcite known as "vital

effects". The respiration products are relatively depleted in heavier isotopes (Lane and Doyle, 1956) and their utilization for shell secretion results in lower $\delta^{18}O$ values. Furthermore, planktonic foraminifera inhabits different depths at various stages of their ontogeny. In the later part of their lifecycles, they tend to secrete shells at deeper and cooler waters resulting in enhanced $\delta^{18}O$ values (Bouvier-Soumagnac and Duplessy, 1985; Emiliani, 1971). $\delta^{18}O$ of planktic foraminifera has been found to decrease with increasing light intensities which enhances the photosynthetic activity. The $\delta^{18}O$ was found to vary with changing carbonate ion concentrations as well. Previous studies show that foraminiferal shell $\delta^{18}O$ drops to -0.002‰ to -0.004 ‰ per μmol/kg carbonate ion increase for some species of foraminifera (Spero et al, 1997).

The disequilibrium due to vital effects can be minimized by selecting a species which precipitates their shells in equilibrium with seawater. Also picking intact shells from a fixed size range is helpful in reducing the vital effect. The $\delta^{18}O$ values of planktonic foraminifera from warm subtropical seas are particularly sensitive to alteration as the secondary calcite precipitates in equilibrium with the cold pore fluids at the sediment-water interface (Schrag, 1999). Also, diagenetic alteration after the death of the organism can modify its isotopic composition significantly. This obstacle can be overcome by selected pristine shells, which appear glassy under the microscope and are without any overgrowths. All foraminifera used in this research has been carefully handpicked to as far as possible avoid most of the above complications.

2.4.2 Carbon Isotope of the Planktic Foraminifera

The carbon isotope signature defined by the carbon isotopic ratio of the dissolved inorganic carbon in the oceanic water. Processes linked to ventilation rates and primary productivity primarily governs this isotopic signature. Carbon isotopic record from the foraminiferal carbonates has huge importance in paleoclimate reconstruction because they help to understand the movement of carbon in different reservoirs, primary productivity and paleocirculation of oceans (Kroopnick, 1980). The two stable isotopes of carbon ^{12}C and ^{13}C have an abundance of 98.89% and 1.11% respectively. Kinetic isotope effects during photosynthesis cause preferential uptake of ^{12}C in the organic matter. On the contrary isotope equilibrium reactions within the inorganic carbon system, "atmospheric CO_2 ↔ dissolved bicarbonate ↔ solid carbonate" cause enrichment of heavier isotopes (Hoefs, 1997) in the carbonates. The carbonate equilibrium in the marine system is given by the equation below (Faure, 1986)

$$CaCO_3\,(s) + H^+ \leftrightarrow Ca^{2+}\,(aq.) + HCO_3^-\,(aq.) \qquad \textbf{(2.5)}$$

These equilibrium reactions govern the carbon and oxygen isotopic variations among various chemical species.

HCO^{3-} (aq.), CO_3^{2-} and CO_2 (aq.) constitute the dissolved inorganic carbon. The net equation for carbonate precipitation can be represented as:

$$Ca^{2+}\,(aq.) + 2HCO_3^-\,(aq.) \leftrightarrow CaCO_3\,(s) + H_2O + CO_2\,(g) \qquad \textbf{(2.6)}$$

The equilibrium fractionation factors for carbon isotope in this system at 20°C are

(Emrich et al, 1970):

$$\alpha\ CaCO_3\ (s)\text{-}\ HCO_3^-\ (aq.) = 1.00185 \quad \textbf{(2.7)}$$

$$\alpha\ HCO_3^-\ (aq.)\ -\ CO_2\ (g) \quad = 1.00838 \quad \textbf{(2.8)}$$

$$\alpha\ CaCO_3\ (s)\ -\ CO_2\ (g) \quad = 1.01017 \quad \textbf{(2.9)}$$

Lower temperature favours the high fractionation between the dissolved CO_2 and the bicarbonate ion. The bicarbonate ion is the dominant species at the pH of seawater (7.5 – 8.3) and DIC can be measured by HCO_3^-(aq.).

Thus, the temperature has a negligible effect on the $\delta^{13}C$ of calcite in comparison to the effect due to the productivity variations (Emrich et al., 1970; Grossman, 1984). However, geochemical analysis of core top and surface sediments collected along the western continental margin of India suggests that primary productivity is the major controlling factor of the $\delta^{13}C$ distribution (Calvert et al., 1995). Similar to oxygen isotopes the size of the foraminifera, pH of the oceanic water and light intensity also influences the carbon isotopes in the foraminifera (Oppo and Fairbanks, 1989). Many studies also, reveals that the changes in benthic $\delta^{13}C$ can be linked to factors like shifts in the deep ocean circulation (Boyle and Keigwin., 1982; Curry and Lohaman., 1982; Shackleton et al., 1983), air sea exchange (Charles et al., 1993) and physiological and environmental effects (McCorkle et al., 1990; Mackensen et al., 1993). As the organism dies it settles at the bottom of the ocean where it gets oxidized releasing CO_2 depleted in ^{13}C. Thus the DIC in the upper water column has the highest $\delta^{13}C$ with a minimum at the base of it i.e., thermocline depth after which it increases a little and stays more or less uniform.

As discussed earlier, different reservoirs have different $\delta^{13}C$ values. For example, organic-rich reservoirs have lower $\delta^{13}C$ values due to preferential intake of lighter isotope during photosynthesis (O'Leary, et al., 1980, O'Leary, 1981). Thus, a higher $\delta^{13}C$ value probably corresponds to an enhanced rate of photosynthesis in the euphotic layer that indicates an increase in productivity. The vital effect again creates disequilibrium in the $\delta^{13}C$ values as discussed in the case of oxygen isotopes. There are symbionts present in the foraminifera shells that carry out photosynthesis in which they preferentially utilize the lighter isotope. Photosynthesis also increases with an increase in irradiance resulting in enhanced $H^{13}CO_3$- in the ambient microenvironment, results in higher $\delta^{13}C$ (Spero and Lea, 1993). $\delta^{13}C$ in foraminiferal carbonate decreases with increasing carbonate ion concentration similar to the effect experienced by $\delta^{18}O$ (Spero et al, 1997). The diagenetic alteration also makes the ambient water depleted in heavier isotopes and shifts $\delta^{13}C$ values toward the lighter side. Hence, the combined effect of all these factors highly complicates and biases the interpretation of $\delta^{13}C$ records. To minimize the effect of above mentioned processes, intact, monospecies and clean foraminifera of a fixed size have been chosen.

2.4.3 Trace metal (Mg/Ca) of planktic foraminifera

The reconstruction of oceanic water temperatures as well as salinities is a crucial step for a complete understanding of the hydrological component of the climate during the past. The Mg/Ca is one of the rapidly growing advanced proxies for oceanic water temperature (Villiers, et al., 2002; Anand et al., 2003). Calibration of

foraminifera Mg/Ca ratios with temperature, including culture, sediment trap and core-top studies have given very consistent results. Mg/Ca-based paleothermometry has been greatly refined and applied frequently to paleoceanographic research concerning temperature variability at different timescales (Hastings et al., 1998; Lea et al., 1999, 2000, 2002; Mashiotta et al., 1999; Elderfield and Ganssen, 2000; Koutavas et al., 2002; Stott et al., 2002; Pahnke et al., 2003; Visser et al., 2003).

The advantage of Mg/Ca of planktonic foraminifera is that it gives an independent estimate of temperature (Nurnberg et al., 1996; Lea et al., 1999; Mashiotta et al., 1999; Anand et al., 2003; Russell et al., 2004; von Langen et al., 2005; Groeneveld and Chiessi, 2011) and oxygen isotopic analysis from the same foraminifera species can be used to determine the oxygen isotopic composition of seawater and thus the oceanic salinity (Elderfield and Ganssen, 2000; Lear et al., 2000). Thus, coupled measurement of Mg/Ca and $\delta^{18}O$ can help in quantifying the climate change of a region in terms of exact SST and salinity (can be related to precipitation) (Waelbroeck et al., 2002; Mahesh et al., 2014; Tiwari et al., 2015).

Mg/Ca-based paleothermometry has also been applied to benthic foraminifera species to generate records of bottom water temperature (Lear et al., 2002; Martin et al., 2002; Skinner et al., 2003; Elderfield et al., 2006; Rosenthal et al., 2006; Marchitto et al., 2007; Rosenthal et al., 2011; Healey et al., 2008; Yu and Elderfield, 2008). It has been observed that elemental ratio (e.g., Mg/Ca, Sr/Ca) of several calcifying organisms like ostracods, corals and coccoliths have also been shown to be sensitive to changes in temperature (Izuka, 1988; Dwyer et al., 1995; Rathburn and De Deckker, 1997; Rosenthal et al., 1997; Mitsuguchi et al., 1996; Lear et al., 2000;

Toyofuku et al., 2000; Martin et al., 2002; Martin and Lea 2002; Billups and Schrag, 2003).

The planktic foraminifera has been calibrated for oceanic temperature by using core-tops, sediment traps and lab-cultures studies (Nurnberg et al., 1996; Mashiotta et al., 1999; Lea et al., 1999, 2000; Elderfield, et al., 2000; Elderfield and Ganssen, 2000; Dekens et al., 2002; Anand et al., 2003; McConnell and Thunell, 2005). Most of these studies have demonstrated a ~9-10% exponential increase in Mg/Ca per degree Celsius in most species (Lea et al., 1999). *G. sacculifer* have a nearly uniform inter-chamber distribution of Mg and Ca (Eggins et al., 2003). The biological and thermodynamical processes into the foraminifera shells (Rosenthal et al., 1997; Lea et al., 1999; Erez, 2003) affect the incorporation of Mg. In addition to the vital effect, the interspecies variability of Mg/Ca is also observed in planktic foraminifera (Anand et al., 2003; Lea et al., 1999). Understanding of processes, which can influence Mg/Ca concentration should be taken into account before the interpretation and calculating the oceanic temperature.

2.5 Measurements of different proxies

2.5.1 Analysis of squeezed cake sediments for TOC/TN and isotopes of Carbon and Nitrogen

5–15 cm long whole-round core sections at the interval of every core or every alternate core were squeezed at ~35000 lbs using titanium steel squeezing device to obtain the interstitial water. The remaining sediments are named '**squeeze cake**'. The samples were dried to remove the moisture at 45 °C before processing. Around

10 to 20 g of sediment aliquots were taken for further analysis. Dried samples were finely ground for homogenization. Homogeneous samples were divided into two batches for geochemical and isotopic analyses (i) 2 N HCl treatment for total organic carbon (TOC) and $\delta^{13}C$ of organic carbon measurement and (ii) untreated for determination of total nitrogen (TN) content and $\delta^{15}N$ values. 20 ml of 2 N HCl solutions was added to 5–10 g of fine sediment powder for removing the inorganic carbon. The mixture was shaken mechanically and allowed to stand for ~12 hours. The acid treatment is done to decarbonize the sediment for removing inorganic carbon. However, the acid treatment can alter the nitrogen isotopes in the sediment, which makes it unsuitable for nitrogen isotope analysis (Schlacher et al., 2014). Previous studies show up to ~1.5 ‰ difference in nitrogen isotopes in treated and untreated sediments (Brodie et al., 2011a,b). Therefore, the nitrogen isotope ratio was measured using untreated sediment samples.

The sample was then washed with ultrapure demineralized water and approximately 10 mg of the treated sample was used for TOC and $\delta^{13}C$ analysis. For TN and $\delta^{15}N$ measurement, approximately 40 mg of bulk ground sediment was used. The $\delta^{15}N$ and $\delta^{13}C$ values were determined using isotope ratio mass spectrometer coupled with an element analyser at Marine Stable Isotope Lab, National Centre for Polar and Ocean Research, Goa, India. The standard used was ammonium sulphate (IAEA-N-1) and cellulose (IAEA-CH-3). The analytical precision for $\delta^{15}N$ and $\delta^{13}C$ is 0.12‰ and 0.06‰ (1σ standard deviation), respectively. The analytical precision is obtained by running standard during the analysis. Similarly, TN and TOC were determined using sulphanilamide as the standard. The analytical precision for TN and TOC is 0.63% and 0.84% (n=20) respectively.

Table 2.2 Details of the standards used in the bulk sediment analysis

	Elements	**Standards**	**Precision (1σ)**
1	Carbon ($\delta^{13}C$)	IAEA-CH-3	0.06 ‰
2	Nitrogen ($\delta^{15}N$)	IAEA-N-1	0.12 ‰
3	TOC and TN	Sulphanilamide	0.84% and 0.62%

2.5.2 Analysis of Quaternary Sediments for TOC/TN and isotopes of carbon and nitrogen

Briefly, each sample was oven-dried overnight at 45°C to remove the moisture. Dried samples were finely grounded for homogenization. The sample was then washed with ultrapure demineralized water and approximately 8-10 mg of the treated sample was used for TOC and $\delta^{13}C$ analysis. For TN and $\delta^{15}N$ measurement, approximately 200 mg of bulk ground sediment was used.

The $\delta^{15}N$ and $\delta^{13}C$ values were determined using isotope ratio mass spectrometer coupled with an element analyzer at Marine Stable Isotope Lab, National Centre for Polar and Ocean Research, Goa, India. The $\delta^{13}C$ and $\delta^{15}N$ are calibrated to the VPDB and Air-N_2 scale using international standard IAEA-CH-3 and IAEA-N-1, respectively. The analytical precision for $\delta^{15}N$ and $\delta^{13}C$ is ± 0.12‰ and ± 0.06‰ obtained through repeatedly running ammonium sulphate (IAEA-N-1) (n=36) and cellulose (IAEA-CH-3) (n=36) standards, respectively. Similarly, analytical precision for TN and TOC was determined using sulfanilamide as the standard. The analytical precision for TN and TOC is ± 0.70 % and ± 0.09%, respectively, obtained through repeatedly analysing sulfanilamide standard (n = 30).

Table 2.3. Details of the standards used in the bulk sediment analysis

	Elements	Standards	Precision (1σ)
1	Nitrogen ($\delta^{15}N$)	IAEA-N-1	0.12 ‰
2	Carbon ($\delta^{13}C$)	IAEA-CH-3	0.06 ‰
3	TOC and TN	Sulphanilamide	0.09 % and 0.70 %

2.5.3 Separation from sediment and Oxygen and carbon isotopic analysis of planktic foraminifera

About 10 g of sediment samples were taken in a 400 ml beaker filled with ~200 ml of distilled water. It is soaked overnight to breakdown the sediment. If the sediment is hard to disperse using distilled water, sodium hexametaphosphate (Calgon) was added. Calgon acts as a dispersing agent and easily disintegrates the sediment. The Calgon mixture was heated (not to boil, for ~15 minutes) only when sediments are agglutinated and hard to disperse. After this, around 10 cc of 30% H_2O_2 was added to remove any organic matter that might be present and sticking to the foraminifera shells. Subsequently, wet sieving was carried out using the sieve of the sizes 63 μm. The foraminifera were then transferred to 50 ml beakers containing distilled water and were ultrasonicated to remove any particles sticking to the shells. The foraminifera thus separated from the sediments were dried in the oven at 50° C. The size fraction 250 to 350 μm was then separated using dry sieving. The separated foraminifera were kept in pre-cleaned plastic vials and properly labelled. The planktonic species *G. sacculifer* was then handpicked under a stereoscopic microscope from the size range 250 μ to 350 μ. For isotopic analysis, 8-10 tests were picked and kept in the clean and dry glass vials. For Mg/Ca analysis, 15-20 tests

were picked. The foraminifera were chosen for their pristine appearance and particular attention was paid to species morphotypes to yield mono-specific samples. From each sample, 8-10 tests of *G. sacculifer* were selected from the 250 -350 μm fractions for $\delta^{18}O$ and $\delta^{13}C$ analyses by Isoprime Dual Inlet Isotope Ratio Mass Spectrometer with Multiprep device at the NCPOR's Marine Stable Isotope Laboratory (MASTIL). $\delta^{13}C$ and $\delta^{18}O$ are reported in per mil (‰) calibrated to the VPDB scale using international standard IAEA-603, Calcite (all the data is presented and discussed in Chapter 5).

Table 2.4. Details of the standards used in the foraminifera isotope analysis

	Elements	**Standards**	**Precision (1σ)**
1	Oxygen ($\delta^{18}O$)	IAEA-603; n= 18	0.15 ‰
2	Carbon ($\delta^{13}C$)	IAEA-603; n= 18	0.06 ‰

2.5.4 Measurements of Mg/Ca

Methods of preparing and analysing foraminiferal samples for Mg/Ca measurement vary between laboratories; there is no standardised method per se. Different methods and analysis could lead to offsets in the results between laboratories. Thus, it is important to know what differences exist and how these might affect the determination of Mg/Ca ratios. These questions have been addressed by an inter-laboratory comparison study by Rosenthal et al. (2004). Several foraminifera samples and standard solutions were run by many laboratories to assess the relative accuracy, precision and reproducibility of their methodologies. Results from this work suggest that analytical techniques used by a selection of laboratories produced generally good precision but poor inter-lab consistency. This was probably caused

by inaccuracies during the preparation of calibration standard solutions within particular laboratories and may be addressed in the future by use of a universal accuracy standard. The different techniques have their own limitations and produce offsets in the results. The findings also point towards the more significant disparities caused by sample preparation methods. Modern analytical techniques for analysing bulk foraminiferal Mg/Ca ratios include Inductively Coupled Plasma Mass Spectrometry (ICP-MS) (Rosenthal et al., 1999, 2002, 2006) and ICP-AES (Atomic Emission Spectrometry) also known as optical emission spectrometer (ICP-OES) (Villiers et al., 2002). Both of these techniques provide high precision measurements of Mg/ Ca ratios. The electron microprobe (Nurnberg, 1996) and Laser Ablation (LA–ICP–MS/OES) techniques can help find the heterogeneity in the measurement of Mg/Ca in a single test (Nurnberg, 1996; Eggins et al., 2003).

Using best fit statistical methods, several empirical equations of the following form are obtained:

$$\mathbf{Mg/Ca\ (\mu Mol\ Mol^{-1}) = b\ e^{mT}} \qquad \mathbf{(2.10)}$$

Where *b* is the pre-exponential constant, *m* the exponential constant, and *T* the temperature. The exponential constant determines the magnitude of temperature change calculated from variations in Mg/Ca, while the pre-exponential constant determines the absolute temperature. The calibration equation is chosen based on the oceanography of the region.

A known NIST standard solution with a fixed concentration of Mg/Ca was run after every fifth sample to check the instrumental consistency. More than 100

measurements of the NIST standards spread over the analytical period yielded a mean of 2.18 ± 0.09 μmol/mol indicating that the Mg/Ca data presented in this study is of high precision (data shown in table 2.6, 2.7 and 2.8). The Fe, Mn and Al were also measured to monitor contamination by clays and oxides. To check contamination, the criterion chosen was to reject any sample with Fe/Mg ratio exceeding 1 mol/mol (Barker et al., 2003). Some studies monitor the Fe/Ca, Al/Ca and Mn/Ca (Barker et al., 2003,). In the present study, the correlation between Al/Ca versus Mg/Ca yielded insignificant correlations (R^2 < 0.08) indicating contamination-free Mg/Ca data (all the data is presented and discussed in Chapter 5).

The chemical treatment and cleaning of foraminifera

The foraminifera were cleaned before the measurement was conducted in order to remove any potential contaminants such as clay, sand and organic materials. The cleaning method was a modified version of the one laid out by Barker et al., 2003 (the steps repeated more number of times for less duration to avoid loss of samples and the samples were observed visually more frequently to avoid dissolution and loss). There are many clay minerals present in the marine sediments containing between 1 to 10 wt % Mg (Deer et al., 1992) therefore the presence of clay can potentially influence the Mg/Ca content. This makes it necessary to remove the maximum amount of clays impurities for accurate measurement. The cleaning procedures described by Barker et al., 2003 have dedicated steps to remove clay contamination.

- There are several methods in order to examine whether this method is effective. Correlation between Mg/Ca and Al/Ca can be useful in determining the cleaning effectiveness. A linear relationship between the two would indicate that the samples are contaminated (Barker et al. 2003). However, a weak correlation between Mg/Ca and Al/Ca (R^2 value of just 0.08, this value is from analysed data of this work) indicates that the cleaning was successful (Barker et al., 2003).
- Before cleaning commenced, the specimens were partially crushed between two glass slides in order to open up all the chambers. If the foraminifera shells were found to be very weak as observed under the microscope, a blunt stainless needle was used to open the chambers individually to avoid over crushing and loss of samples. The ease with which the foraminifera were crushed was noted as it indicates how well they were preserved. Once the crushing was complete, the broken shells were transferred to a micro-centrifuge tube and ultrapure deionized water is added.
- In order to remove clay from the crushed shells, 500 µl of water was added to each vial. Air bubbles were removed by gently tapping the micro-centrifuge tubes. Superfluous water was removed carefully using a pipette. The microcentrifuge tubes filled with 500 µl of deionized water were placed in an ultrasonic bath at normal strength baths for two minutes. Air bubbles were removed again and superfluous water was removed.
- Once cleaning with water was completed, 250 µl of analytical grade methanol was added to the microcentrifuge tubes and were placed in an ultrasonic bath for two minutes. Once the microcentrifuge tubes were removed from the ultrasonic bath the superfluous methanol was removed like the previous step. This procedure was

repeated until the transparency appears in the solution. Thereafter, it was rinsed with 500 µl of water to remove the methanol completely from the sample (this method was repeated to remove any traces of methanol from the crushed sample).

- In order to remove organic material from the sample, an oxidation step was included. A solution of fresh alkali buffered 1% H_2O_2 was prepared for every batch. Alkali buffered solution is prepared by mixing 100 ml H_2O_2 (Aristar Grade) to 10 ml 0.1 M NaOH (Aristar Grade). 250 µl of this solution was then added to each vial. The vials were then placed in warm water for a total of ten minutes. Every two and half minutes the microcentrifuge tube were removed and tapped in order to remove air bubbles.
- After every fifth and tenth minute in the water bath, the vials were placed in the ultrasonic bath for a short duration of time (time ~30 seconds). Once the procedure was completed the solution was removed. This step was repeated twice. The samples were then washed by adding and removing 500 µl of water three times.
- The final cleaning stage was an acid leach. The samples were transferred to new microcentrifuge tube and 250 µl of 0.001 M HNO_3 was added to each microcentrifuge tube. The samples were then transferred to the ultrasonic bath and left for 30 seconds. Once removed from the ultrasonic bath the acid was removed quickly and twice rinsed with 500 µl of ultrapure deionized water to avoid dissolution.
- After the acid leach was completed, the sample has to be dissolved for analysis using ICP-OES. For this, 500 µl of 0.075 M HNO_3 was added and the sample was placed in the ultrasonic bath until the entire sample was dissolved. Before analysis, the samples were diluted in order to achieve an optimal amount of calcium in the

samples (10-80 ppm Ca). The extent of dilution varied depending on the amount of material that was remaining.

- The measurements were performed using Inductively Coupled Plasma-Optical Emission Spectrometer (ICP-OES) in Paleothermometry Lab, National Centre for Polar and Ocean Research, Goa, India.

2.5.5 Analysis using Inductively Coupled Plasma-Optical Emission Spectrometry (ICP-OES)

ICP-OES is a spectrometric technique used to determine elemental concentrations in aqueous solutions. The instrument measures characteristic emission spectra by optical spectroscopy. In this technique, a sample solution is aspirated (i.e., nebulized) continuously into an argon plasma where analytes of interest (crushed, cleaned and dissolved foraminifera for present research) are converted into gas-phase atoms or ions in excited state. As the excited-state atoms or ions return to their ground state, they emit energy in the form of light at wavelengths that are characteristic of a specific element. The spectra are dispersed by a diffraction grating and the intensities of the emission lines are monitored by a photosensitive solid-state Charge Injection Device. The intensity of the energy emitted at the chosen wavelength is proportional to the concentration of the element in the analysed sample. See table 2.8 for proportional decrease in intensity (cps) with concentration of synthetic standards. Thus, by finding which wavelengths are emitted by a sample and their respective intensities (known as intensity ratio calibration), the elemental composition of the given sample relative to a reference

standard may be quantified. This method is used in simultaneous determination of many elements' concentration.

Table 2.5. Instrument parameter during trace metal analysis

Parameter		
RF Power	1150 W	
Pump Speed	50 rpm	
Exposure Time	Axial View	
	UV 10 s	Visible 5 s
Nebulizer	V-groove type	
Nebulizer Gas Flow	0.50 L/min	
Auxiliary Gas Flow	0.50 L/min	
Coolant Gas Flow	12 L/min	

Table 2.6. NIST carbonate standard with fixed Mg/Ca value ran throughout during different batches of Mg/Ca analysis

	Sample name	**Mg**	**Ca**	**Mg/Ca**
1	CRM-1	0.100	46.107	2.162
2	CRM-2	0.040	18.452	2.152
3	CRM-3	0.167	76.771	2.175

4	CRM-4	0.040	18.258	2.206
5	CRM-5	0.103	46.025	2.236
6	CRM-6	0.055	25.329	2.175
7	CRM-7	0.019	8.069	2.338
8	CRM-8	0.018	7.493	2.351
9	CRM-9	0.082	39.343	2.078
10	CRM-10	0.082	39.728	2.052
11	CRM-11	0.084	39.234	2.138
12	CRM-12	0.084	39.247	2.142

Mean Mg/Ca = 2.18 ± 0.10

Table 2.7. NIST standard measurement-1 for matrix effect

	Sample name	Mg	Ca	Mg/Ca
1	CRM-1	0.028	11.300	2.546
2	CRM-1	0.027	11.168	2.422
3	CRM-1	0.027	10.914	2.490
4	CRM-1	0.027	11.084	2.467
5	CRM-1	0.025	10.489	2.420
6	CRM-1	0.025	9.761	2.556
7	CRM-1	0.027	10.456	2.652
8	CRM-1	0.025	10.602	2.315

Mean Mg/Ca = 2.48 ± 0.10

Table 2.8. NIST standard measurement-2 for matrix effect

S No.	Sample list	Mg	Ca	Mg/Ca
1	CRM2	0.0270	10.8601	2.4822
2	CRM2	0.0266	10.7585	2.4718
3	CRM2	0.0245	10.4777	2.3405
4	CRM2	0.0247	10.3529	2.3900
5	CRM2	0.0219	10.0723	2.1710
6	CRM2	0.0228	9.8716	2.3073
7	CRM2	0.0234	9.6530	2.4268
8	CRM2	0.0226	9.5177	2.3787

Mean Mg/Ca = 2.37 ± 0.10

Table 2.9. The intensity of Mg and Ca at different concentration of multi-element standard

Multi element standard	Mg 280.270 (Axial)	Mg 285.213 (Axial)	Ca 422.673 (Axial)	Ca 315.887 (Axial)
	Y (cps)	Y (cps)	Y (cps)	Y (cps)
10 ME	2624928	659209	1502468	237444
1 ME	307301	72420	181146	23186
0.5 ME	157377	37236	97574	10886
0.1 ME	31417	7300	20814	560

Chapter 3

Published in Scientific Reports
DOI: 10.1038/srep43056

3. First evidence of denitrification vis-à-vis monsoon in the Arabian Sea since Late Miocene

Shubham Tripathi[1], Manish Tiwari[1], Jongmin Lee[2], Boo-Keun Khim[2]& IODP Expedition 355 Scientists[†]

1. National Centre for Antarctic and Ocean Research, Vasco-da-Gama, 403804, Goa, India.
2. Department of Oceanography, Pusan National University, Busan, 46241, Korea.

†A comprehensive list of consortium members appears at the end of the chapter

Abstract

In the Arabian Sea, South Asian monsoon (SAM)-induced high surface water productivity coupled with poor ventilation of intermediate water results in strong denitrification within the oxygen minimum zone (OMZ). Despite the significance of denitrification in the Arabian Sea, we have no long-term record of its evolution spanning the past several million years. Here, we present the *first* record of denitrification evolution since Late Miocene (~10.2 Ma) in the Eastern Arabian Sea, where the SAM generates moderate surface water productivity, based on the samples retrieved during the International Ocean Discovery Program (IODP) Expedition 355. We find that (i) the SAM was persistently weaker from ~10.2 to 3.1 Ma; it did not intensify at ~8 Ma in contrast to a few previous studies, (ii) on tectonic timescale, both the SAM and the East Asian Monsoon (EAM) varied synchronously, (iii) the first evidence of denitrification and productivity/SAM intensification was at ~3.2–2.8 Ma that coincided with Mid- Pliocene Warm Period (MPWP), and (iv) the modern

strength of the OMZ where denitrification is a permanent feature was attained at ~1.0 Ma.

3.1 Introduction

Oxygen minimum zones (OMZs) - the regions of dissolved oxygen deficient (O_2< 20 μM) water located in the tropical oceans - have been proposed to expand in the present scenario of global warming[1,2]. OMZs play a significant role in producing N_2O - a powerful greenhouse gas through the process of denitrification (a process by which nitrate and nitrite are reduced to nitrogen gas) when the dissolved O_2 levels fall below 1 μ M [3]. A perennial OMZ develops between 150 and 1000 m water depth in the Arabian Sea due to various natural factors such as high surface water productivity and reduced ventilation of intermediate water[4]. The anoxic zones of these OMZs occupy only ~0.8% of the world ocean but are responsible for the highest production of N_2 through denitrification (~35% of the global production) out of which the Arabian Sea contributes the largest proportion (~17% of global N_2 production)[5]. The balance between nitrogen fixation and its removal through N_2 production is a key to carbon assimilation by primary production and CO_2 regulation in the atmosphere[3,6]. In the Arabian Sea, most of the studies have examined denitrification variability over the past 100 kyr or younger; the longest record available goes back to 1 Ma in the Western Arabian Sea[7]. Hence, there is a lack of information regarding the long-term evolution of denitrification spanning the past several million years, especially from the Eastern Arabian Sea. Here, we examine samples from Site U1456 in the Eastern Arabian Sea retrieved during the IODP Expedition 355[8] (Fig. 1). To reveal the long-term OMZ variability and its coupling with surface water productivity, we analyzed multiple isotopic and geochemical proxies viz. nitrogen and carbon isotopic ratios ($\delta^{15}N$

and $\delta^{13}C$), total organic carbon and total nitrogen (TOC and TN) concentrations, and carbon to nitrogen (C/N) weight ratio of sedimentary organic matter (SOM).

3.1.1 Study Area

Site U1456 is located at 16°37.28′ N, 68°50.33′ E in the Eastern Arabian Sea (EAS) (Fig. 1), ~475 km away from the Indian coast, and ~820 km from the modern mouth of the Indus River, and within the Laxmi Basin which is flanked by the Laxmi Ridge to the west and the Indian continental shelf to the east. The Laxmi Basin is characterized by a 200–250 km wide depression that runs in a northwest–southeast direction parallel to the west coast of India[8]. The site is situated at a water depth of 3640 m, which lies well above the modern lysocline (~3800 m).

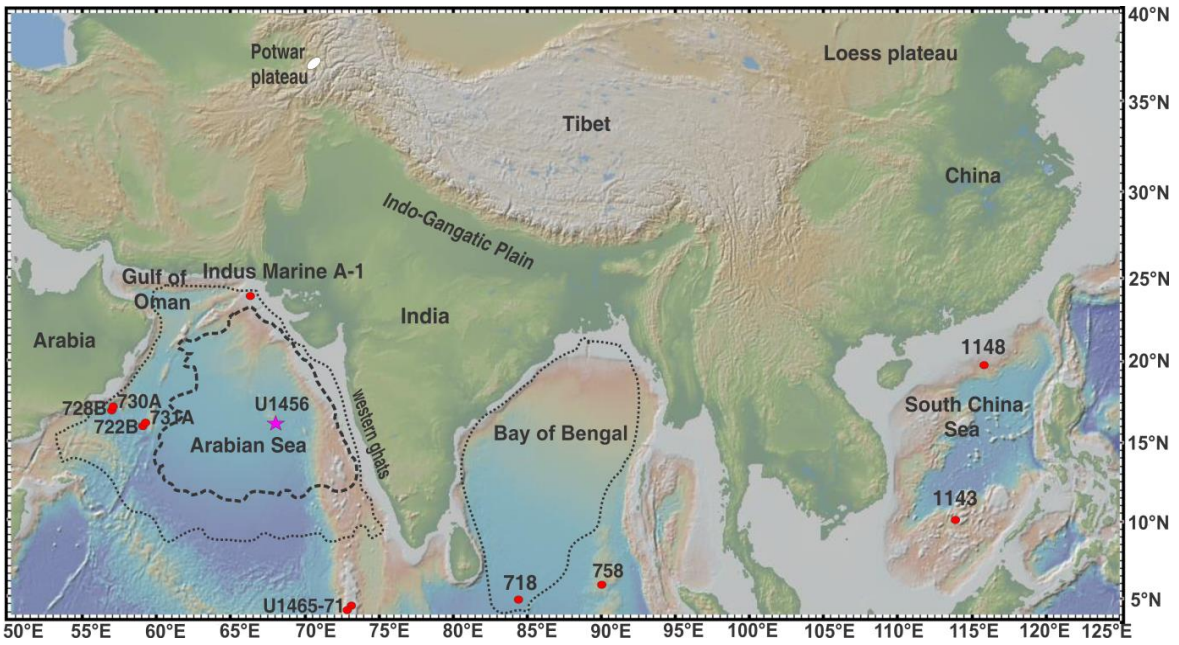

Figure 1. Locations of the IODP Expedition 355 Site U1456 in the Eastern Arabian Sea (3640 m of water depth, 16°37.28′N, 68°50.33′E) denoted by pink star[8]. The red circles represent ODP and IODP sites in the Arabian Sea[7,27,28,29,32] Bay of Bengal[33,34] and South China Sea[38,41] which have been discussed in the present study. The white patch represents Potwar plateau[31]. The thin dotted curves in the Arabian Sea and the Bay of Bengal show

modern anoxia[1] based on WOA 2005 climatology. The thick black dotted curve in the Arabian Sea represents the approximate extent of denitrification zone[42] (Figure created using GeoMapApp3.6.0, www. geomapapp.org).

in the Arabian Sea[8]. Three distinct water masses identified by Rochford[9] in the Arabian Sea are Arabian Sea High Salinity Water (~50 m to 75 m) (ASHSW), Persian Gulf Water (~25 m to 70 m) (PGW), and Red Sea Water (~600 m to 900 m) (RSW)[10]. ASHSW shows greater seasonal variability than PGW and RSW and is considered as the main source of oxygen in the Western Arabian Sea (WAS)[9,11]. Thus, the subsurface denitrification intensity in the WAS is controlled by the surface productivity as well as the supply of oxygen from the water masses[11]. However, in the EAS, the subsurface denitrification is expected to be controlled mainly by the extent of surface productivity[12]. An Argo float-based study in the Arabian Sea revealed the presence of high salinity water with inter-seasonal to inter-annual variability[13]. The vertical mixing of PGW and RSW between ~250 m to ~800 m result in the formation of the Arabian Sea Intermediate Water[14]. The deep water masses of the Indian Ocean comprise

Antarctic Bottom Water (AABW), Circumpolar Deep Water (CDW), and Indian Deep Water (IDW). IDW forms in the Indian Ocean itself by the process of diffusion and upwelling and is characterised by low oxygen content and relatively enriched nutrients because of its aging[15]. The present-day bottom water in the Arabian Sea flows northward and upwells into the layer of North Indian Deep Water (~1500–3500 m)[16].

3.2 Results and Discussion

The drilled section at Site U1456 is divided into four lithologic units based on a variety of sediment properties (Fig. 2a); Unit I (~121 m thick and Pleistocene nannofossil ooze

interbedded with very thin turbidities), Unit II (~240 m thick and late Pliocene to early Pleistocene sand and silt), Unit III (~370 m thick and late Miocene to late Pliocene clay/claystone, sand/sandstone, nannofossil chalk, and nannofossil-rich claystone), and Unit IV (~380 m thick and older than late Miocene claystone, calcarenite, calcilutite, and conglomerate/breccia). These lithologies are characterized by different mineralogical and geochemical properties8. Since the drilled core is very long (1109.4 m) and the site is quite deep (3640 m)[8], the isotopic ratios of the SOM should be evaluated for the diagenetic alterations related to the lithology. Diagenesis of the organic matter begins within the photic zone of the water column, which continues during sinking. It further maintains unceasingly within the bioturbated mixed layer of sediment (a few cm to ~10 cm depth) and only a few percent (1 to 0.01%) of organic matter is finally buried/preserved in the sediment[17]. Although microbial activity has been found even upto several hundred meters deep into the sedimentary sequence[18], diagenesis reduces significantly with increasing depth. Popp *et al.*[19] suggested that despite the loss of organic matter due to remineralization, the $\delta^{13}C$ of OM remains almost unchanged with increasing depth. Similarly, a very small $\delta^{15}N$ offset was found between core top sediments and sinking particles in the equatorial Pacific region; the loss of organic matter due to diagenesis in the upper section of the core top shows no corresponding $\delta^{15}N$ change[11]. Core top studies from the Western Arabian Sea reported no correlation between TN and $\delta^{15}N$, which indicates that diagenesis does not affect $\delta^{15}N$ variation[7]. We also obtain no relationship between TN and $\delta^{15}N$ (r^2 = 0.19; Supplementary Fig. 1). Thus, diagenesis appears to cause no significant alteration in $\delta^{13}C$ and $\delta^{15}N$ values of SOM at Site U1456. The C/N ratio of marine organic matter generally ranges from 8 to 10[20]. Terrestrial organic matter predominantly consists of compounds like cellulose and lignin with much low nitrogen

content. The C/N ratios of land-derived organic matter, therefore, are much high in the range between 20 and 100[20]. The mean $\delta^{13}C$ values

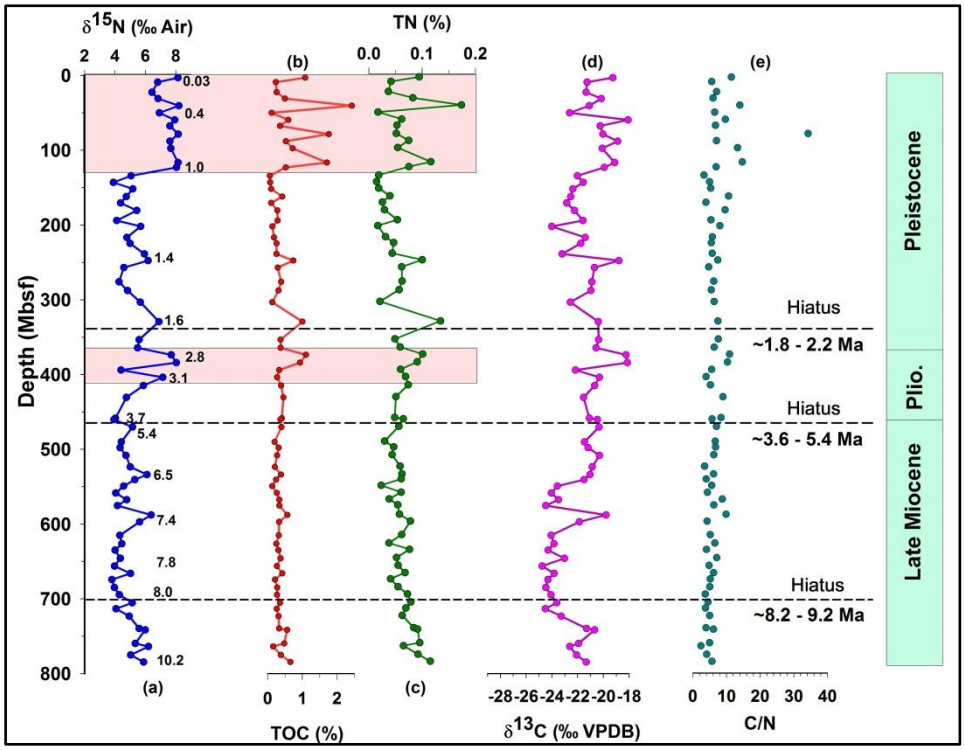

Figure 2. Record of denitrification, surface water productivity, and provenance of the Sedimentary Organic Matter (SOM) in the Eastern Arabian Sea since Late Miocene. **(a)** Lithostratigraphy of site U1456, (**b**) denitrification variability ($\delta^{15}N$ of SOM), (**c,d**) paleoproductivity variability (weight percent total organic carbon [TOC] and total nitrogen [TN] of SOM), (**e,f**) SOM provenance indicators ($\delta^{13}C$ and C/N ratio). The coloured, rectangular boxes show the intensified OMZ coupled with surface water productivity when denitrification occurred in the basin. The horizontal dotted lines indicate the position of the hiatuses. The vertical dashed line over panel '**b**' show denitrification threshold and horizontal brown lines separates different lithological units. The age data (in Ma) at Site U1456, shown by the Indo-Arabic numerals in 'panel **b**', are based on calcareous

nannofossil and planktonic foraminifera biostratigraphy, together with magnetostratigraphy[8].

of the marine organic matter, C4, and C3 plants are about − 21‰, − 13‰, and − 27‰, respectively[21]. The C/N ratio together with $\delta^{13}C$ of SOM has been widely used to determine the origin of organic matter[20]. At Site U1456, the $\delta^{13}C$ values vary from − 18‰ to − 25‰ and most of the C/N ratios range from 6 to 10, indicating that SOM is mostly of marine origin (Fig. 2 e,f and Supplementary Fig. 2). Based on surface sediment analysis of more than 100 locations in the Central and Eastern Arabian Sea (most of them are located in the Eastern Arabian Sea), the $\delta^{15}N$ values of SOM have been found to vary from 6‰ to 11‰ [22]. In most of the oxygenated basins, the $\delta^{15}N$ values do not exceed 6‰ while those from the oxygen deficient basins are highly enriched with mostly higher than 6‰[7, 22, 23, 24]. Thus, the periods with $\delta^{15}N$ values higher than 6‰ may signify denitrification associated with strong OMZ. At Site U1456, the $\delta^{15}N$ values of SOM vary between 2.4‰ to 8.2‰ (Fig. 2b). The maximum TOC and TN values are 2.42% and 0.17%, respectively (Fig. 2c, d). The Mid-to Late Pliocene (~3.2 to 2.7 Ma) is characterized by high $\delta^{15}N$ values (> 6‰) along with high TOC and TN values, indicating denitrification/strong OMZ (Fig. 2). Another, period of denitrification/OMZ intensification ($\delta^{15}N$ > 6‰) takes place from ~1.0 Ma to the core top (0.03 Ma) (Fig. 2b). During these periods of intense denitrification, the surface water productivity indicators viz. TOC and TN contents also represent an increasing trend (Fig. 2c, d). Intense wind-induced productivity and particle flux occur in the Arabian Sea during the monsoon seasons[25]. Modern climatological chlorophyll *a* data show that the surface water productivity in the Eastern Arabian Sea is driven by both the summer and the winter monsoons[26]. Thus, surface water productivity variability in the Eastern Arabian Sea is a manifestation of the SAM variability, which can be linked to

denitrification/OMZ intensification. The origin and evolution of the SAM are still a topic of debate. According to the previous hypothesis based on a study from the Western Arabian Sea (Ocean Drilling Program (ODP) Site 722), the initiation/intensification of the SAM occurred at around 8.5 Ma and continued until 6 Ma[27] (Fig. 3g). Another study from the same ODP Site 722 shows that the onset of the SAM took place at ~12.9 Ma and a major intensification occurred at ~7 Ma[28]. In contrast, a decrease in *G. bulloides* abundance was found at 8.5 Ma (Fig. 3f) from the ODP Site 722 implying reducing SAM[29]. A recent study from the inner seas of the Maldives (IODP sites U1465-71) postulates a proto-monsoon from 25–12.9 Ma and an abrupt increase in the monsoon at ~12.9 Ma[30] (Fig. 3d). The $\delta^{13}C$ values of paleosols from the Siwalik Group sediments in the northern Pakistan spanning the past 18 Myr showed a marked shift from C-3 to C-4 dominated plants at ~7.4 Ma, which may be associated with SAM inception and again the flood plains were mostly occupied by C-4 grassland in Plio-Pleistocene[31] indicating monsoon intensification (Fig.3h). Recent records of Himalayan weathering represented by the chemical index of alteration (CIA) and K/Al ratios (Fig. 3c) demonstrated that SAM attained the maximum strength at 15 Ma, remained high until 10.5 Ma, gradually weakened until ~3.5 Ma, and again increased from the Late Pliocene to Pleistocene[32].

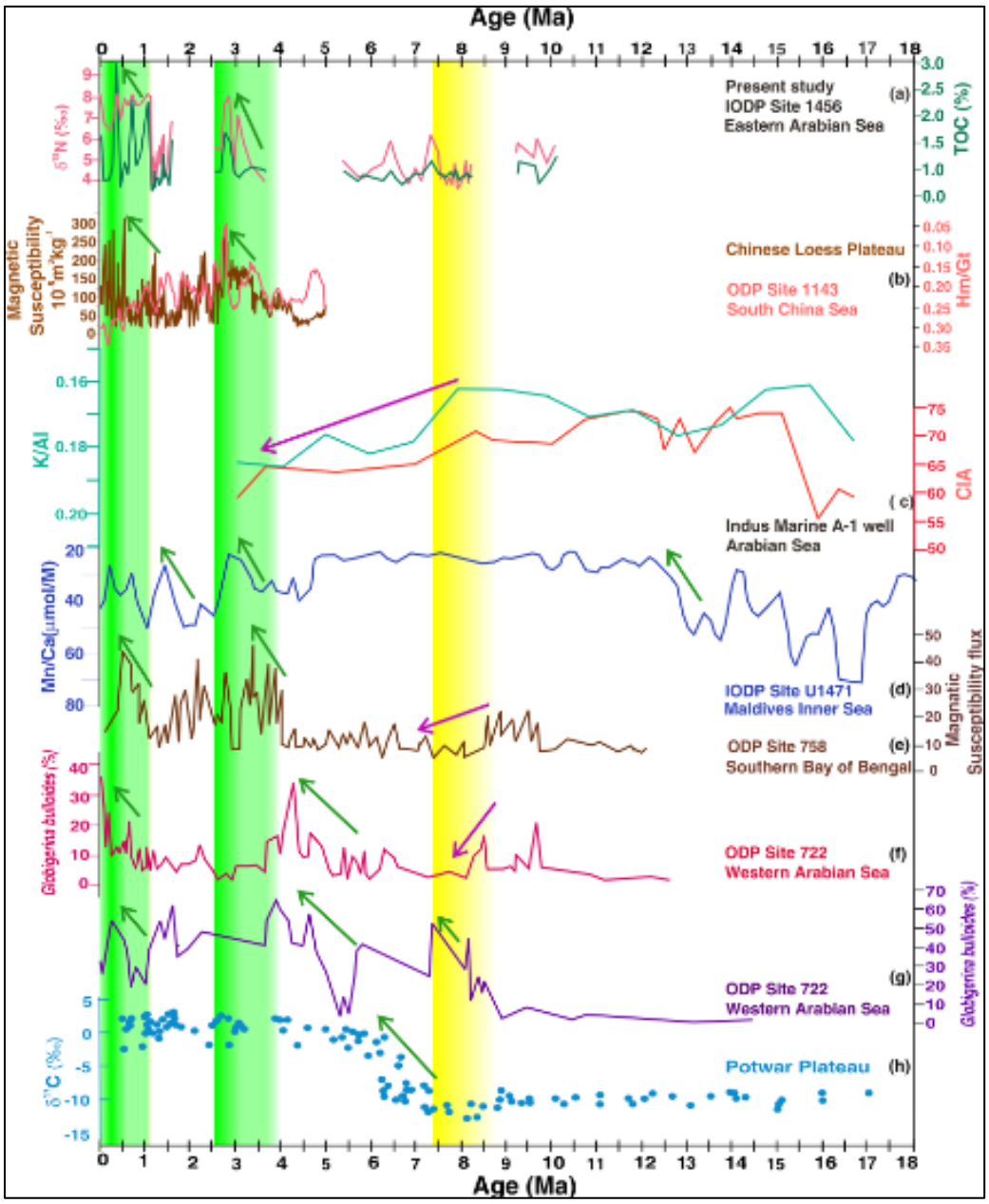

Figure 3. Comparative records of the South Asian Monsoon and East Asian Monsoon since Mid-Miocene. (**a**) $\delta^{15}N$ and total organic carbon (TOC) from IODP site U1456, (**b**) Magnetic susceptibility record[37] of Chinese loess plateau and Hm/Gt (40 point moving average) from the South China Sea ODP site 1143[38], (**c**) Chemical Index of Weathering (CIA) from the Indus river fan[32], (**d**) Mn/Ca record from the Maldives inner Sea[30] (**e**) Magnetic susceptibility record of the southern Bay of Bengal ODP site 758[34], (**f**) *G. bulloides* abundance from ODP site 722[29], (**g**) *G. bulloides* abundance from ODP site

722[27], and (**h**) $\delta^{13}C$ of calcretes from the Potwar Plateau[31]. The green arrows represent the strengthening of monsoon and the purple indicate the weakening of monsoon. The yellow band marks the arid period when many of the studies including the present study show the weakened monsoon while the green bands indicate the periods of strengthened monsoon.

The Sr isotope and clay mineral data also suggested weaker SAM after 8 Ma[33]. Our record from Site U1456 spans ~10.2 to 0.03 Ma, but includes several hiatuses dated to ~8.2–9.2 Ma, ~3.7–5.4 Ma, and ~1.6–2.2 Ma[8]. Nevertheless, we interpret that surface water productivity in the Eastern Arabian Sea was low from 10.15 Ma to 3.2 Ma as evident from uniformly low values of TOC and TN (3a and 2b). Additionally, during this period, the $\delta^{15}N$ did not reach the threshold value (~6‰) indicative of denitrification (Fig. 3a). This implies that neither the surface water productivity (TOC, TN) nor the OMZ intensity supports any major intensification in SAM strength from ~10 to ~3.2 Ma, which is also documented in the different regions (the South China Sea, the Northern Arabian Sea and the Bay of Bengal) [32, 34]. These studies[32, 34] reported that SAM and EAM were reduced more or less in parallel albeit with a time-lag; the EAM started declining at ~10 Ma while the SAM began decreasing at ~8 Ma. But, we find that the SAM was weak at ~10 Ma indicating that EAM and SAM varied in consonance, without any apparent time lag, on tectonic timescale. This Late Miocene reduction in monsoon strength could be a result of global cooling after the Middle Miocene Climatic Optimum[35]. At around 8 Ma, $\delta^{15}N$ values vary between 3.7‰ to 5.8‰, i.e., the OMZ was not intense enough to cause denitrification and the surface water productivity was diminished (Figs 2 and 3a), which implies that SAM did not intensify at ~8 Ma. During the study period, for the first time, the OMZ intensified to the level that denitrification takes place was at ~3.2–2.8 Ma (Fig. 2b). During this period, the surface water productivity (Fig. 2c,d) was also enhanced, indicating

stronger SAM, which coincides with MPWP[36]. Earlier studies, based on magnetic susceptibility (Chinese Loess Plateau, Fig. 3b; southern Bay of Bengal, Fig. 3e) and hematite to goethite ratio (Hm/Gt, South China Sea, Fig. 3b), also reported the enhanced SAM and EAM during ~3.6–2.6 Ma[34,37,38]. A new magnetostratigraphy study from Chinese Loess Plateau spanning from ~8.2 Ma to 2.6 Ma documented long-term East Asian Summer Monsoon (EASM) intensification. Both proxy, as well as numerical climate model assessment, show that the Antarctic glaciation was an important driver for the long-term trend of late Miocene-Pliocene EASM intensification[39]. To examine the responsible mechanisms, a modeling experiment, using the NCAR climate model CCM3, with idealized Himalayan-Tibetan Plateau elevations explains the observed increase of the EAM as a result that the Himalayan-Tibetan Plateau attained modern extension along its eastern and northern margins[34]. It was speculated that it might not have affected the SAM circulation pattern[34]. The present study, based on the multi-proxy records, suggests that the SAM was also enhanced in parallel with the EAM and therefore the intensification can be ascribed to the same mechanism. A recent review [40] investigated the role of the Tibet Plateau in affecting SAM, and found that it simply acts as a physical barrier for northerly cool, dry winds. Its role as an elevated heat source is of secondary importance in affecting the SAM. EAM dynamics is also affected by the Tibet Plateau, which is located in the path of subtropical jet streams[40]. The increase in both the EAM and SAM during ~3.6–2.6 Ma could have resulted in the increased weathering and organic carbon burial, as evident by higher TOC (Fig. 2c), leading to atmospheric CO_2 drawdown that would have possibly contributed to Northern Hemisphere Glaciation (NHG) at 2.7 Ma[40]. Thereafter, from 2.8 Ma to ~1.0 Ma, $\delta^{15}N$ values as well as the surface water productivity declined in parallel, indicating relatively weaker SAM. Previous studies also reported the weakened EAM and SAM after ~2.6 Ma[34, 36, 37], confirming our results, which coincide with the onset of NHG.

Finally, the OMZ reached its modern strength, i.e., denitrification became a permanent feature, at about ~1.0 Ma closely following the enhanced surface water productivity. It implies that SAM intensified from ~1.0 Ma as reported in earlier studies viz. the enhanced sedimentation rate in the Indus Fan[32], the increased chemical weathering from the Bengal Fan[33] and the South China Sea[41], the rise of magnetic susceptibility (Fig. 3b) and mean sediment flux from the Indian Ocean[38].

3.3 Methods

The samples used in the present study were obtained on board the JOIDES Resolution. 5–15 cm long whole-round core sections at the interval of every core or every alternate core were squeezed using titanium steel squeezing device to obtain the interstitial water. The remaining sediments are named 'squeeze cake'. The samples were dried to remove the moisture at 45 °C before processing. Around 10 to 20 g of sediment aliquots were taken for further analysis. Dried samples were finely grounded for homogenization. Homogeneous samples were divided into two batches for geochemical and isotopic analyses - (i) 2N HCl treatment for total organic carbon (TOC) and $\delta^{13}C$ measurement and (ii) untreated for determination of total nitrogen (TN) content and $\delta^{15}N$ values. 20 ml of 2N HCl solution was added to 5–10 g of fine sediment powder. The mixture was shaken mechanically and allowed to stand for ~12 hours. The sample was then washed with ultrapure demineralized water and approximately 25 mg of treated sample was used for TOC and $\delta^{13}C$ analysis. For TN and $\delta^{15}N$ measurement, approximately 40 mg of bulk ground sediment was used. The $\delta^{15}N$ and $\delta^{13}C$ values were determined using isotope ratio mass spectrometer coupled with an element analyzer at Marine Stable Isotope Lab, National Centre for Antarctic and Ocean Research, Goa, India and Department of Oceanography, Pusan National University, Busan, Korea. The standard used was ammonium sulfate (IAEA-N-1) and cellulose (IAEA-CH-3).

The analytical precision for $\delta^{15}N$ and $\delta^{13}C$ is ± 0.12‰ and ± 0.06‰, respectively. Similarly, TN and TOC were determined using sulfanilamide as the standard. The analytical precision for TN and TOC is ± 0.63% and ± 0.84%, respectively.

References

1. Paulmier, A. & Ruiz-Pino, D. Oxygen minimum zones (OMZs) in the modern ocean. Prog. Oceanogr. 80, 113–128 (2009).
2. Stramma, L. et al. Ocean oxygen minima expansions and their biological impacts. Deep-Sea Res. I 57, 587–595 (2010).
3. Bange, H. W. et al. Nitrous oxide emissions from the Arabian Sea: A synthesis. Atmos. Chem. Phys. 1, 61–71 (2001).
4. Naqvi, S. W. A. et al. Marine hypoxia/anoxia as a source of CH4 and N2O. Biogeosciences 7, 2159–2190 (2010).
5. Ward, B. B. et al. Denitrification as the dominant nitrogen loss process in the Arabian Sea. Nature 461, 78–81 (2009).
6. Altabet, M. A., Higginson, M. J. & Murrey, D. W. The effect of millennial-scale changes in Arabian Sea denitrification on Atmospheric CO2. Nature 415, 159–162 (2002).
7. Altabet, M. A., Murray, D. W. & Prell, W. L. Climatically linked oscillations in Arabian Sea denitrification over the past 1 m.y.: Implications for the marine N cycle. Paleoceanography 14, 732–743 (1999).
8. Pandey, D. K., Clift, P. D., Kulhanek, D. K. & The Expedition 355 Scientists. Site 1456. In The Proceedings of the International Ocean Discovery Program 355, 1–61, doi: 10.14379/iodp.proc.355.103.2016 (2016).
9. Rochford, D. J. Salinity maximum in the upper 100 meters of the north Indian Ocean. Aust. J. Mar. Freshwater. Res. 15, 1–24 (1964).
10. Prasanna, K. S. & Prasad, T. G. Formation and spreading of Arabian Sea high-salinity water mass. Journal of Geophysical Research. 104, 1455–1464 (1999).

11. Altabet, M. A., Francois, R., Murray, D. W. & Prell, W. L. Climate related variations in denitrification in the Arabian Sea from sediment 15N/14N ratios. Nature. 373, 506–509 (1995).
12. Agnihotri, R., Bhattacharya, S. K. & Sarin, M. M. Changes in surface productivity, sub-surface denitrification and SW monsoon during the Holocene: A multi proxy record from the eastern Arabian Sea. The Holocene 13(5), 701–713 (2003).
13. Chowdary, J. S., Gnanaseelan, C., Thompson, B. & Salvekar, P. S. Water mass property and transports in the Arabian Sea form Argo Observations. Journal of Atmospheric & Ocean Science 10, 235–260 (2007).
14. Premchand, K., Sastry, J. S. & Murty, C. S. Water mass structure in the Western Indian Ocean- Part 2: The spreading and transformation of the Persian Gulf Water. Mausam 37, 179–186 (1986).
15. Tally, L. D., Pickard, G. L., Emery, W. J. & Swift, J. H. Descriptive physical oceanography: An Introduction. Elsevier, China, 387–399 (2012).
16. Shetye, S. R., Gouveia, A. D. & Shenoi, S. S. C. Circulation and water masses of the Arabian Sea. Proc. Indian Acad. Sci. 103, 107–123 (1994).
17. Rullkötter. J. Organic matter: driving force for early diagenesis. In (ed. Schulz, H. D., Zabel, M.) Marine geochemistry, Springer, Berlin, 125–206 (2006).
18. Parkes, J. R. et al. Deep bacterial biosphere in Pacific Ocean sediments. Nature 371, 410–413 (1994).
19. Popp, B. N., Parekh, P., Tilbrook, B., Bidigare, R. R. & Laws, E. A. Organic carbon variation in sedimentary rocks as chemostratigraphic and paleoenvironmetal tools. Palaeogeogr.Palaeoclimat. Palaeoecol. 132, 119–132 (1997).
20. Meyers, P. A. Preservation of elemental and isotopic source identification of sedimentary organic matter. Chem Geol. 114, 289–302 (1994).

21. Farquhar, G. D., Ehleringer, J. R. & Hubick, K. T. Carbon isotope discrimination and photosynthesis. Ann. Rev. Plant Physiol. Plant Molecul. Biol. 40, 503–537 (1989).
22. Gaye-Haake, B. et al. Stable nitrogen isotopic ratios of sinking particles and sediments from the northern Indian Ocean. Mar. Chem. 96, 243–255 (2005).
23. Ganeshram, R. S., Pedersen, T. F., Calvert, S. E. & Murray, J. W. Large changes in oceanic nutrient inventories from glacial to interglacial periods. Nature 376, 755–758 (1995).
24. Liu, K. & Kaplan, I. R. The eastern tropical Pacific as a source of ^{15}N-enriched nitrate in seawater off southern California. Limnol. Oceanogr. 34, 820–830 (1989).
25. Nair, R. R. et al. Increased particle flux to the deep ocean related to monsoon. Nature 338, 749–751 (1989).
26. Cabarcos, E., Flores, J. A., Singh, A. D. & Sierro, F. J. Monsoonal dynamics and evolution of the primary productivity in the eastern Arabian Sea over the past 30 ka. Palaeogeogr. Palaeoclimat. Palaeoecol. 411, 249–256 (2014).
27. Kroon, D., Steens, T. N. F. & Troelstra, S. R. Onset of monsoonal related upwelling in the western Arabian Sea. In: Prell, W. L. et al. (eds) Proceedings of the ODP Sci. Results. 117, 257–264 (1991).
28. Gupta, A. K., Yuvaraja, A., Prakasam, M., Clemens, S. C. & Velu, A. Evolution of the South Asian monsoon wind system since the late Middle Miocene. Palaeogeogr. Palaeoclimat. Palaeoecol. 438, 160–167 (2015).
29. Huang, Y., Clemens, S. C., Liu, W., Wang, Y. & Prell, W. L. Large-scale hydrological change drove the late Miocene C4 plant expansion in the Himalayan foreland and Arabian Peninsula. Geology 35, 531–534 (2007).
30. Betzler, C. et al. The abrupt onset of the modern South Asian Monsoon winds. Sci. Rep. 6, 29838 (2016).

31. Quade, J., Cerling, T. E. & Bowman, J. R. Development of Asian monsoon revealed by marked ecological shift during the latest Miocene in northern Pakistan. Nature 342, 163–165 (1989).
32. Clift, P. D. et al. Correlation of Himalayan exhumation rates and Asian monsoon intensity. Nature geoscience 1, 875–880 (2008).
33. Derry, L. A. & France-Lanord, C. Neogene Himalayan weathering history and river 87Sr/86Sr: impact on the marine Sr record. Earth Planet. Sci.Lett. 142, 59–74 (1996).
34. An, Z., Kutzbach, J. E., Prell, W. L. & Porter, S. C. Evolution of Asian monsoons and phased uplift of the Himalaya-Tibetan plateau since Late Miocene times. Nature 411, 62–66 (2001).
35. Zachos, J., Pagani, M., Salon, L., Thomas, E. & Billups, K. Trends, rhythms and aberrations in global climate 65 Ma to Present. Science 292, 686–693 (2001).
36. Haywood, A. M., Dowsett, H. J. & Dolan, A. M. Integrating geological archives and climate models for the mid-Pliocene warm period. Nature communications 7, 1–14, doi: 10.1038/ncomms10646 (2016).
37. Sun, Y., Lu, H. & An, Z. Grain size of loess, palaeosol and Red Clay deposits on the Chinese Loess Plateau: Significance for understanding pedogenic alteration and palaeomonsoon evolution. Palaeogeogr. Palaeoclimat. Palaeoecol. 241, 129–138 (2006).
38. Zhang, Y. G., Ji, J., Balsam, W., Liu, L. & Chen, J. Mid-Pliocene Asian monsoon intensification and the onset of Northern Hemisphere glaciation. Geology 37, 599–602 (2009).
39. Ao, H., Roberts, A. P., Dekkers, M. J., Liu, X., Rohling, E. J., Shi, Z., An, Z. & Zhao, X. Late Miocene–Pliocene Asian monsoon intensification linked to Antarctic ice-sheet growth. Earth Planet. Sci. Lett. 444, 75–87 (2016).

40. Molnar, P., Boos, W. R. & Battisti, D. S. Orographic Controls on Climate and Paleoclimate of Asia: Thermal and Mechanical Roles for the Tibetan Plateau. Annu. Rev.Earth Planet. Sci. 38, 77–102 (2010).
41. Wang, P. et al. Site 1148. Proc. Ocean Drill. Prog. Init. Rep. 184, 121 (2000).
42. Naqvi, S. W. A. Geographical extent of denitrification in the Arabian Sea in relation to some physical processes. Oceanol. Acta 14, 281–290 (1991).

Acknowledgements

This research used samples and data provided by IODP, collected onboard the vessel *JOIDES Resolution* (IODP Expedition 355-Arabian Sea Monsoon). M.T. and S.T. thank the Secretary, Ministry of Earth Sciences (MoES), Govt. of India and Director, National Centre for Antarctic and Ocean Research (NCAOR) for support and encouragement (NCAOR Contribution no. 03/2017). B.K.K. and J.L. appreciate the National Research Foundation of Korea grant (2016R1A2B4008256) and K-IODP program by the Korea government. This research has also been supported by the Research Council of Norway (RCN) and MoES, Govt. of India through the Ind-Nor programme (grant No. 248793 and MoES/Ind-Nor/PS-8/2015). We also thank the anonymous reviewers and the editor for constructive comments that helped to improve the manuscript.

Author Contributions

M.T. and B.K.K. designed the research and collected the samples onboard *JOIDES Resolution* aided by IODP Expedition 355 Scientists; S.T. and J.L. did the sample

processing and analysis; S.T. and M.T. supported by B.K.K and J.L. wrote the manuscript, which was edited by all the IODP Expedition 355 Scientists.

Additional Information

Supplementary information accompanies this paper at http://www.nature.com/srep

Consortia

IODP Expedition 355 Scientists:

Dhananjai K. Pandey[1], Peter D. Clift[3], Denise K. Kulhanek[4], Sergio Andò[5], James A.P. Bendle[6], Sophia Aharonovich[7], Elizabeth M. Griffith[8], Gundiga P. Gurumurthy[9], Annette Hahn[10], Masao Iwai[11], Anil Kumar[12], A. Ganesh Kumar[13], Hannah M. Liddy[14], Huayu Lu[15], Mitchell W. Lyle[16], Ravi Mishra[1], Tallavajhala Radhakrishna[17], Claire M. Routledge[18], Rajeev Saraswat[19], Rakesh Saxena[20], Giancarlo Scardia[21], Girish K. Sharma[22], Arun D. Singh[23], Stephan Steinke[24], Kenta Suzuki[25], Lisa Tauxe[26], Zhaokai Xu[27], Zhaojie Yu[28].

3. Department of Geology and Geophysics, Louisiana State University, E 253 Howe-Russell-Kniffen, Geoscience Complex, Baton Rouge, LA 70803, USA.
4. International Ocean Discovery Program, Texas A&M University, 1000 Discovery Drive College Station TX 77845, USA.
5. Department of Earth and Environmental Sciences, University of Milano Bicocca, Piazza della Scienza 4, 20126 Milan, Italy.
6. School of Geography, Earth and Environmental Sciences, University of Birmingham, Edgbaston, Birmingham B152TT United Kingdom.

7. Department of Earth and Planetary Sciences, Faculty of Science and Engineering, Macquarie University Level 2, The Australian Hearing Hub, 16 University Avenue, Sydney NSW 2109, Australia.
8. Department of Earth and Environmental Sciences, University of Texas at Arlington, Geosciences Building, Room 107, 500 Yates Street, Arlington TX 76019 USA.
9. Manipal Centre for Natural Sciences, Manipal University, Dr. T.M.A. Pai Planetarium Building, Manipal 576104, India.
10. MARUM, University of Bremen, Leobener Strasse 28359 Bremen, Germany.
11. Center for Advanced Marine Core Research/Natural Science Cluster, Kochi University, 2-5-1 Akebono-cho, Kochi 780-8520, Japan.
12. Wadia Institute of Himalayan Geology, 33 GMS Road, Dehradun, Uttrakhand 248001, India.
13. Marine Biotechnology Department, National Institute of Ocean Technology, Velachery-Tambaram Main Road Pallikaranai, Chennai 600100, India.
14. Department of Earth Sciences, University of Southern California, 3651 Trousdale Parkway Los Angeles CA 90089, USA.
15. School of Geographical and Oceanographical Sciences, Nanjing University, 163 Xianlin Avenue, Nanjing 210023, China.
16. College of Earth, Ocean and Atmospheric Sciences, Oregon State University, 104 CEOAS Administration Building, Corvallis OR 97331 USA.
17. Geosciences Division, National Centre for Earth Science Studies, Aakkulam, Trivandrum 695031, India.
18. University College London, Gower Street, London WC1E 6BT, United Kingdom.
19. Geological Oceanography Division, National Institute of Oceanography, Dona Paula, Goa 403004, India.

20. ONGC 11 High, Bandra-Sion Link Road, Mumbai 400017, India.
21. Instituto de Geociências e Ciências Exatas, Universidade Estadual Paulista, 1515 Avenida 24-A Rio Claro SP 13506- 900, Brazil.
22. Department of Geology, Kumaun University, Nainital 263002, India.
23. Department of Geology, Banaras Hindu University, Varanasi, Uttar Pradesh 221005, India.
24. Department of Geological Oceanography, College of Ocean and Earth Sciences, Xiamen University, Xiping Building, Xiang'an South Road, Xiang'an District, Xiamen 361102, China.
25. Graduate School of Environmental Science, Hokkaido University, N10W5, Kita-ku Sapporo 060-0810, Japan.
26. Scripps Institution of Oceanography, 9500 Gilman Drive, La Jolla CA 92093-0220, USA.
27. Key Laboratory of Marine Geology and Environment, Institute of Oceanology,Chinese Academy of Sciences 7 Nanhai Road, Qingdao Shandong 266071, China.
28. Laboratoire Geosciences Paris-Sud (GEOPS, UMR8148-CNRS) University de -Paris-sud (Orsay) Batiment 50491405, Orsay Cedex, France.

Chapter 4

Published in current Science
DOI:10.18520/cs/v119/i2/282-290

3. Evolution and dynamics of the denitrification in the Arabian Sea on millennial to million-year timescale

Shubham Tripathi, Padmasini Behera, Manish Tiwari

National Centre for Polar and Ocean Research, Ministry of Earth Science, Vasco da Gama, Goa, India

Abstract

Denitrification - the reduction of nitrate to oxidize organic matter in the absence of oxygen in the OMZs - may provide positive feedback to global warming as it releases N_2O, which is a powerful greenhouse gas and also reduces oceanic nitrate inventory resulting in the reduced drawdown of the CO_2. A perennial OMZ exists in the Arabian Sea where intense denitrification takes place and contribute a large amount of N_2O. Therefore, it is important to understand the evolution and dynamics of the denitrification in the Arabian Sea during different time periods of the earth. We present here denitrification and productivity variability in the Eastern Arabian Sea spanning the last ~600 thousand years (kyr). It is based on ~300 new measurements ($\delta^{15}N$ and total nitrogen concentration) generated from the Site U1457 drilled during the IODP Expedition 355. To further study the factors governing the denitrification on other timescales, we compare existing records of denitrification variability spanning the last several million years and since the last glacial period (~past 70 kyr) from the Northeastern and the Western Arabian Sea. During the last 10 million years (Myr), the first evidence of denitrification in the Arabian Sea was

observed at ~3 Myr ago (Ma) coinciding with the Mid-Pliocene Warm Period. The modern strength of denitrification in the Arabian Sea was established at ~ 1 Ma. On glacial-interglacial timescale, we find stronger denitrification during interglacials and weaker denitrification during glacial periods. During the Holocene, we observe declining denitrification in the Western Arabian Sea in response to the reduced monsoon-induced productivity but find increasing denitrification in the Northeastern Arabian Sea due to reduced ventilation. This diminished ventilation occurred as the sea level rise led to the inflow of oxygen-poor water from the Red Sea and the Persian Gulf that hindered the inflow of oxygen-rich water from the Southern Ocean

4.1 Introduction

The Arabian Sea has one of the strongest perennial oxygen minimum zones (OMZ) of the world oceans where oxygen concentration drops to less than 20 µM (*Paulmier and Ruiz-Pino*, 2009). This perennial OMZ is formed at a water depth of around 150 m to 1200 m due to high oxygen consumption for the respiration of a large amount of organic matter produced in the upwelling dominated Western Arabian Sea (*Qasim* 1982; *Naqvi*, 1987). The organic matter produced in the Western Arabian Sea during the southwest monsoon is advected towards the Eastern Arabian Sea and the central Arabian Sea. Thus, a continuous organic matter supply stabilizes the perennial OMZ in the Eastern Arabian Sea. The development of this OMZ is further supported by poor ventilation by subsurface currents and a strong stratification due to tropical thermocline because of relatively high SST that inhibits the mixing with the oxygen-rich surface water (*Qasim* 1982; *Naqvi*, 1987). As the Arabian Sea is closed by land mass on its northern border so there is an absence of any major oxygen-rich deep to intermediate water inflow from that side as well (*Olson et al*., 1993). Once the oxygen level falls below 1µM (*Bange et al*., 2001), nitrate (NO_3^-) is used

as an oxidizing agent (electron acceptor) for the bacterial respiration (oxidation) of organic matter resulting in denitrification. During denitrification, the nitrate (oxidation state, OS: +5) is reduced to nitrite (NO_2^-; OS: +3), nitric oxide (NO; OS: +2), nitrous oxide (N_2O; OS: +1), and finally to gaseous nitrogen (N_2; OS: 0). Thus,denitrification releases gaseous products like N_2O and N_2 that, to a large extent, are lost to the atmosphere so there is a net loss of fixed nitrogen from the ocean during denitrification (*Codispoti and Richards*, 1976; *Ward et al*., 2009).

Post-industrialization, anthropogenic climate change is projected to enhance sub-oxic conditions in large regions of the world ocean (*Cocco et al*., 2013; *Keeling et al*., 2010) that would result in the expansion of the OMZs. It would increase the production of nitrous oxide, which is a major greenhouse gas.Additionally, denitrification reduces the oceanic nitrate inventory - a limiting nutrient - that would result in a lower drawdown of CO_2 due to reduced productivity and thus provides positive feedback to the global warming (*Altabet et al*., 1995; *Ganeshram* et al., 1995). Considering the importance of denitrification to climate change, it is important to understand the denitrification variability in the Arabian Sea and its controlling mechanisms on various time scales. The turnover time of fixed nitrogen in the ocean is ~3000 years thus the marine nitrogen inventory is altered in several-thousand-years (Altabet et al., 2002). Here, we present a new record of denitrification spanning a period from 600 thousand years before present (kyr BP) to 50 kyr BP from the eastern Arabian Sea using sediment cores recovered during the IODP 355 expedition. This is a unique record spanning such a long period at millennial scale resolution. We also examine the existing records of denitrification to discuss the evolution and denitrification mechanism in the Arabian Sea on millennial to million-year time scales.

4.1.1 Nitrogen Isotopes of Nitrate as a Proxy of Denitrification Intensity in the Arabian Sea

Nitrogen has two stable isotopes namely ^{14}N and ^{15}N with abundances of 99.64% and 0.36%, respectively. The nitrogen isotopes mostly undergo 'Kinetic Fractionation' in the marine nitrogen cycle as most of the reactions are biologically mediated. The isotope fractionation (ε) in this case can, therefore, be expressed as the deviation of the ratio of the 'rate coefficients' *viz*. ^{14}k and ^{15}k of the reaction for the reactants containing lighter (^{14}N) and heavier (^{15}N) isotopes, respectively, from unity. As it is a small number so it is further multiplied by 1000 for ease of comprehension and is expressed in per mil. So, ε (‰) = $(^{14}k/^{15}k - 1)10^3$. The isotope fractionation during the process 'Nitrogen Fixation' - the reduction of N_2 to NH^{+4}, and oxidation to NO_2^-, and NO_3^- and their subsequent assimilation into the organic matter - is less than 2‰ resulting in a slight decrease of the $\delta^{15}N$ values of the particulate nitrogen. Nitrate uptake/utilization also results in small fractionation (ε = ~5‰) and a slight increase in $\delta^{15}N$ values; more the *relative* nutrient (nitrate) utilization, more will be the $\delta^{15}N$ value. The isotope fractionation for benthic denitrification (occurring due to anoxia within the sediments) is negligible (ε = ~0‰) because nitrate is almost 100% consumed in the sediment pore environment. The largest isotopic fractionation takes place during the denitrification process in the water column at the depth of ~200-300 m - the pelagic denitrification (Naqvi et al., 2006a). The isotope fractionation value is around 25‰ resulting in very high $\delta^{15}N_{NO3-}$ that can go up to 15‰ and above (*Brandes et al*., 1998). In the Arabian Sea, previous studies have shown that nitrate utilization does not play an important role in affecting $\delta^{15}N_{NO3-}$ (*Schafer and Ittekkot*, 1993). Nitrogen fixation can be an important process in oligotrophic, stratified waters and in waters overlying denitrifying zones resulting in lower surface $\delta^{15}N_{NO3^-}$ (*Karl et al*., 2002). But, the waters overlying the

Arabian Sea denitrification zone have high δ^{15}Nvalues reflecting the fact that denitrification in the Arabian Sea is the dominant process governing the $\delta^{15}N_{NO3^-}$values. This nitrate enriched in heavier isotope is upwelled to the euphotic zone and is consumed by the organic productivity a fraction of which finally gets preserved in the sediments resulting in relatively higher δ^{15}Nvalues of the sedimentary organic matter (SOM) underlying the denitrification zones.

4.1.2 Oceanic Circulation at Intermediate Depth in the Arabian Sea

There are three distinct water masses present at the intermediate depth (200 - 1000 m) of the Arabian Sea originating from Northwestern (Red Sea Water (RSW), Persian Gulf Water (PGW)) and Southern (Indian Central Water (ICW)) Indian Ocean (*Wyrtki*,1973; *Swallow*, 1984; *You*, 1998). Other water masses like aged Antarctic Intermediate Water (AAIW) and Banda Sea Water (BSW) also enter the Arabian Sea through Southwestern boundary and move towards the Northeastern Arabian Sea via Somali Current (*Sharma et al*., 1978; *You*, 1998). Presently, the AAIW spreads up to 5 ºN in the Indian Ocean and from there it feeds to ICW (*You*, 1998). The inflow of AAIW to the Arabian Sea varies with the mean sea level and the fronts created by other water masses.During Glacial periods, the decrease in sea level reduces the inflow of high saline water (RSW and PGW) to the Arabian Sea. The absence of this very saline water from marginal seas with strongly reduced BSW (low salinity front created along the equator) favors the northward circulation of the oxygen-rich AAIW (shown in Fig. 1a by thick blue arrows). But during interglacial periods, the increase in sea level favours the expansion of a strong frontal system along the equator and the inflow of highly saline marginal water to the Arabian Sea. This causes the reduced inflow of the southern oxygen-rich AAIW into the Arabian Sea (shown by the thin blue arrow in Fig. 1b).

4.2 Materials and Methodology

4.2.1 Site Setting and Core Description

The Site U1457 (17°9.95′N, 67°55.80′E, water depth 3534m) was drilled in the Laxmi Basin located in the eastern part of the Indus Fan during IODP Expedition 355 (Fig. 1). IODP Site U1457 is located ~490 km west of the Indian coast and ~760 km south from the modern mouth of Indus River. In this study, we used the upper ~43 mbsf of sediment core (U1457A) corresponding to the last ~40kyr to ~600 kyr (*Pandey et al*., 2016). The lithology of the studied sections consists of light brown to light green nannofossil ooze including foraminifer-rich nannofossil ooze and nannofossil-rich clay, interbedded with silty clay and silty sand (*Pandey et al*., 2016).

4.2.2 Nitrogen isotope ratio and concentration analysis

Bulk sediment samples were powdered, and 200 mg were used for nitrogen concentration and nitrogen isotope ratio analysis of the sedimentary organic matter. Samples of ~130 mg weighed out into 8-6 mm tinfoil cups and analysed using Elemental Analyser coupled with 'Isoprime Dual Inlet Isotope Ratio Mass Spectrometer' at the Marine Stable Isotope Laboratory (MASTIL) of National Centre of Polar and Ocean Research (NCPOR), Goa, India. The isotopic values are expressed in term of delta (δ) notation, which is the relative difference of isotopic ratios in the sample from an international standard. Thus: $\delta^{15}N = \{(^{15}N/^{14}N)_{sample}/(^{15}N/^{14}N)_{standard}\}-1$; where, $(^{15}N/^{14}N)_{sample}$ and $(^{15}N/^{14}N)_{standard}$ are the ratios of the abundances of the less abundant (heavier, *i.e*., ^{15}N) to more abundant (lighter, *i.e*., ^{14}N) isotope in the sample and standard, respectively. The $\delta^{15}N$ value is multiplied by 10^3 for the ease of readability and comprehension and is therefore expressed in per mil (‰).

The reproducibility of $\delta^{15}N$ measurement is ± 0.12 ‰ (1σ standard deviation) based on the repeat measurement of the IAEA-N1 Ammonium Sulphate standard. The $\delta^{15}N$ values are quoted with respect to Air-N_2. The reproducibility of Total Nitrogen measurement is ±0.70 % (1σ) based on the repeat measurement of the Sulphanilamide standard.

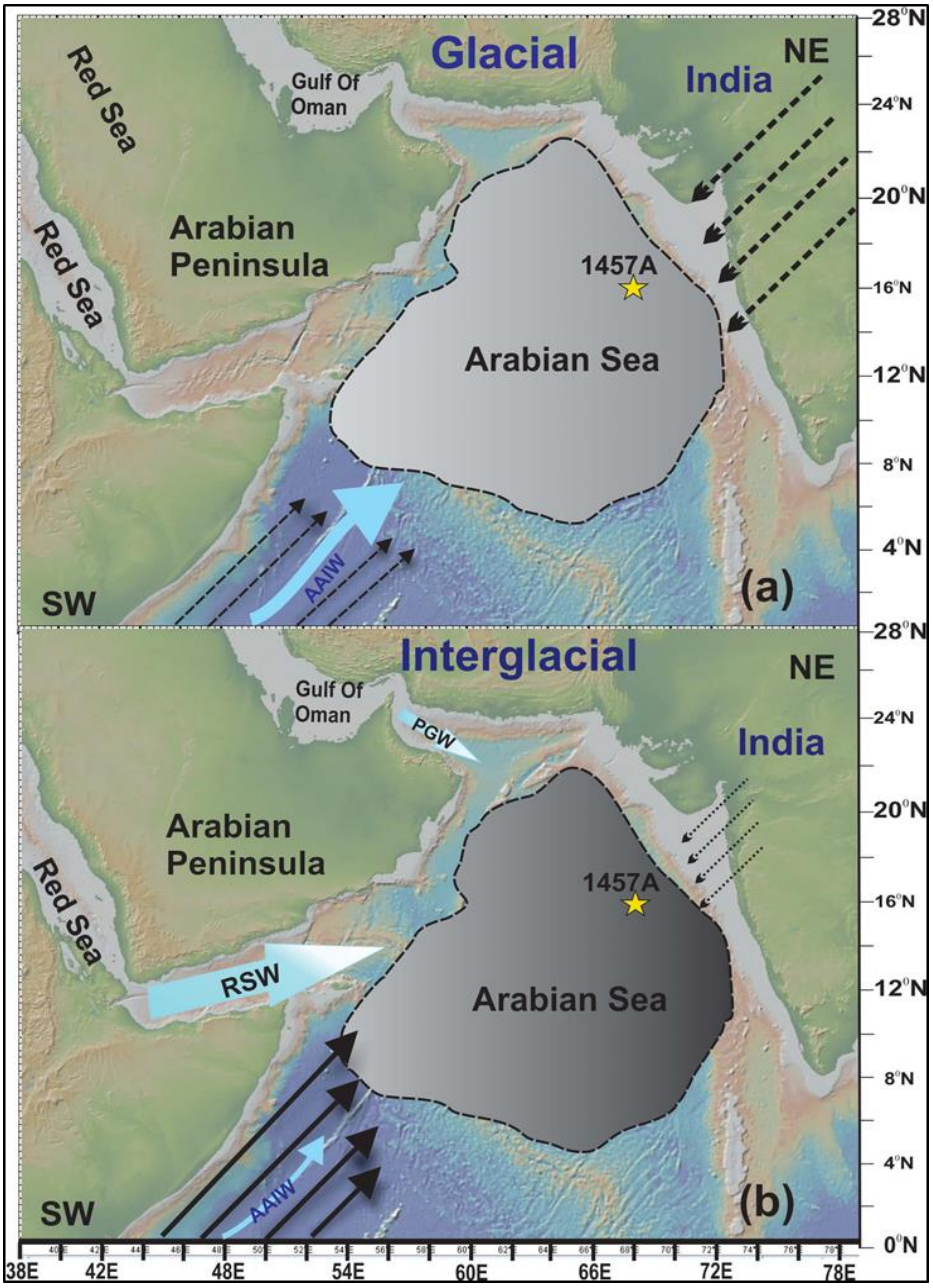

Fig. 1. Location Map and schematic diagram of the Arabian Sea. (a) and (b) shows southwest and northeast monsoon wind (black arrows) and intermediate water flow (blue arrows) during glacial and interglacial periods, respectively. Thicker arrows reflect

stronger winds/circulation. The present study site (U1457) is shown by yellow star. Denitrification gradient during the glacial and interglacial period is shown in grey colour (darker colour indicates stronger denitrification).

4.3 Age-Depth Model

The age model of IODP Site U1457 is based on linear sedimentation rate using the age-depth model generated on-board *JOIDES Resolution*. The on-board age-depth model was based on the first and the last appearance of planktic foraminifera, nannofossils and paleomagnetic reversals (*Pandey et al*., 2016). The age model, the upper 43 mbsf of IODP Site U1457 provides a continuous record of the last ~600 kyr, with an average linear sedimentation rate of approximately ~7.0 cm/kyr.

4.4 Results and Discussion

4.4.1 Denitrification on million-year time scale

Although there is a paucity of data to describe denitrification through geological time scale, we revisited some records from different ocean basins of the world which extend past into deep geological time. *Algeo et al*., (2008) reported $\delta^{15}N$ and C/N ratio from the black shales of Carboniferous period. He argued that the variation in denitrification ($\delta^{15}N$ of SOM) is because of eustatic changes during the glacial and interglacial periods. An increase (decrease) in denitrification is observed during the sea level rise (fall) in interglacials (glacial). A similar pattern in denitrification was observed in Eastern Tropical Pacific Ocean during the Quaternary, reflecting ice ages have produced similar oceanographic effects and nitrogen cycle patterns over past ~300 Ma (*Algeo et al*., 2008). The$\delta^{15}N$data from the anoxic ocean of lower Jurassic carbon-rich shales show a distinct positive $\delta^{15}N$ increase (*Jenkyns et al*., 2001). This was attributed to the upwelling of sub-oxic water mass similar to the Arabian Sea, Californian gulf, and the Peruvian coast. This

development during the early Jurassic is also linked to increased organic productivity (*Jenkyns et al*., 2001). Only one record of sub-oxic conditions in the Arabian Sea since early Miocene (~25 Ma to present) exists from Maldives based on cores collected during the IODP Expedition 359 (*Betzler et al*., 2016). They studied the redox-sensitive element Mn and found that from 25 to ~12.5 Ma, the sub-oxic conditions show a slightly increasing trend. At ~13 Ma, the sub-oxic condition suddenly strengthened showing the expansion of Arabian Sea OMZ to the core site and was stable till 5 Ma. Thereafter, the OMZ exhibits strong variability and finally retraction from the Maldives at around 0.8 Ma (*Betzler et al*., 2016). The only record that reported denitrification (δ^{15}Nof SOM)from the Arabian Sea since late Miocene (~10 Ma) suggests that the surface water productivity and OMZ remain weak from ~10 to ~3.2 Ma based on samples collected during the IODP Expedition 355 (Fig. 2) (*Tripathi et al*., 2017). Prior to that, the δ^{15}Nrecord in the Arabian Sea extended till the last one million years only (*Altabet et al*., 1999).

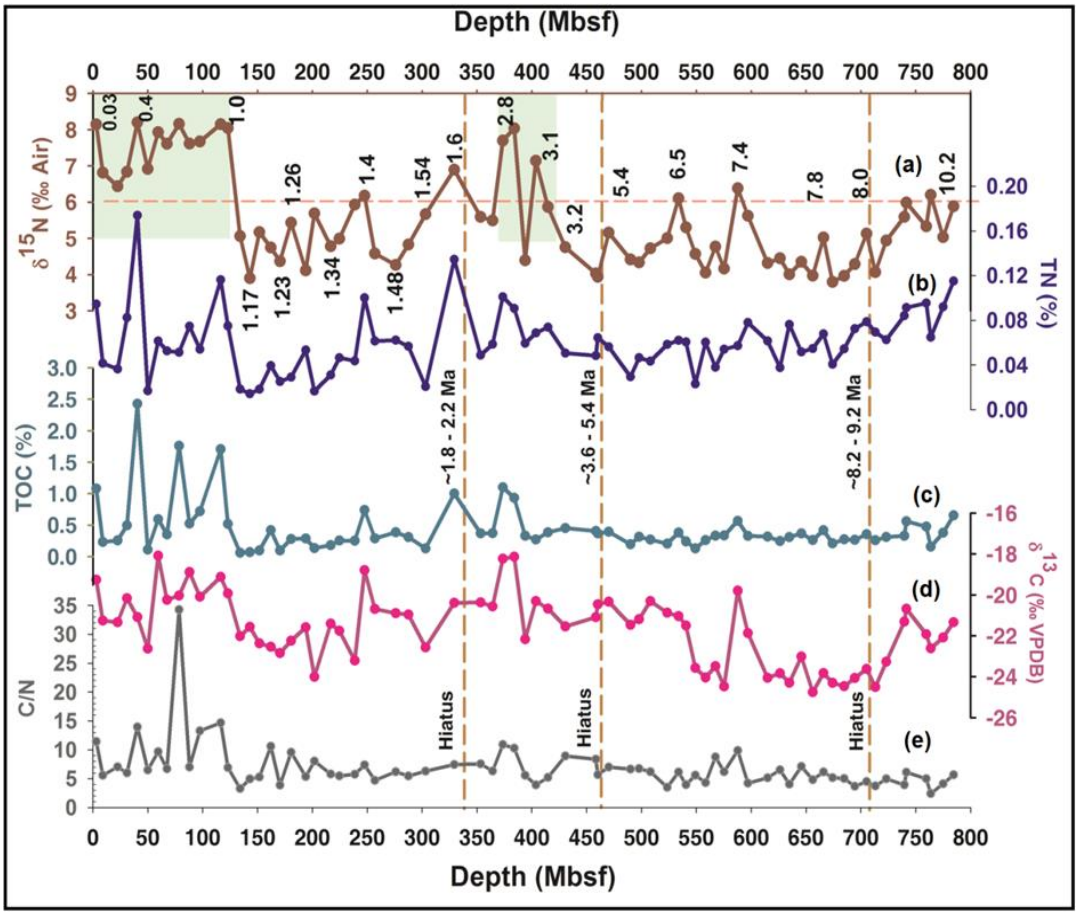

Fig. 2: Denitrification record from the Eastern Arabian Sea since the Late Miocene. (a) denitrification variability ($\delta^{15}N$ of SOM); (b, c) past productivity variability (weight percent of total organic carbon and total nitrogen of SOM); (d, e) Provenance indicators ($\delta^{13}C$ and C/N ratio of SOM). The vertical broken lines indicate the position of the hiatuses. The horizontal dashed line over panel 'a' show denitrification threshold (*Tripathi et al*., 2017). The age data (in million years ago, Ma) at Site U1456 is shown by the Indo-Arabic numerals in 'panel a.

Figure 2 which is based on data from *Tripathi et al*., 2017, shows the relation between denitrification variability and productivity from 10.2 Myr to present in Eastern Arabian Sea (Fig. 2a, b, c). The provenance of organic matter at the core site is determined from the

$\delta^{13}C$ value of SOM and C/N ratio (Fig. 2d, e). These provenance proxies indicate that productivity is mostly of marine origin.*Gaye-Haake et al*., 2005 showed that the $\delta^{15}N$ values of SOM vary from 6‰ to 11‰ in the Arabian Sea, which is based on surface sediment analysis of more than 100 locations in the Central and Eastern Arabian Sea. This is also noted by other studies (*Tripathi et al*., 2017; *Gaye et al*., 2018). Therefore, we consider a $\delta^{15}N$ value of 6 ‰ as an empirical threshold value indicating the presence of denitrification (shown by an orange dashed line in Fig. 2a). The first time the $\delta^{15}N$values are more than 6‰ is during the Mid-Pliocene Warm Period (MPWP; ~3 Ma). It suggests that the first appearance of denitrification occurred during MPWP and was supported by an increase in surface water productivity (Fig. 2b, c). MPWP is a period with similar conditions as today with similar atmospheric CO_2 concentration ~400 ppm (*Pangani et al*., 2010), the mean annual temperature higher by 2.7-4°C (*Haywood et al*., 2013), and the sea level higher by ~20 m than today (*Miller et al*., 2012). The productivity increase during the MPWP could have further contributed the intensification of the northern hemisphere glaciation by causing higher drawdown of CO_2. During 1.5 to 1 Ma, *Tripathi et al*., 2017 found that the denitrification was either absent or very weak in the Arabian Sea. The denitrification again appeared at ~1 Ma as shown in Fig. 2a reflecting the fact that the modern conditions in the Arabian Sea were attained by ~1 Ma.

4.4.2 Denitrification during Marine Isotope Stage (MIS) 15 to MIS 3 (~600 to 40 kyr) on multi-millennial timescale

The drilled section of U1457-A (17ºN, 67ºE; 3534 m water depth) is divided into 4 sections based on the sedimentology and we analyzed sediment samples from the Unit I

(~120 m thick; Pleistocene nannofossil ooze interbedded with thin turbidites). This section spanned from ~600 kyr (MIS 15) to ~40 kyr (MIS 3). We further evaluated the SOM for digenetic alteration related to lithology. If there is any diagenesis then there should be a correlation between TN and $\delta^{15}N$.

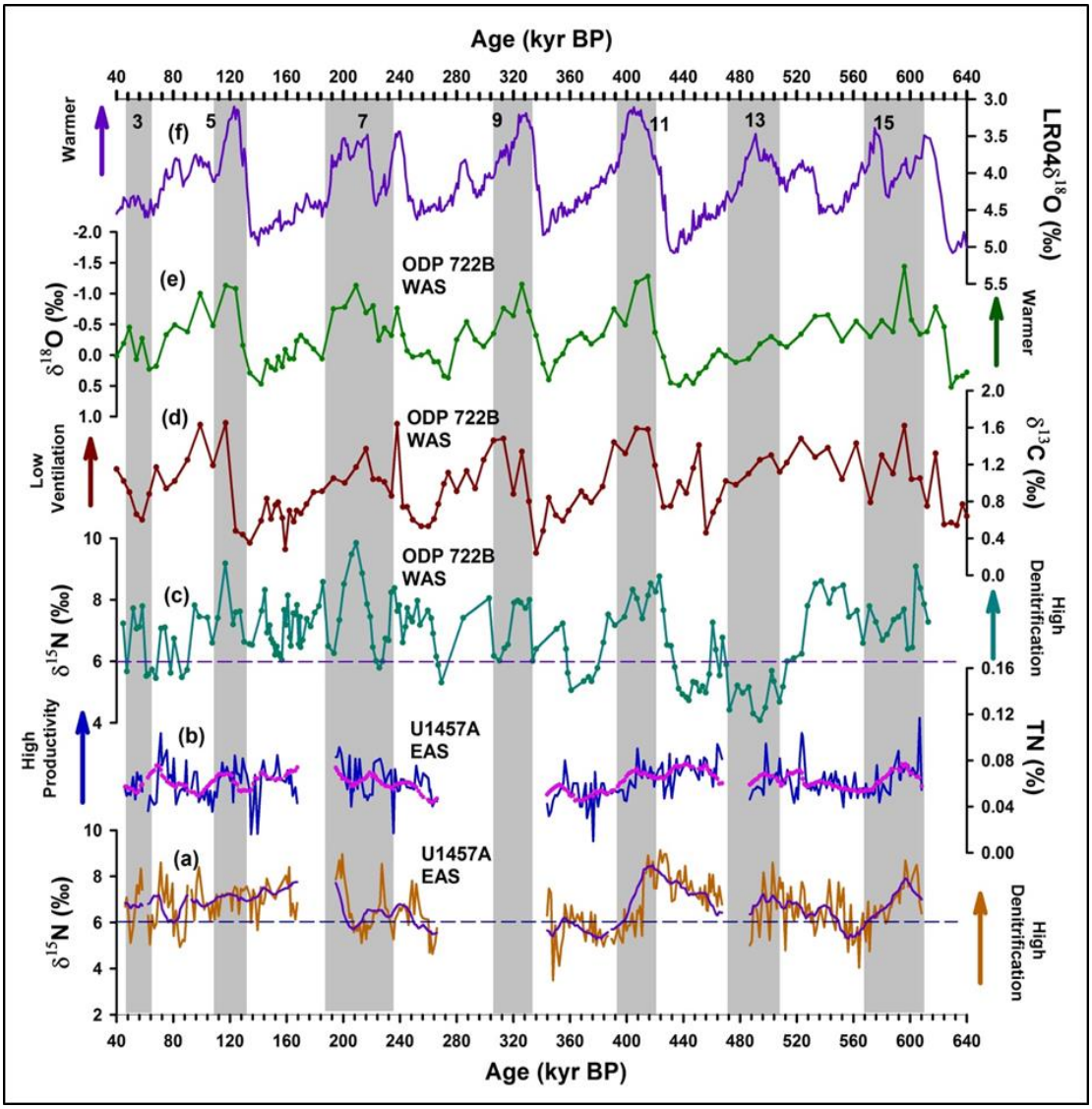

Fig.3. High-resolution denitrification variability from the Eastern Arabian Sea (present study; Site 1457A; panel 'a') and its comparison with denitrification in the Western Arabian Sea (Altabet et al., 1999; Site 722B; panel 'c'). Panel (b) represents TN concentration of core 1457A related to productivity; (d) and (e) represent $\delta^{13}C$ and $\delta^{18}O$ variability from Site 722B related to ventilation and global ice volume, respectively

(*Clemens et al*., 1996); panel (f) shows the LR04 stack (*Lisiecki and Raymo*, 2005) representing the glacial-interglacial cycles (the grey bands show the interglacial periods with corresponding MIS numbers).

Earlier studies from the Western Arabian Sea (*Altabet et al*., 1999) reported no correlation, which indicates that diagenesis does not affect $\delta^{15}N$ variation. We also obtain no relationship between $\delta^{15}N$ and TN (r^2 = 0.19; Supplementary Fig. 1). Thus, diagenesis appears to cause no significant alteration in $\delta^{15}N$ values of SOM at Site U1457.

High-resolution $\delta^{15}N$ measurements from sediment samples of site U1457A show large variability; the $\delta^{15}N$ values range from around 3.4 to 9.1‰ with a mean value of 6.6‰. The marine denitrification causes an increase in $\delta^{15}N$ value which is significantly higher than the global ocean average nitrate value 4.5-6 % as explained above (*Sigman et al*., 1997). Figure 3 shows the comparison of denitrification from both the Eastern (Fig. 3a; present study; Site U1457) and Western Arabian Sea (Fig. 3c; *Altabet et al*., 1999; ODP 722 B) with productivity (Fig. 3b; present study; Site U1457), and ventilation (Fig. 3d; *Clemens et al*., 1996). Productivity is shown by the total nitrogen concentration at the core site (Fig. 3b). The ventilation variability is based on the $\delta^{13}C$ of the benthic foraminifera from the ODP Site 722B from a water depth of ~2000 m (*Clemens et al*., 1996). In the Arabian Sea, there is no record of ventilation of intermediate depths by AAIW (the depth in which denitrification takes place) for the long period spanning the last 600 kyr. Therefore, we have chosen another record from the Site 722B, which although belongs to a deeper depth but represents the strength of the influx of southern water masses into the Arabian Sea. So, it can indirectly indicate the AAIW variability. The $\delta^{13}C$ values of the benthic foraminifera have been used to reconstruct the past ventilation changes related to the age of the water (*Pierre et al*., 1991). The older water mass has more nutrient and

lower $\delta^{13}C$ due to respiration, which releases the lighter isotope (^{12}C) into water. Presently, the North Indian Deep Water (NIDW) occupies the deeper parts of the Arabian Sea (~1500–3500 m). The NIDW is formed by the upwelling of the deep water from below 3500 m (*Shetye et al*., 1994). The deep water is made up of high salinity cores of Antarctic Bottom Water (AABW), Circum Polar Deep Water (CDW), North Atlantic Deep Water (NADW), and Indian Deep Water (IDW) (*Tally et al*., 2012). This deep water contains high nutrient and is aged water (*Tally et al*., 2012) and will, therefore, have lower $\delta^{13}C$. As observed in Fig. 3d, higher (lower) $\delta^{13}C$ values during interglacial (glacial) show weakened (strengthened) ventilation by the southern water masses including AAIW. During MIS 15, the denitrification is strong but declines towards the glacial period (MIS 14) in both the Eastern Arabian Sea (Fig. 3a) and Western Arabian Sea (Fig. 3c). During interglacial periods like MIS 13, 11, and 9 (shown by grey bands, Fig. 3), the denitrification is stronger in both the Western and Eastern Arabian Sea. The denitrification in the Eastern Arabian Sea follows the productivity (Fig. 3b) and ventilation (Fig. 3d) variability within the chronological uncertainty. The increase in denitrification in both Western and Eastern Arabian Sea during interglacials can be explained by the increase in productivity and a low influx of oxygen-rich intermediate water (AAIW) to the core sites. The glacial periods (MIS 14, 12, 10 and 8) show low denitrification (lower $\delta^{15}N$ value) in both Eastern (Fig. 3a) and Western (Fig. 3c) Arabian Sea. The decrease in productivity during the glacial period results in the low denitrification. Further, the enhancement of oxygen-rich water during the colder period reduces the denitrification in both the Eastern and Western Arabian Sea. Earlier studies from the Arabian Sea and the Eastern Pacific, which reconstructed denitrification during Late Quaternary, found stronger denitrification during interglacials and weaker denitrification during glacial periods (*Altabet et al*., 1995, 1999; *Ganeshram et al*., 2000) similar to the present study. From MIS 7 to MIS 3, the

denitrification shows an overall decreasing trend, which is supported by enhanced ventilation by AAIW. The high-frequency variability shown by denitrification matches well with the productivity; denitrification was weak/strong during periods of low/high productivity.

4.5 Denitrification Variability since the Last Glacial Period (~ 70 kyr BP) on millennial timescale

4.5.1 Denitrification during Heinrich Events

Fig. 4 shows the denitrification variability in the northern (Fig. 4d) and the western (Fig. 4e, f) Arabian Sea since the last glacial period along with the productivity (Fig. 4h, g) and ventilation (Fig. 4c) variability. The ventilation variability of the intermediate depth by the AAIW is based on the $\delta^{13}C$ of epibenthic foraminifera *Cibicidoides kullenbergi* (*Jung et al*., 2009). Since the AAIW has higher $\delta^{13}C$ values than other water masses, so high $\delta^{13}C$ reflects more ventilation by AAIW (*Jung et al*., 2009). It is further compared with the GISP2 $\delta^{18}O$ record (*Groot & Stuiver*, 1997) showing past climate (temperature) variability. During colder periods (Heinrich events, H1 to H6 shown by grey bands), the decrease in sea level reduces the influx of marginal sea water (highly saline) to the Arabian Sea and it favours the northward circulation of southern water mass (low saline) (*You*, 1998; *Jung et al*., 2009). Further, the low saline water coming from Indonesian throughflow (Banda Sea water) to the Arabian sea (*Sharma et al*., 1978; *You*, 1998) also acts as a barrier during the warmer period but its influx is lower during colder period (*Pichevin et al*., 2007). Thus, the meridional progression of oxygen-rich Southern water mass to the Arabian Sea is enhanced during the colder period and it ventilates both the thermocline and intermediate depth in the Arabian Sea (shown by higher $\delta^{13}C$values in Fig. 4c; *Jung et al*., 2009). The ventilation

of intermediate depth reduces the OMZ as well as the denitrification during colder periods (lower δ^{15}Nvalues in Fig. 4d, e and f). However, the Southwest monsoon has an immense impact on denitrification and OMZ development. During colder period, the weakened Southwest monsoonal upwelling results in lowered productivity in both Western and Northeastern Arabian Sea (Fig. 4g, h; *Ivanochko et al*., 2005; *Ganeshram et al*., 2000; *Sirocko et al*., 1993; *Singh et al*., 2011), which coincides with the decreased denitrification (grey bands in Fig. 4). It leads to the fact that the low organic matter influx due to lower productivity and the enhanced AAIW reduces the denitrification intensity during Heinrich events in Western, Northern and Northeastern Arabian Sea. During LGM (~23 kyr), the decrease in SW monsoonal upwelling (*Anderson and Prell*., 1993, *Niitsuma et al*., 1991, *Pattan et al*., 2003), reduced productivity coupled to enhanced ventilation by AAIW decreases denitrification intensity in the western region. In the northern Arabian Sea as well, the denitrification intensity is low. This may again be because of low organic matter advection from the western Arabian Sea coupled with higher ventilation. Although a few studies have suggested an increase in productivity during LGM (*Thamban et al*., 2001; *Cabarcos et al*., 2014) in the northern Arabian Sea due to an increase in winter monsoon-induced mixing but the reduced advection of organic matter along with higher ventilation reduces denitrification intensity (*Rostek et al*., 1997; *Schulte et al*., 1999;).

4.5.2 Denitrification during Last Deglacial and Holocene period

The last deglaciation (18 kyr BP to 11kyr BP) covers various colder (H1 and Younger Drays, YD) and warmer (Bølling-Allerød, B-A) periods that experienced varying inflow of AAIW in to the Arabian Sea (Fig. 4c) (*Jung et al., 2009*; *Yu et al*., 2018).

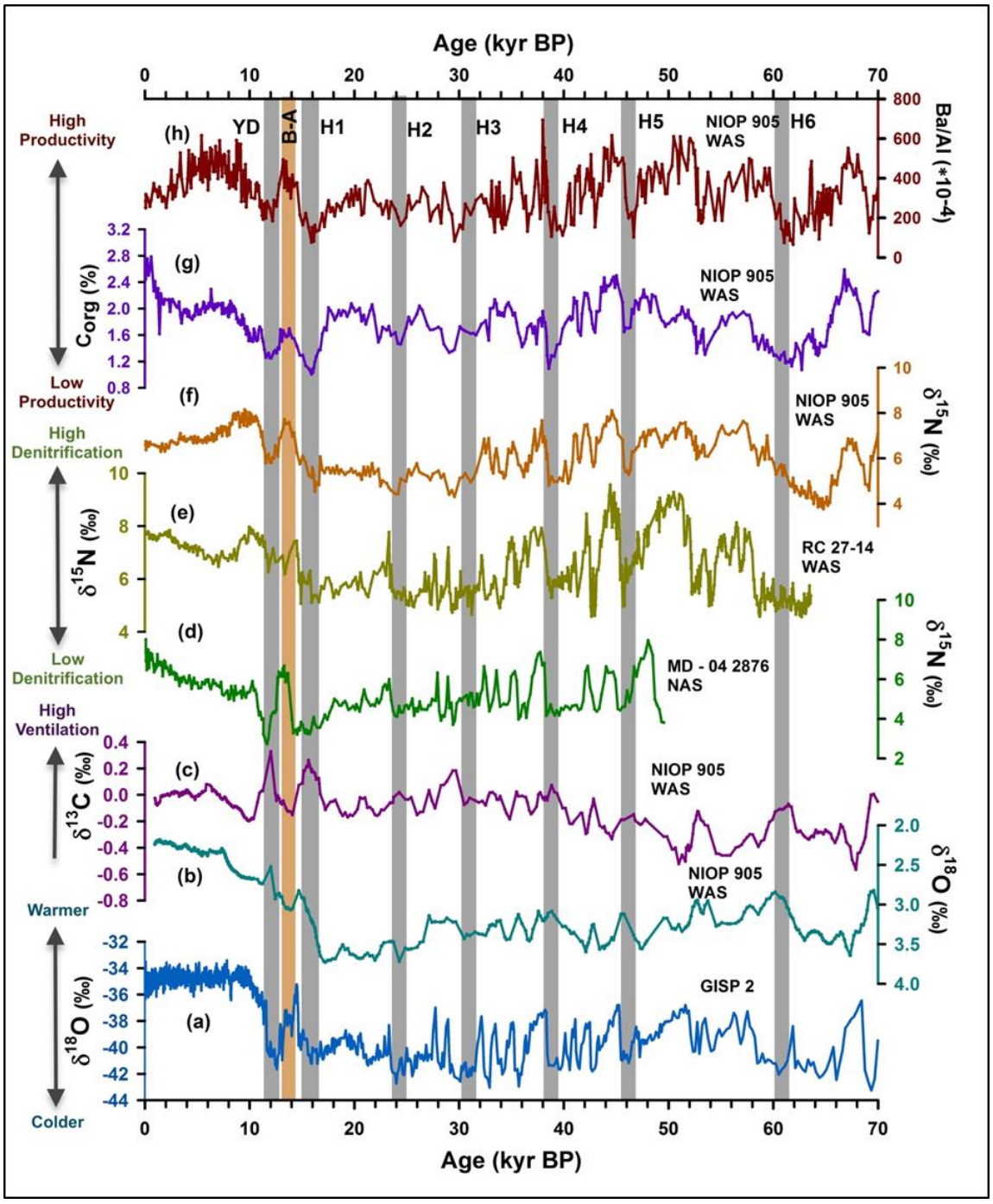

Fig. 4: Comparison among denitrification variability from the Western and Eastern Arabian Sea, Northern Hemisphere temperature, and productivity from the western Arabian Sea. (a) The Greenland ice core $\delta^{18}O$ record GSIP 2 (*Groot and Stuiver*., 1997). (b) $\delta^{18}O$ and (c) $\delta^{13}C$ of benthic foraminifera (*C. kullenbergi*) of core NIOP 905 (*Jung et al., 2009*). (d) $\delta^{15}N$ of core MD- 04 2876 from North Arabian Sea (*Pichevin et al., 2007*)

(e) $\delta^{15}N$ of core RC 27-14 from Oman margin (*Altabet et al*., 2002) (f) $\delta^{15}N$ (g) organic carbon percentage and (h) Ba/Al ratio of core 905P (*Ivanochko et al*., 2005). Grey bands represent colder periods (Henrich events, H1 to H6); dark orange bar indicates the Bølling-Allerød warm period; YD denotes Younger Dryas.

The enhanced/reduced inflow of oxygen-rich water results in decreasing/increasing denitrification during colder/warmer periods of the deglaciation in both the Northern and the Western Arabian Sea (Fig. 4d, e, f). Further, the decrease (increase) in productivity (Fig. 4g, h) in the Western Arabian Sea during the colder (warmer) periods adds to the decrease (increase) of the denitrification intensity (*Suthhof et al*., 2001; *Altabet et al*., 2002).

The South Asian Summer Monsoon (SASM) was intensified in the early Holocene and declined from mid-Holocene (~5 kyr) to present (*Hong et al*., 2003; *Tiwari et al*., 2015; *Nagoji and Tiwari*, 2017). The productivity trend in the Western Arabian Sea follows Southwest monsoon variability and the denitrification declines (Fig. 4f) during reduced monsoon-induced productivity as shown by Ba concentration (Fig. 4h, *Ivanochko et al*., 2005). At the same time, the denitrification intensifies in North and Northeastern Arabian sea during the Holocene period (Fig. 4d, *Pichevin et al*., 2007). This increase in denitrification is explained through intermediate water ventilation. The rise in sea level during the warmer period leads to increased inflow of oxygen-poor water from the Red Sea (RSW) and Persian Gulf (PGW) (*Peichvin et al*., 2007). The front created by this water acts as a barrier to the oxygen-rich Southern water mass inflow to the Northern Arabian Sea. Thus, the denitrification in the Northern and Northeastern Arabian Sea is heavily influenced by the ventilation of the intermediate water. But in the Western Arabian Sea, the denitrification is mostly governed by the huge Southwest monsoon-induced

productivity variability leading to the divergent trends in the denitrification in the western and northern Arabian Sea during Holocene.

4.6 Conclusion

The denitrification variability in the Arabian Sea is an interplay of monsoon-induced productivity and the ventilation by oxygen-rich southern water masses. The oldest record of $\delta^{15}N$ variability indicating denitrification intensity from the Arabian Sea spans the last 10 Myrs. It shows that the denitrification first appeared at ~3 Ma, declined thereafter and attained modern strength by ~1 Ma. During the Late Quaternary (last 600 kyrs), the new data based on IODP Expedition 355 shows that the denitrification intensified during interglacials and weakened during the glacial periods. The comparison of denitrification variability from the Eastern and Western Arabian Sea since the last glacial period (past ~70 kyr) for which chronologically well-constrained records are available shows similar variability i.e., stronger (weaker) denitrification during warmer (colder) periods. During the Holocene, the sea level rise led to the influx of Red Sea Water and the Persian Gulf Water (poor in oxygen) that hindered the inflow of oxygen-rich water from the Southern Ocean resulting in reduced ventilation of the Northeastern Arabian Sea ensuing increasing denitrification in contrast to the Western Arabian Sea.

Acknowledgement

We are grateful to the Secretary, Ministry of Earth Sciences and Director, NCPOR for support and encouragement (NCAOR Contribution no. xxx/xxxx). We thank the IODP and the colleagues and the crew onboard IODP Expedition 355 for making this study possible. This research has also been supported by the Research Council of Norway (RCN) and

MoES, Govt. of India through the Ind-Nor programme (grant No. 248793 and MoES/Ind-Nor/PS-8/2015).

References

Algeo, T., Rowe, H., Hower, J. C., Schwark, L., Herrmann, A. and Heckel, P., Changes in ocean denitrification during Late Carboniferous glacial–interglacial cycles. *Nat. Geosci*., 2008, **1** (10), 709.

Altabet, M. A., R. Franqois, Murray, D.W. and Prell, W.L., Climate-related variations in denitrification in the Arabia Sea from 15N/14N ratios. *Nature*, 1995, **373**, 506-509.

Altabet, M. A., Murray, D. W. and Prell, W. L., Climatically linked oscillations in Arabian Sea denitrification over the past 1 m.y.: Implications for the marine N Cycle, *Paleoceanogr.*, 1999, **14**, 732-743.

Altabet, M. A., Higginson, M. J. and Murray, D. W., The effect of millennial-scale changes in Arabian Sea denitrification on atmospheric CO_2. *Nature*, 2002, **415**(6868), 159.

Anderson, D. M. and Prell, W. L., A 300 kyr record of upwelling off Oman during the late Quaternary: evidence of the Asian southwest monsoon. *Paleoceanogr. Paleoclimatol*., 1993, **8**(2), 193-208.

Bange, H. W., Rapsomanikis, S. and Andreae, M. O., Nitrous oxide cycling in the Arabian Sea. *J.Geophys. Res*., 2001, **106**, 1053-1066.

Betzler, C., Eberli, G. P., Kroon, D., Wright, J. D., Swart, P. K., Nath, B. N., ... and Guo, J. A., The abrupt onset of the modern South Asian Monsoon winds. *Sci. Rep*., 2016, **6**, 29838.

Brandes, J. A., Devol, A. H., Yoshinari, T., Jayakumar, D. A. and Naqvi, S. W. A., Isotopic composition of nitrate in the central Arabian Sea and eastern tropical North Pacific: A tracer for mixing and nitrogen cycles, *Limnol. Oceanogr*., 1998, **43**, 1680-1689.

Cabarcos, E., Flores, J. A., Singh, A. D. and Sierro, F. J., Monsoonal dynamics and evolution of the primary productivity in the eastern Arabian Sea over the past 30 ka. *Palaeogeogr. Palaeoclimatol. Palaeoecol*., 2014, **411**, 249-256.

Clemens, S. C., Murray, D. W. and Prell, W. L., Nonstationary phase of the Plio-Pleistocene Asian monsoon. *Science*, 1996, **274**(5289), 943-948.

Cocco, V., Joos, F., Steinacher, M. et al., Oxygen and indicators of stress for marine life in multi-model global warming projections. *Biogeosciences*, 2013, **10**, 1849–1868.

Codispoti, L. A. and F. A. Richards., An analysis of the horizontal regime of denitrification in the eastern tropical North Pacific. *Limnol. Oceanogr*., 1976, **21**, 379-388.

Ganeshram, R. S., Pedersen, T. F., Calvert, S. E. and Murray, J. W., Large changes in oceanic nutrient inventories from glacial to interglacial periods. *Nature*, 1995, **376**, 755–758.

Ganeshram, R. S., Pedersen, T. F., Calvert, S. E., McNeill, G. W. and Fontugne, M. R., Glacial-interglacial variability in denitrification in the world's oceans: Causes and consequences, *Paleoceanogr*., 2000, **15**(4), 361– 376.

Gaye-Haake, B., Lahajnar, N., Emeis, K. C. et al., Stable nitrogen isotopic ratios of sinking particles and sediments from the northern Indian Ocean. *Mar. Chem*., 2005, **96**(3– 4), 243– 255.

Gaye, B., Böll, A., Segschneider, J., Burdanowitz, N. et al., Glacial–interglacial changes and Holocene variations in Arabian Sea denitrification. *Biogeosciences*, 2018, **15**(2), 507-527.

Grootes, P. M. and Stuiver, M., Oxygen 18/16 variability in Greenland snow and ice with 10− 3-to 105-year time resolution. *J. Geophy. Res. - Oceans*, 1997, **102**(C12), 26455-26470.

Haywood, A. M., Dowsett, H. J. and Dolan, A. M. Integrating geological archives and climate models for the mid-Pliocene warm period. *Nat. Commun*., 2016, **7**, 1–14, doi: 10.1038/ncomms10646.

Hong, Y. T., Hong, B., Lin, Q. H., Zhu, Y. X., Shibata, Y., Hirota, M., ... and Wang, H., Correlation between Indian Ocean summer monsoon and North Atlantic climate during the Holocene. *Earth Planet Sci. Lett*., 2003, **211**(3-4), 371-380.

Ivanochko, T. S., Ganeshram, R. S., Brummer, G. J. A., Ganssen, G., Jung, S. J., Moreton, S. G. and Kroon, D., Variations in tropical convection as an amplifier of global climate change at the millennial scale. *Earth Planet Sci. Lett*., 2005, **235**(1-2), 302-314.

Jenkyns, H. C., Gröcke, D. R. and Hesselbo, S. P., Nitrogen isotope evidence for water mass denitrification during the early Toarcian (Jurassic) oceanic anoxic event. *Paleoceanogr.*, 2001, **16**(6), 593–603.

Jung, S. J., Kroon, D., Ganssen, G., Peeters, F. and Ganeshram, R., Enhanced Arabian Sea intermediate water flow during glacial North Atlantic cold phases. *Earth Planet Sci. Lett.*, 2009, **280**(1-4), 220-228.

Karl, D., Michaels, A., Bergman, B., Capone, D., Carpenter, E., Letelier, R., Lipschultz, F., Paerl, H., Sigman, D. and Stal, L. Dinitrogen fixation in the world's oceans. *Biogeochemistry*, 2002, **57/58**, 47–98.

Keeling, R. F., Körtzinger, A. and Gruber, N. Ocean deoxygenation in a warming world. Ann. Rev. Mar. Sci., 2010, **2**(1), 199-229.

Miller, K. G., Wright, J. D., Browning, J. V., Kulpecz, A., Kominz, M., Naish, T. R., Cramer, B.S., Rosenthal, Y., Peltier, W. R. and Sosdian, S., High tide of the warm Pliocene: Implications of global sea level for Antarctic deglaciation. *Geology*, 2012, **40**(5), 407-410.

Naqvi S.W.A., Some aspects of the oxygen deficient conditions and denitrification in the Arabian Sea. *Marine Res*., 1987, **29,** 459–469.

Naqvi, S.W.A. Narvekar, R.V. & Desa, E. Coastal biogeochemical processes in the North Indian Ocean. In: A. Robinson and K. Brink, editors, The Sea, Vol. 14, Harvard University Press, 2006a, pp. 723-780.

Nagoji, S. S. and Tiwari, M., Organic carbon preservation in Southeastern Arabian Sea sediments since mid-Holocene: Implications to South Asian Summer Monsoon variability. *Geochem. Geophys*., 2017, **18**(9), 3438-3451.

Niitsuma, N., Oba, T. and Okada, M. Oxygen and carbon isotope stratigraphy at site 723, Oman margin. *Proc. Ocean Drilling Prog., Sci. Results*, 1991, **117**, 321-341.

Olson, D. B., Hitchcock, G. L., Fine, R. A. and Warren, B. A., Maintenance of the low-oxygen layer in the central Arabian Sea. *Deep Sea Res.-II*, 1993, 40 (3), 673-585.

Pagani, M., Liu, Z., LaRiviere, J. and Ravelo, A. C., High Earth-system climate sensitivity determined from Pliocene carbon dioxide concentrations. *Nat. Geosci*., 2012, **3** (1), 27.

Pandey, D. K., Clift, P. D., Kulhanek, D. K. et al., Site 1456. Proc. International Ocean Discovery Prog., 2016, **355**, 1–61.

Pattan, J. N., Masuzawa, T., Naidu, P. D., Parthiban, G. and Yamamoto, M., Productivity fluctuations in the southeastern Arabian Sea during the last 140 ka. *Palaeogeogr. Palaeoclimatol. Palaeoecol*., 2003, **193**, 575-590.

Paulmier, A. and Ruiz-Pino, D., Oxygen minimum zones (OMZs) in the modern ocean. *Prog. Oceanogr*., 2009, **80**, 113-128.

Pichevin, L., Bard, E., Martinez, P. and Billy, I., Evidence of ventilation changes in the Arabian Sea during the late Quaternary: Implication for denitrification and nitrous oxide emission. *Global Biogeochem. Cycles*, 2007, **21**(4), GB4008.

Pierre, C., Vergnaud-Grazzini, C. and Faugeres, J. C. Oxygen and carbon stable isotope tracers of the water masses in the Central Brazil Basin. *Deep Sea Res. Part A*, 1991, ***38***(5), 597-606.

Qasim S. Z., Oceanography of the northern Arabian Sea. *Deep Sea Res*., 1982, **29**, 1041–1068.

Rostek, F., Bard, E., Beaufort, L., Sonzogni, C. and Ganssen, G., Sea surface temperature and productivity records for the past 240 kyr in the Arabian Sea. *Deep Sea Res.-II*, 1997, **44**, 1461-1480.

Schäfer, P. and Ittekkot, V., Seasonal variability of $\delta^{15}N$ in settling particles in the Arabian Sea and its palaeogeochemical significance. *Naturwissenschaften*., 1993, **80**, 511–513.

Schulte, S., Rostek, F., Bard, E., Rullkötter, J. and Marchal, O., Variations of oxygen-minimum and primary productivity recorded in sediments of the Arabian Sea. *Earth Planet Sci. Lett*., 1999, **173**(3), 205-221.

Sharma, G. S., Gouveia, A. D. and Satyendranath, S., Incursion of Pacific Ocean water into Indian-Ocean, Proc. *Indian Acad. Sci. Section A*., 1978, **87**(3), 29– 45.

Shetye, S. R., Gouveia, A. D. and Shenoi, S. S. C. Circulation and water masses of the Arabian Sea. *Proc. Indian Acad. Sci*., 1994, 103, 107–123.

Sigman, D. M., Karsh, K. L. and Casciotti, K. L., Ocean process tracers: nitrogen isotopes in the ocean, in Encyclopedia of Ocean Sciences (2nd Ed.), edited by J.H. Steele, K.K. Turekian, and S.A. Thorpe, 2009, Academic Press, London, 40-54.

Singh, A. D., Jung, S. J., Darling, K., Ganeshram, R., Ivanochko, T. and Kroon, D. Productivity collapses in the Arabian Sea during glacial cold phases. *Paleoceanogr. Paleoclimtol*., 2011, **26**(3).

Sirocko, F., Sarnthein, M., Erlenkeuser, H., Lange, H., Arnold, M. and Duplessy, J. C., Century-scale events in monsoonal climate over the past 24,000 years. *Nature*, 1993, **364** (6435), 322.

Suthhof, A., Ittekkot, V. and Gaye-Haake, B., Millennial-scale oscillation of denitrification intensity in the Arabian Sea during the Late Quaternary and its potential influence on atmospheric N2O and global climate. *Global Biogeochem Cycles*., 2001, **15** (3), 637-649.

Swallow, J. C., Some aspects of the physical oceanography of the Indian Ocean. Deep Sea Res Part A, 1984, **31** (6-8), 639-650.

Tally, L. D., Pickard, G. L., Emery, W. J. and Swift, J. H., Descriptive physical oceanography: An Introduction. *Elsevier, China*, 2012, 387–399.

Thamban, M., Rao, V. P., Schneider, R. R. and Grootes, P. M., Glacial to Holocene fluctuations in hydrography and productivity along the southwestern continental margin of India. *Palaeogeogr. Palaeoclimatol. Palaeoecol*., 2001, **165** (1-2), 113-127.

Tiwari, M., Nagoji, S. S. and Ganeshram, R. S., Multi-centennial scale SST and Indian summer monsoon precipitation variability since the mid-Holocene and its nonlinear response to solar activity. *Holocene*, 2015, **25**(9), 1415-1424.

Tripathi, S., Tiwari, M., Lee, J., Khim, B. K., IODP Expedition 355 Scientists, First evidence of denitrification vis-à-vis monsoon in the Arabian Sea since Late Miocene. *Sci. Rep*., 2017, **7**, 43056.

You, Y., Intermediate water circulation and ventilation of the Indian Ocean derived from water-mass contributions. *Marine Res*., 1998, **56**(5), 1029-1067.

Yu, Z., Colin, C., Ma, R. et al., Antarctic Intermediate Water penetration into the Northern Indian Ocean during the last deglaciation *Earth Planet Sci. Lett*., 2018, **500**, 67-75.

Ward, B. B., Devol, A. H., Rich, J. J. et al., Denitrification as the dominant nitrogen loss process in the Arabian Sea. *Nature*., 2009, **461**, 78–81.

Wyrtki, K., Physical oceanography of the Indian Ocean. In The biology of the Indian Ocean,1973, Springer, Berlin, Heidelberg, 18-36.

Supplementary Fig. 1. Cross-plot between $\delta^{15}N$ and total nitrogen (TN) concentration to test the effect of diagenesis on the sedimentary organic matter. No correlation indicates that the effect of the diagenesis is negligible in the present study.

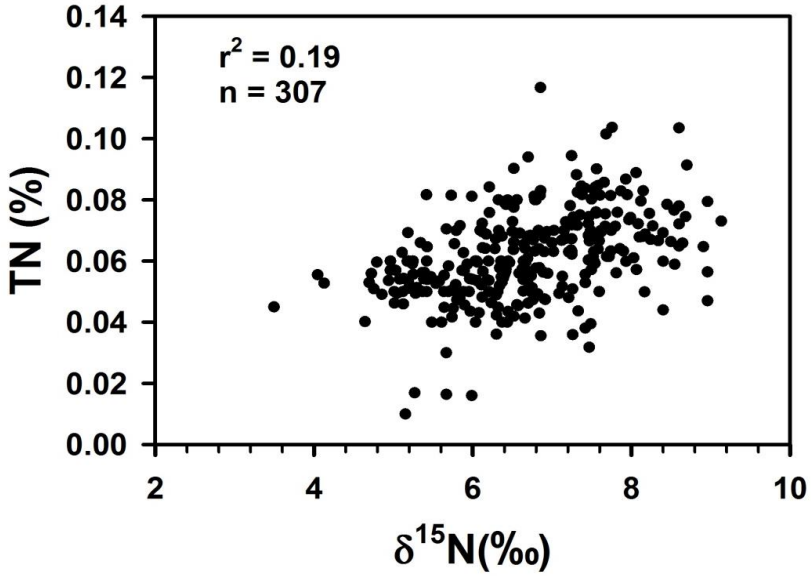

Chapter 5

4. Quantification of Eastern Arabian Sea Climate Change during Mid-Pleistocene Transition

5.1 Introduction

Most of the earlier studies from the eastern Arabian Sea spanning the MPT are qualitative in nature. We for the first time have quantified the climate variability of this region during MPT in terms of accurate oceanic temperature and salinity. We have also reconstructed the denitrification and productivity variability during MPT. Salinity and temperature variability have been used to reconstruct past monsoon changes from the coastal Arabian Sea (Tiwari et al., 2015 and references therein). Besides, Oceanic salinity and temperature have been also used to resolve ocean density structure and the spreading of deep water masses (Munk, 1950; Stommel and Arons, 1959). Knowledge of salinity is critical in characterizing deep water masses in the past ocean with respect to glacial-interglacial changes (Emery and Meincke, 1986; Broecker, W. S., 1998). Mid-Pleistocene Transition is one of the important climate transitions during the Quaternary period of the earth history (Fig 5.1). During MPT, a prolongation and intensification is observed in the glacial-interglacial cycles with no corresponding change in the orbital parameters (Hays et al., 1976; Maslin et al., 2015, Ford et al., 2016). The smooth transitions from glacial to interglacial became more abrupt (Maslin et al., 2015) and the glacial-interglacial cycle shifted from 41 kyr to quasi-100 kyr cyclicity. The MPT, therefore, can help to understand the mechanisms of climate variability. Most of the earlier studies regarding the MPT comes from Atlantic and Pacific Oceans (Shackleton, 1967; Pisias and Moore, 1981; Labeyrie et al., 1987;

Maasch, 1988; Ruddiman et al., 1989; Saltzman and Maasch, 1991; Mudelsee and Schulz, 1997; Rutherford and D'Hondt, 2000; Lisiecki and Raymo, 2005, 2007). There is a dearth of productivity, denitrification variability, and oceanic temperature and oceanic salinity record during the MPT from the Eastern Arabian Sea. A detailed discussion about MPT is already done in the Introduction chapter (section 1.2). In summary, from a geological perspective, it was postulated that the emergence of crystalline basement in Northern Hemisphere provided a base for the growth of the thicker ice sheets (Clark and Pollard, 1998). At 0.9 Ma (mid-point of the MPT), it was observed that the ice volume over Antarctica increased markedly (Elderfield et al., 2012). The feedbacks between poleward heat transport and meridional overturning is also considered as the main factor of the 100 kyr cycles (Imbrie et al., 1993). This is further corroborated as a recent study found changes in thermohaline circulation at 0.90 Ma (Pena and Goldstein, 2014). Lear et al., 2016 proposed that the carbon sequestration in deep ocean can amplify the 100 kyr cycle. Tzedakis et al., 2017 emphasized the role of climate feedback and found that due to a weak response to solar-maxima, the ice growth period is extended resulting in the 100 kyr periodicity. Although CO_2 is a factor influencing the climate, its role in affecting the MPT is ambiguous. Ice-core records spanning continuously the entire MPT are not available (Wolff et al., 2010). Here, we present the high-resolution record of productivity, denitrification variability, provenance, oceanic temperature and salinity variability from MIS 18 to MIS 28 spanning a major part of MPT. We also developed a new, higher resolution age-depth model using oxygen isotope stratigraphy.

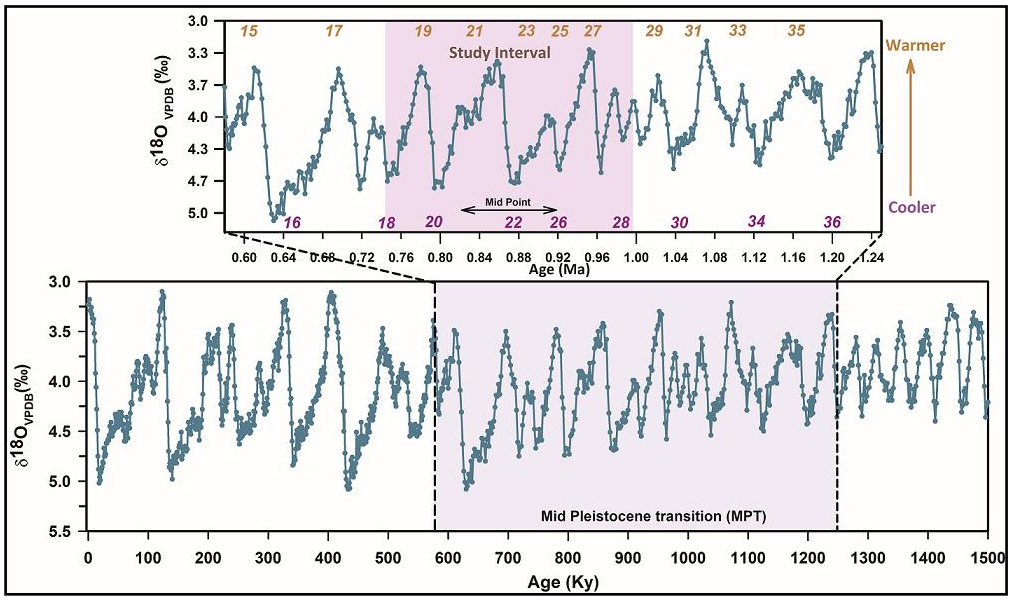

Figure 5.1. The Span of MPT. Benthic foraminiferal $\delta^{18}O$ record is shown by the greenish grey curve. The MPT and the present study interval are shown by coloured boxes. Marine Isotope Stages (MIS) are mentioned in the upper graph (Indo-Arabic numerals; Lisiecki and Raymo, 2005). Mudelsee and Schulz, 1997 noted the MIS 24-21 as the mid-point of the MPT.

5.1 Age Depth Model

The first age model of IODP Site U1457 was generated onboard *JOIDES Resolution* and is based on the first and the last appearance of planktic foraminifera, nannofossils and paleomagnetic reversals (Pandey et al., 2016). It was further refined by the addition of new biostratigraphic, paleomagnetic and strontium isotope data (Routledge et al., 2019). But, it is still very coarse resolution model. For example, during the MPT, a ~400 kyr long period, only three tie-points are available making it unsuitable for millennial to multi-millennial scale studies. Therefore, to further refine the age-depth

model, we have generated a new oxygen isotope stratigraphy for the MPT using the oxygen isotope values of *G. ruber*. The three dates available during MPT from Routledge et al., 2019 are taken to constrain our age-depth model. We consider these three dates as the basis for the development of our age-depth model. Using them as guidelines, we carefully did the graphic correlation so that our tie-points fall broadly in the range provided by Routledge et al., 2019. The three control points used as guidelines for the age-depth model are 0.61 Ma (42.75 m), 0.91 Ma (52.42 m), and 1.14 Ma (81.62 m). Graphic correlation requires a good judgement to find out matching features. For a more objective correlation, computerized correlation algorithms are also used. However, it is suggested that each alignment should be evaluated visually. The disturbances caused by the hiatuses, coring gaps etc. can induce errors in the computerized correlation (Lisiecki and Raymo, 2005). Therefore, we visually identified tie-points using the three dates from Routledge et al., 2019 as guidelines. As per our new oxygen isotope stratigraphy, the sediments range from MIS-18 to MIS-28. The comparison of our oxygen isotope curve with that of the LR-04 to identify the tie-points (Table 5.1) for developing the age model is shown in Fig 5.2. The sedimentation rates are highly variable during this 0.3 Myr long period. The error in the LR-04 record from all the possible sources of uncertainty like orbital tuning, global climate reorganization etc. is estimated to be 4 kyr for 0 to 1 Ma.

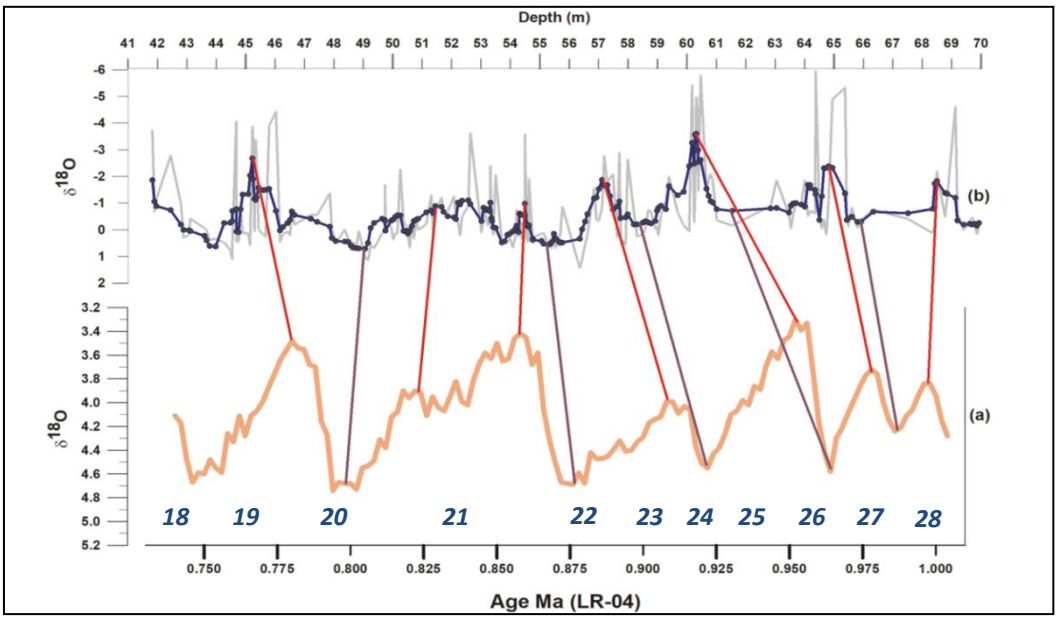

Figure 5.2. Comparison with LR-04 stack (bottom panel) and oxygen isotope curve from the present study (top panel). The original data points are shown by grey colour while the dark blue lines represent the 3-point running average. The red lines mark the tie-points at peak interglacials and purple lines show the tie-lines connecting maximum $\delta^{18}O$ values, which represents the glacial periods. The Indo-Arabic numerals in italics represent marine isotope stages.

Table 5.1. The tie points for the development of the age-depth model based on oxygen isotope stratigraphy

S. No.	Age (Ma)	Depth (m)
1	0.778	47.150
2	0.794	49.060
3	0.819	51.470
4	0.858	54.490
5	0.880	56.360
6	0.909	57.490
7	0.922	58.690
8	0.952	60.180
9	0.964	61.540
10	0.986	65.800
11	0.998	68.500

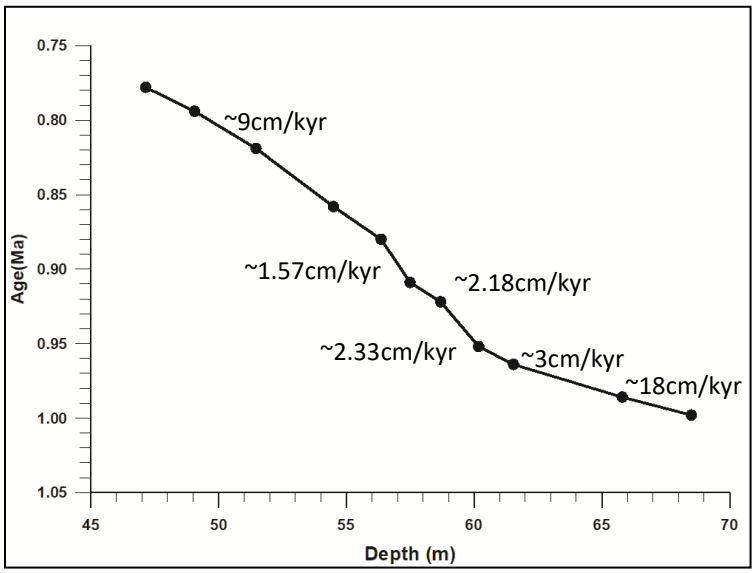

Figure 5.3. Age-depth model and sedimentation rate of the site 1457 based on new stratigraphic tie points.

5.2 Methodology

The materials and detailed analytical techniques used are discussed in the Methodology chapter (Section 2.3). For the completeness, the methodology with the calibration equation used in the study is discussed in brief in this section. The planktic foraminifera *Globigerinoides sacculifer* is selected, which is a mixed-layer thriving species (Hemleben et al., 1989). It is one of the most abundant and is relatively unaffected by dissolution (Delaney et al., 1985; Dekens et al., 2002, Farmer et al., 2007). Thus, *G. sacculifer* is a suitable species for the present study. The reconstruction of oceanic water temperatures as well as salinities is a crucial step for a complete understanding and quantifying the hydrological component during the MPT. Empirical calibration equations based on core-top, sediment trap, and culture studies have been developed for relation between foraminifera Mg/Ca ratios with ambient temperature that have given very consistent results. Mg/Ca based paleothermometry has been used widely for determining the past temperature variability at different timescales (Hastings et al., 1998; Lea et al., 1999, 2000, 2002; Mashiotta et al., 1999; Elderfield and Ganssen, 2000; Koutavas et al., 2002; Stott et al., 2002; Pahnke et al., 2003; Visser et al., 2003). There are several planktic foraminifera based calibration equation for oceanic temperature by using core-tops, sediment traps and lab-cultures studies (Nurnberg, 1995; Nurnberg et al., 1996; Mashiotta et al., 1999; Lea et al., 1999; Lea et al., 2000; Elderfield and Ganssen, 2000; Dekens et al., 2002; Anand et al., 2003; McConnell and Thunell, 2005). The incorporation of Mg is affected by the biological and thermodynamical processes into the foraminifera shells (Rosenthal et al., 1997; Lea et al., 1999; Erez, 2003; Bentov and Erez, 2006). These studies show a ~9-10% increase in Mg/Ca per degree Celsius increase in temperature in most species (Lea et al., 1999). *G.*

sacculifer has a nearly uniform distribution of Mg and Ca in its test (Eggins et al., 2003). In the present study, the following calibration equation provided by Dekens et al., 2002 for *G. sacculifer* is used for converting the Mg/Ca ratios (mmol/mol) into calcification temperatures:

$$Mg/Ca = 0.37\, e^{0.09\,[T - 0.36\,(\text{core depth in km}) - 2\,^{\circ}C]} \quad \textbf{(5.1)}$$

This calibration is used because it is species-specific (*G. sacculifer*). Also, the derived temperatures are close to modern values, which show that this calibration equation can be applied to the Arabian Sea. The measurement shows repeatability of ~0.01 mmol/mol (1σ standard deviation) for a standard solution of Mg/Ca = 2.18 (mmol/mol). The analytical repeatability for $\delta^{18}O$ analysis is ~0.15 ‰. Bemis et al., 1998 provided the following equation to determine the $\delta^{18}O$ of seawater:

$$\delta^{18}O_{sw} = 0.27 + [\{SST - 17 + 4.59 \times \delta^{18}O_{sac}\}/4.59] \quad \textbf{(5.2)}$$

Singh et al., 2010 put together oxygen isotope and salinity data collected over almost two decades (1987 - 2009) from the northern Indian Ocean. Due to the long period of collection, it is more representative of the conditions in that part of the Arabian Sea. The equation provided by them is: Salinity = $(\delta^{18}O_{sw} + 8.6)/0.26$. Salinity was obtained using this equation using the *Ice volume corrected* $\delta^{18}O_{sw}$ values.

For denitrification, paleoproductivity and provenance we measured the $\delta^{15}N$, TN, $\delta^{13}C$ and TOC content of SOM. Each sample was oven dried overnight at 45°C to remove the moisture. Dried samples were homogenized by grinding. The grinded samples were divided into two batches for geochemical and isotopic analyses. One portion is treated with 2 N HCl total organic carbon (TOC) and $\delta^{13}C$ of organic carbon measurement and

the other untreated is used for determination of total nitrogen (TN) content and $\delta^{15}N$ values. The acid treated samples were washed with Milli-Q water to remove the residual acid. Around 8-10 mg of treated sample was used for For TOC and $\delta^{13}C$ analysis. And 200 mg of untreated grinded sediment was used for TN and $\delta^{15}N$ measurement. In addition to this the detailed method and analytical measurements are discussed in section 2.4.2 and in method section of chapter 3 and chapter 4.

5.3 Results and Discussion

5.3.1 Diagenesis and provenance of Sedimentary Organic Matter (SOM)

The sediment samples used in the study are from the section 5H to 8H of the site U1457 (17ºN, 67ºE; 3534 m water depth). It is divided into 4 units based on the sedimentology and we analyzed sediment samples from ~ 41 m to ~70 m (Unit I, ~120 m thick composed of nannofossil ooze interbedded with thin turbidites) (Pandey et al., 2016). This section spanned from ~ 1.017 Ma (MIS 28) to ~0.714 Ma (MIS 18). Before doing the interpretation, we looked into the diagenetic alteration and provenance of the SOM. Diagenesis of the SOM initiates from the upper water column and continues during the sinking. It continues within the bioturbated mixed layer of sediment (~10 cm depth) and less than 1% of organic matter is finally preserved (Rullkötter, 2006). However, as the organic matter is buried deeper, the diagenesis reduces considerably (Parkes et al., 1994).

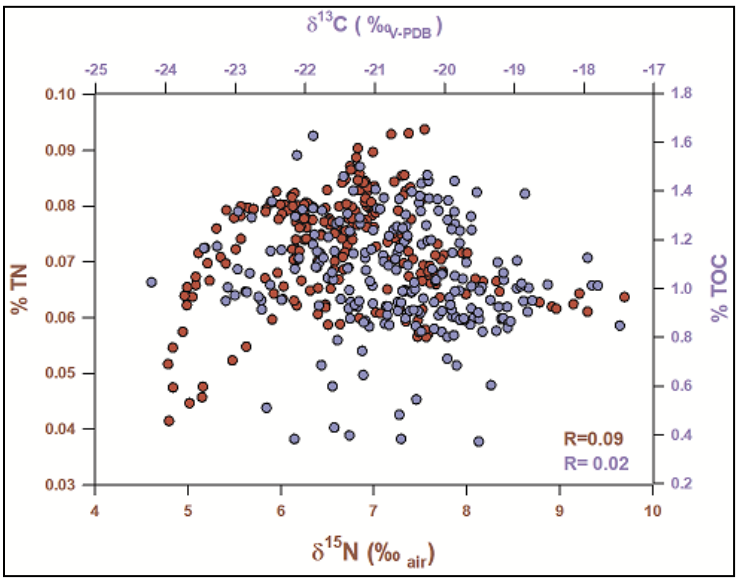

Figure 5.4. Cross-plot between $\delta^{15}N$ and total nitrogen (TN); $\delta^{13}C$ and total organic carbon (TOC) concentration to test the effect of digenesis on the sedimentary organic matter.

An earlier study showed that although remineralization may lead to the loss of organic matter with increasing depth, the $\delta^{13}C$ of the SOM is nearly unaffected (Popp et al., 2009). Similarly, in the equatorial Pacific, the difference in $\delta^{15}N$ values between core top sediments and sinking particles is very small; the $\delta^{15}N$ values do not change because of diagenesis in the upper section of the core (Parkes et al., 1994). Altabet et al., 1999 based on no correlation between TN and $\delta^{15}N$ in sediment from the Western Arabian Sea concluded that diagenesis does not have any effect on the $\delta^{15}N$ variation. We also found no correlation between TN and $\delta^{15}N$ (Fig. 5.5). We also find no correlation between TOC and $\delta^{13}C$. Thus, we conclude that diagenesis does not significantly change the $\delta^{13}C$ and $\delta^{15}N$ values of SOM at Site U1457.

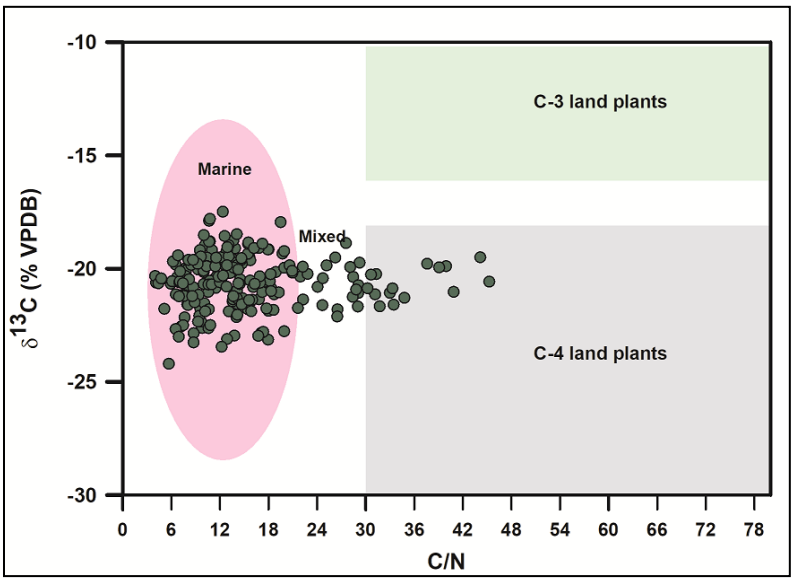

Figure 5.5. The Provenance of SOM of U1457 based on atomic C/N ratios and organic $\delta^{13}C$ values of marine, lacustrine algae, C-3, C-4 plants and Marine biomass.

The $\delta^{13}C_{som}$ ranges from -17 ‰ to -24 ‰ and TOC/TN values range from 4 to 45. The organic matter from terrestrial origin has values between 20 and100 (Premuzic et al., 1982, Meyers, 1994) and organic matter produced in the marine environment has C/N of 8 to 10 (Muller, 1977). The $\delta^{13}C$ value of C-3 plants varies between -20 ‰ and -36 ‰ and for C-4 plants it varies from -9 ‰ to -17 ‰ (discussed in details in methodology section 2.3.3). Thus, the $\delta^{13}C_{som}$ and TOC/TN variability in the core indicates the presence of both marine and terrestrial organic matter (Farquhar et al., 1989). Based on $\delta^{13}C$ and TOC/TN variability in the samples, we find that there are certain periods during which terrestrial influx of organic matter dominates marine organic matter implying a heavy surface runoff.

5.3.2 Productivity and denitrification variability during MPT

Productivity variability during MPT

TOC, TN and $\delta^{15}N$ measurements from MIS 28- MIS 18 show large variability; Figure 5.6 b and f show the comparison of denitrification from both the Eastern and Western Arabian Sea. Fig. 5.6c and d show the productivity variability (shown by the total nitrogen concentration and total organic carbon at the core site). Figure 5.6 g represents the productivity of the Western Arabian Sea. The TN at the core site of present study varies from 0.02 to 0.14 % and TOC varies from 0.26 to 2.33 %. The TOC variability has been used as a proxy to reconstruct the SAM variability. The increase in TOC implies the strengthening of SAM (Kessarkar et al., 2010; Singh et al., 2011). However, sedimentation rate and redox conditions are also shown to affect the TOC concentration depending on the regional oceanic settings (Calvert and Pedersen, 1993; Nagoji et al., 2017).

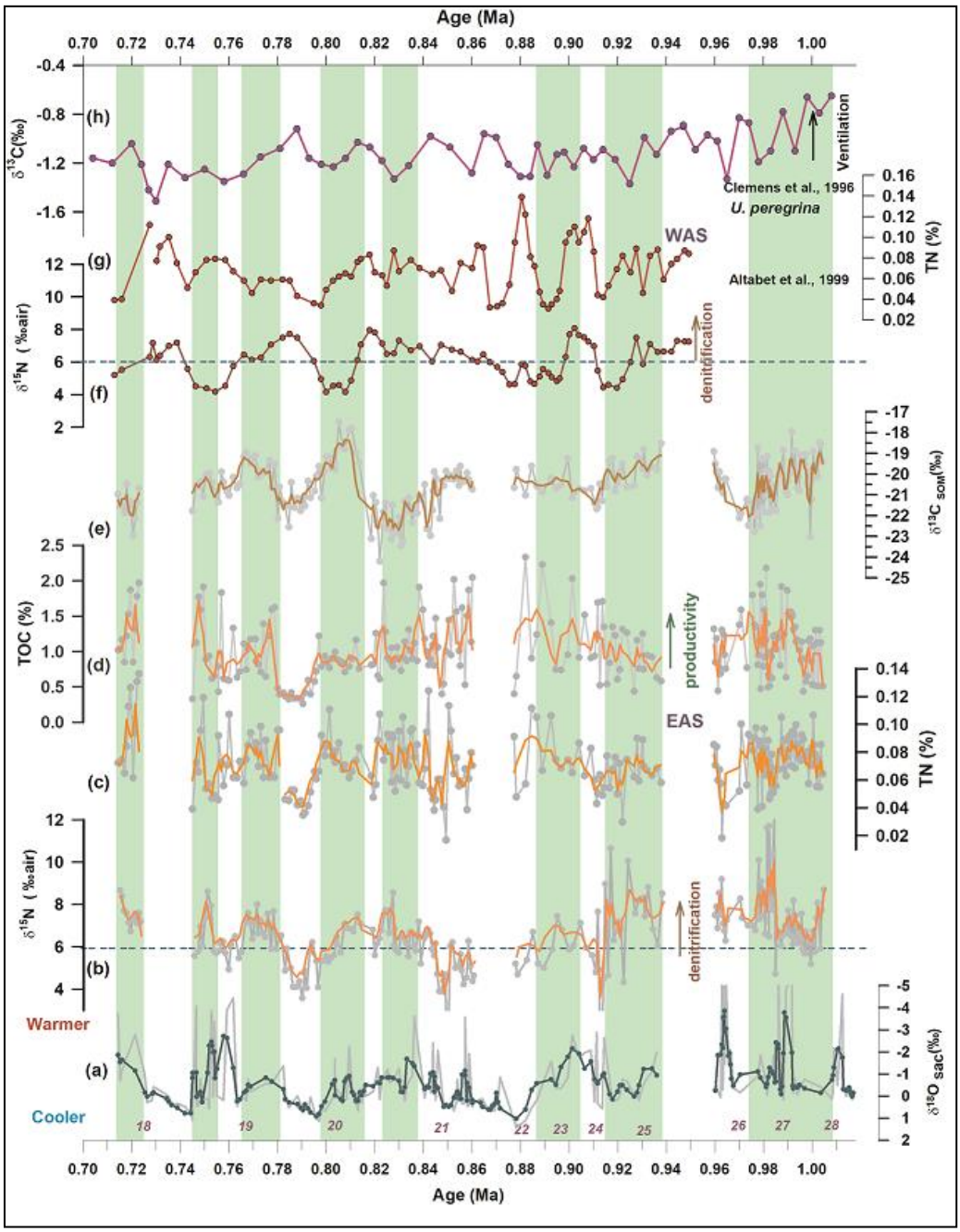

Figure 5.6. High-resolution denitrification and productivity variability during MPT from the Eastern Arabian Sea. Panel (a) represents the $\delta^{18}O$ of G *sacculifer* (present study), the lower values represent the warmer condition and higher values represent cooler condition; (b) represents down core variability of $\delta^{15}N$ of SOM from Site U1457A, which shows the denitrification during MPT (present study); (c), (d) represent

TOC and TN variability from present study both representing productivity; (f) shows $\delta^{15}N$ variability of ODP site 722, which represents the denitrification variability from the WAS (Altabet et al., 1999), (g) shows the TN variability from WAS (Altabet et al., 1999), and (h) shows the benthic $\delta^{13}C$ variability showing the ventilation during MPT in WAS (Clemens et al., 1996). The light green bands show the periods with high productivity, high denitrification and strong monsoon.

Productivity represents an important component of global climate cycle, is responsible for removal of CO_2 from the atmosphere and transfers it to the ocean floor in the form of organic matter - a process defiend as "biological pump" (Broecker, 1982; Mix, 1989). Thus, marine productivity regulates the concentration of atmospheric and upper-ocean CO_2 (Field et al., 1998; Sarmiento et al., 1990). Investigations of variability in productivity, especially during intervals of extreme climate conditions, can provide useful information on how marine productivity is affected by changes in climate. McClain et al., 2004 noted that the sustained global warming may increase the stratification in the open ocean that may drastically influence the productivity. A mixed view exists about the fate of productivity in the warming world. Several model outputs showed a decrease in the global mean productivity due to reduction in Atlantic meridional overturning circulation and stratification of the upper ocean water column (Schmittner, 2005; Steinacher et al., 2010). However, many of the model output showed an increased rate of phytoplankton growth due to warmer temperature which ultimately led to enhanced global productivity (Sarmiento et al., 2004; Schemittner et al., 2008). It is very crucial to study the variability of productivity during MPT. The monsoon induced productivity and silicate weathering lead to drawdown the CO_2 from the atmosphere (Field et al., 1998; Sarmiento et al., 1990). Many studies claim CO_2 as one

of the drivers of MPT (Martinez-Garcia et al., 2009, Chalk et al., 2017, Haass et al., 2018). Overall, our results show increased productivity in the Eastern Arabian Sea is higher during warmer periods (e.g., MIS 27, 25, 23, 21, and 19). We also compare the productivity record of the Eastern Arabian Sea with the results of the Western Arabian Sea (Altabet et al., 1999) to see the possibility of spatial variability. We find synchronous productivity variation in both the regions during the MPT.

Denitrification variability during MPT

The $\delta^{15}N$ values range from around 3.6 to 12 ‰ with a mean value of 6.6 ‰. The denitrification in the Arabian Sea causes an increase in $\delta^{15}N$ value which is significantly higher than the global ocean average nitrate value 4.5-6 ‰ (Sigman et al., 1997). Similar to productivity, denitrification also shows high variability from MIS 28 to MIS 18. It remained high during most of the period indicated by $\delta^{15}N > 6$ ‰ (Gaye-Haake et al., 2006; Tripathi et al., 2017; Ji-Eun Kim et al., 2018; Gaye et al., 2018) and supported by productivity. The denitrification varies in response to the monsoon activity at various timescales in the Arabian Sea (Naqvi, 1994; Ganeshram et al., 2000; Kao et al., 2015; Ziegler et al., 2010). We find strong denitrification in the Eastern Arabian Sea during interglacial periods (MIS 27, 25, 23, 21, and 19) and a decreasing trend during some of the glacial periods (MIS 28, 22, and 20). We also compared with the only available denitrification record from the western Arabian Sea (Altabet et al., 1999). During the warmer periods, the denitrification is strong in both the Eastern and Western Arabian Sea and is supported by productivity (Fig. 5.6 d, e, and f). The importance of circulation in controlling denitrification on a multi-millennial timescale is well known (e.g., Ganeshram et al., 2000; Ivanochko et al., 2005, Pichevin et al., 2007). But there is no

record of ventilation of intermediate depths by AAIW for the MPT in the Eastern Arabian Sea. Therefore, we compared with the ventilation record ($\delta^{13}C_{benthic}$) from Western Arabian Sea (Clemens et al., 1996). The variability of denitrification during the MPT matches well with the productivity. However, it can only be explained well when productivity is compared with circulation and ventilation record. We find that the ventilation by oxygen-rich water/circulation was weaker during periods of high denitrification. The denitrification record from Western Arabian Sea shows a similarity in the trend of variability but the intensity of denitrification is higher in the Eastern Arabian Sea. It is also observed in the modern oceans that although the productivity is more in the western Arabian Sea, the denitrification is stronger in the eastern Arabian Sea (Olson et al., 1993; Naqvi, 1994). To conclude, the increase in the denitrification during the MPT corresponds to the warmer periods as shown by $\delta^{18}O_{sac}$ values (Fig. 5.6a).

5.3.3. Quantifying hydrographic and monsoon variability during MPT

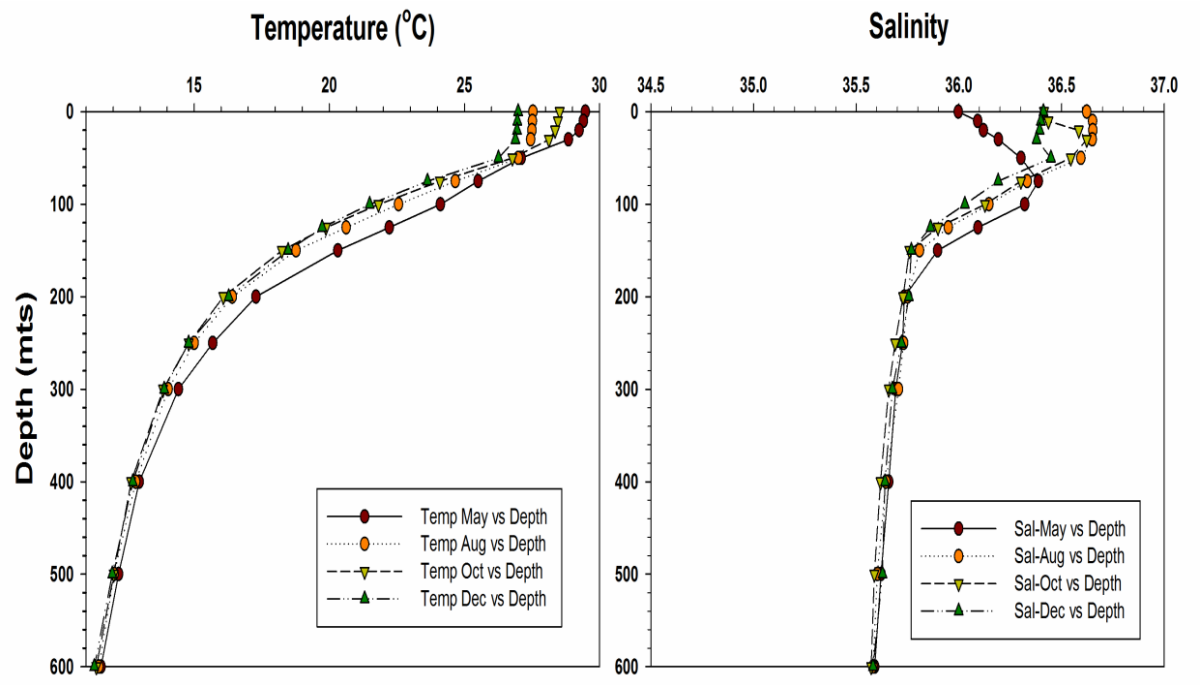

Figure 5.7. Seasonal variability of SST and SSS near the Site U1457 (World Ocean Database 2009 (Boyer et al., 2009)). Summer monsoon season is represented by August (orange circle). Winter monsoon season is shown by December (green triangle). Pre- and post-summer monsoon season is shown by May and October months, respectively (dark red circle and inverted green triangle).

Salinity and SST variability has been used widely to decipher past monsoon variability in the Arabian Sea (Anand et al., 2008; Govil and Naidu, 2010; Kessarkar et al., 2013; Saraswat et al., 2013; Tiwari et al. 2015). During the summer monsoon season, large amount of orographic rainfall falls in the Western Ghats along the Eastern Arabian Sea. This freshwater flows into the coastal Arabian Sea via surface runoff and small rivers, which reduces the salinity along with overhead precipitation. Thus, past monsoon precipitation can be reconstructed using salinity form the eastern Arabian Sea (Tiwari et

al., 2015). During the Southwest monsoon, the salinity reduces by 0.5. Further, during the post-monsoon period, the salinity reduces by up to 0.8 as less saline water from the Bay of Bengal (less salinity is due to the influx of freshwaters from the mainland river system) via the wind-driven North East Monsoon Current. However, our study area is not from the coastal Arabian Sea. Fig 5.7 shows low mixed layer temperature (MLT) during the monsoon periods (shown by August and December respectively). Further, the oceanic salinity is high during the monsoon periods at our study area.

In the present study, *G. sacculifer* is selected which is a spinose mixed-layer dwelling planktic foraminifer (Hemleben et al., 1989). The suitability of this species is already discussed in section 2.3.4 of Chapter 2. It is one of the most abundant species and calcifies in the mixed layer of the ocean (25–40 m) (Farmer et al., 2007). *G. sacculifer* is more resistant to dissolution compared to other planktic foraminifera species (Delaney et al., 1985; Dekens et al., 2002). Thus, it is one of the ideal species for paleoceanographic investigations.

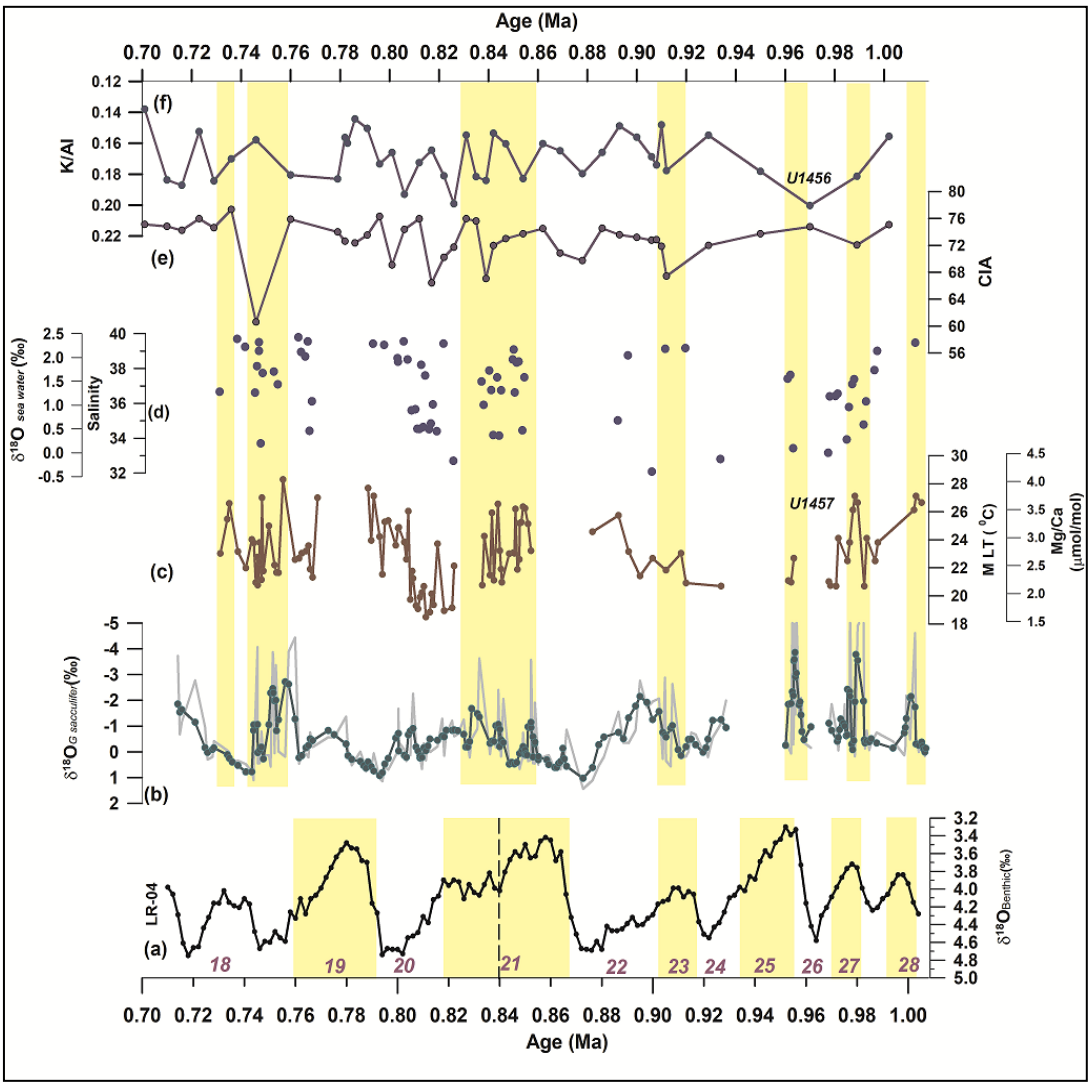

Figure 5.8. (a) LR04 Benthic $\delta^{18}O$ stacks (Lisiecki and Raymo, 2005). (b) $\delta^{18}O_{sac}$ variability from the present study, the dark green curve is the 3-point average. (c) represents the *G. sacculifer* Mg/Ca based mixed layer temperature (MLT) variability, (d) represents the ice volume corrected salinity variability, (e) and (f) represents the chemical index of alteration and K/Al as chemical weathering index from Site U1456 (Cai, et al., 2019). The yellow bands represent the comparatively warm period. The blocks over panel (c) and (d) show three different slices for discussion of MLT variability. The Indo-Arabic numerals in purple indicate the MIS numbers.

Determining the past temperature and salinity of the upper ocean waters column is essential for *quantifying* past changes in climate. The monsoon winds and precipitation have a huge impact on upper ocean temperature and salinity of the Eastern Arabian Sea (Anand et al., 2008). For *quantifying* the hydrography of the Eastern Arabian Sea during MPT, we did the paired measurement of Mg/Ca and $\delta^{18}O$ of *G. sacculifer* to reconstruct the mixed layer temperature (MLT) and salinity record. Our MLT and salinity record spans from the MIS 28 to MIS 18. However, due to the less foraminifera abundance during some periods like MIS 28 to MIS 22, the record is at a coarse resolution and even absent in some intervals. Based on the Mg/Ca and $\delta^{18}O_{sw}$ record, we find that MLT from 28 °C to as low as ~19 °C with a mean value of ~23 °C and $\delta^{18}O_{sw}$ record and salinity ranges from ~39 to ~32 units with a mean value of ~36 units. The MLT varies from 28 °C to 24 °C during MIS 28. Further, we saw an increasing trend in the MLT and it reaches to almost 27 °C from MIS 24 to MIS 22. The MLT show huge variability in MIS 21 with an average value of ~23 °C in the early MIS 21 and further, it shows an abrupt decrease and the MLT reaches to 19 °C in the late phase of MIS 21. During MIS 20 MLT varies from 18 °C to 28 °C and salinity from ~32 to ~38 units. In addition, change in monsoon strength cause changes in the weathering and sediment transport intensity. Strong monsoon periods result in deposition of more altered sedimentary materials than during weaker monsoon times (Clift et al., 2020). Several long term studies found that rapid erosion and increased supply of sediments to the adjoining ocean is linked to the strengthening of the monsoon (Lee et al., 2019, Cai et al., 2018, 2019, Clift et al., 2020). According to some of the previous studies, warmer periods and stronger monsoonal rainfall increase the chemical weathering in a stable tectonic environment (Kump et al., 2000; Liu et al., 2003, Wan et al., 2017). We

compared our MLT and oceanic salinity data with the recently generated chemical weathering record from the adjacent site (U1456; Cai et al., 2019) of the present location (U1457). The chemical weathering intensity can be estimated using the concentration ratios of mobile elements (K, and Mg) to immobile elements like Al, which behaves conservative to weathering (Gaillard et al., 1999; Garzanti et al., 2014). Ratios like K/Al, Mg/Al, have successfully been used for evaluating the intensity of chemical weathering (Gaillard et al., 1999; Garzanti et al., 2014; Wan et al., 2017; Xu et al., 2018). Previous studies show higher K/Al, Mg/Al which indicates less depletion of mobile elements in sediments and thus low chemical alteration; in contrast, lesser K/Al, Mg/Al, and Fe/Al values indicate a high depletion of mobile elements and thus high chemical alteration. However, much care should be taken as these geochemical weathering proxies can be influenced by many factors, such as provenance, grain size, hydraulic sorting, diagenesis (Fralick & Kronberg, 1997; Liu et al., 2007; Limmer et al., 2012; Köhler et al., 2012; Wan et al., 2017; Zhao et al., 2017). The comparison of our record to the chemical index of alteration and K/Al showed a synchronous variation in the strengthening of monsoon and increase in CIA. We find that during the course of study the K/Al and CIA show synchronous variation with the warmer period (high MLT) corresponding to stronger monsoon (high TOC and $\delta^{18}O$). Such periods will bring a high amount of terrestrial organic matter and sediments into the oceans. These episodes of strong monsoon get reflected in various geochemical proxies of provenance $\delta^{13}C$ of organic matter (OM) and trace metals. We reconstructed this high-resolution record of the provenance of sediments at the IODP Site 1457 during MPT (~0.71 Ma to ~1.08 Ma). The $\delta^{13}C_{som}$ ranges from -17 ‰ to -24 ‰ and TOC/TN values range from 4 to 45. The organic matter from terrestrial origin has values between 20 and100 (Premuzic et al., 1982, Meyers, 1994) and organic matter produced in the marine

environment has C/N of 8 to 10 (Muller, 1977). The $\delta^{13}C$ value of C-3 plants varies between -20 ‰ and -36 ‰ and for C-4 plants it varies from -9 ‰ to -17 ‰ (discussed in details in section 2.3.3. of methodology chapter 2). Thus, the $\delta^{13}C_{som}$ and TOC/TN variability in the core indicates the presence of both marine and terrestrial organic matter (Farquhar et al., 1989). Some of the earlier studies have reported that TOC is also influenced by redox conditions, sedimentation rate, and an influx of terrigenous matter depending on the regional oceanic settings and may reflect the degree of preservation (Calvert and Pedersen, 1993, Nagoji et al., 2017). Thus, care should be taken while interpreting TOC/TN. During MIS 28, we saw mostly higher values of $\delta^{13}C_{som}$ and C/N less than 20; at the end of this glacial period, we find an increasing trend in C/N values. During MIS 27, $\delta^{13}C_{som}$ values are less than -21‰ and C/N value increases showing moderate terrestrial input. An increasing trend in K/Al is observed in the same period showing strong monsoon. Further, we don't have any record in MIS 25 and MIS 24, which is a comparatively a small glacial period show no sign of major terrestrial influx. During MIS 23 a clear indication of terrestrial influx is found further supported by weathering proxies. Thus, we find that the warmer periods correspond to stronger monsoon. During MIS 22 we note that the $\delta^{13}C_{som}$ values vary between -19 ‰ to -21 ‰. The C/N values go up to 40 with the majority of values less than 10. During MIS 21 which is along interglacial period, we find dramatic/abrupt increase in terrestrial influx and weathering data also show terrestrial influence. MIS 21 can be divided into three parts in which the early, mid and late MIS 21. The early MIS 21 did not show inputs from the terrestrial region. However, the mid-MIS 21 witnessed a heavy influx of terrestrial organic material implying strong monsoon. During MIS 20, $\delta^{13}C_{som}$ and C/N together show marine to mix the origin of organic matter; however, the weathering

showed high variability during this period. Thus, we find high salinity during the warmer periods (MIS 27, 25, 21 and 19), which indicates the strong SAsM.

5.3.4 Influence of external and internal forcing on the South Asian Monsoon (SAsM)

"Forcing" is defined as the physical process influencing or driving the climate. These forcings exist both outside (external forcing) and inside (internal forcing) of the system. Some of the most important types of forcings include changes in the earth's orbital parameter (Milankovitch Cycles), variations in insolation, changes in the albedo and land-use, and variations in the aerosols and greenhouse gases in the atmosphere. Out of these, the changes in the orbital parameter and solar activity (insolation) are considered as the external forcing while the rest are the internal forcings.

It has been observed that the solar forcing has a large impact on the SAsM on different time scales (Mehta et al., 1997; Agnihotri et al., 2002; Tiwari et al., 2005; Gebregiorgis et al., 2018). Several mechanisms have been proposed to explain how solar forcing affects the global climate and specifically the Asian Monsoon. The first involves heating of the earth's stratosphere by increased absorption of solar radiation by ozone during periods of enhanced solar activity. Increased heating causes high thermal contrast between the Asian landmass and the Indian Ocean, and also increases evaporation from the oceans, thus enhancing the monsoon winds and precipitation. This also involves the release of latent heat to the troposphere by monsoon precipitation, which in turn strengthens the monsoon winds. The second mechanism is that during periods of higher solar activity, the flux of galactic cosmic rays to the earth gets

reduced. This reduction in the cosmic rays results in less cloud condensation nuclei, thus reducing in cloudiness (Schneider, 2005., Friis-Christensen, 1997).

Further, it is proposed that the summer solar radiation intensity changes due to variations in Earth's orbital parameters may influence the monsoon (Kutzbach, 1981). Later studies have shown that the precession cycle primarily influences the monsoon strength [Mediterranean sapropel (Rossignol-Strick, 1983); tropical lakes in Africa (Kutzbach and Street-Perrott, 1985)] suggested that insolation variation at the 23,000-year precession period is the primary control on monsoon intensity, with a small phase lag relative to July insolation. However, Clemens and Prell (1990, 2003) propose a different view. They used marine sediment proxies from the tropical Indian Ocean and calculated the 'summer monsoon factor'. Their conclusion is different from the one in *Kutzbach's hypothesis* (Kutzbach, 1981). Relatively little power is concentrated at 23,000 years, and the average phase of the proxies at the precession period falls in late October, closer to the December solstice than to the July phase in *Kutzbach's hypothesis*. This difference is explained by the transfer of latent heat influx from the southern to the northern hemisphere during the boreal summer monsoon (Clemens and Prell, 1990). Therefore, a contrasting view exists over the orbital scale periodicity and phasing of monsoon variability (Ruddiman, 2006). Thus, whether the northern or southern hemisphere summer insolation govern the Asian monsoon on the Milankovitch timescale is ambiguous (Ruddiman, 2006; Liu and Shi, 2009). The Asian monsoon affects the climate over a large area of the globe, so understanding this disparity is important.

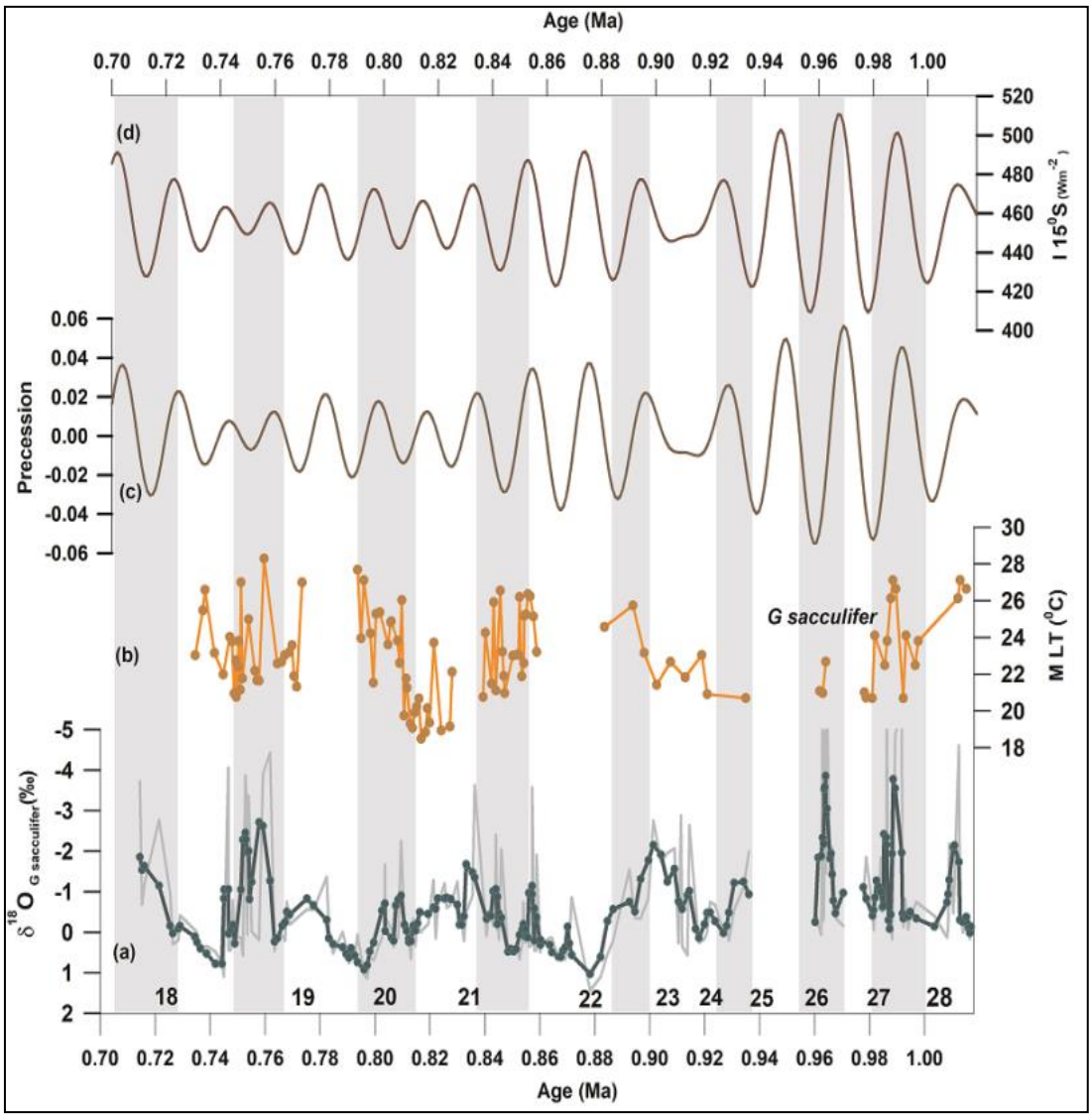

Figure 5.8. (a) $\delta^{18}O_{sac}$ variability from the present study, the dark green curve is the 3-point average, (b) represents the *G. sacculifer* Mg/Ca based mixed layer temperature (MLT) variability, (c) and (e) represent the Precession, and Insolation at 15˚S.

A recent study by *Gebregiorgis et al., 2018* from the southern Indian Ocean found that SAsM was in phase with obliquity minima and responds to warming in southern hemisphere. They further noted that SAsM and East Asian Monsoon precipitation responded differently to orbital forcing and highlights the importance of internal

forcings. We also examined our data and looked for the possible linkage of SAsM to the forcing factors like solar insolation at 15˚S (I15˚S) and precession during MPT. We visibly examine the relationship between the I15˚S and the $\delta^{18}O_{sac}$ variability. We observe that the precession and insolation 15˚S matches well with $\delta^{18}O_{sac}$ and covaried in some of the MISs during the MPT as mentioned in some of the recent studies (Gebregiorgis et al., 2018). From MIS 28 to MIS 23, the I15˚S and precession both seem to vary with $\delta^{18}O_{sac}$. Due to the unavailability and less data of MLT during MIS 28 to MIS 22, we are unable to compare it with the precession as well as I15˚S. From MIS 21 to MIS 18, the amplitude of the precession and I15˚S becomes low. However, during MIS 20 there is an increase in the I15˚S, precession as well as in the $\delta^{18}O_{sac}$. During MIS 19, the amplitude of I15˚S and precession is very low but with notice that $\delta^{18}O_{sac}$ follow the same trend in the early to mid-phase of MIS 19. We also did the continuous wavelet transform (CWT) and redfit analysis on the data to find out the inherent periodicities in the data. Fig. 5.9 a and b represents the wavelet spectrum and redfit curve respectively.

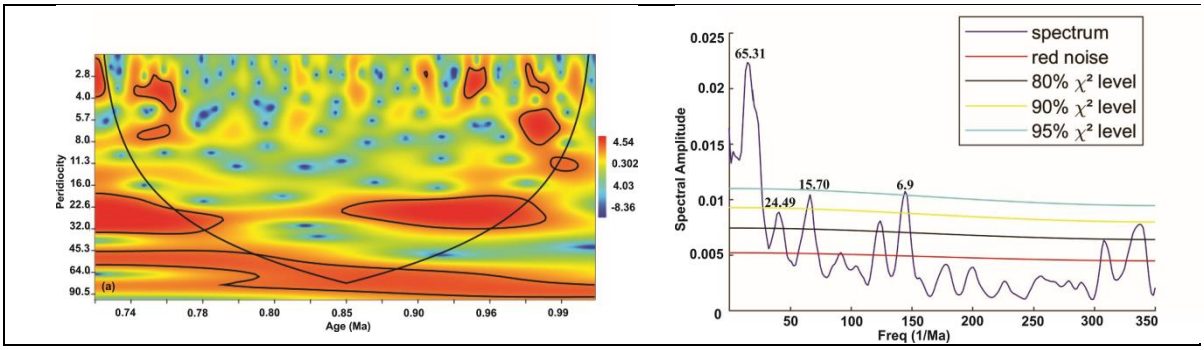

Figure 5.9. Spectral analysis including (a) the CWT and (b) the redfit graph of the $\delta^{18}O_{sac}$.

The redfit analysis shows that periodicities of 65.31 kyr, 24.49 kyr, 15.70 kyr, and 6.9 kyr exits in the data. The periodicities observed possess a significance level of >90%

except for the ~24 kyr. The continuous wavelet transform shows that the ~24 kyr periodicity dominates from 0.97 Ma to 0.85 Ma. The same periodicity is observed during ~0.79 ma to ~0.77 ma. The periodicity of ~65 kyr and ~24 kyr could be explained by precessional cycles. We also find some small scale periodicities of ~ 7 kyr and ~15 kyr which might signify the influence of internal forcings. In conclusion, there is an influence of precession and I15˚S on the South Asian Monsoon. Our new records from the Eastern Arabian Sea reveal and provide evidence that SAM variability is driven by precession. Our record corroborated the findings of Bolton et al., 2013; Gebregiorgis et al., 2018 that the SAsM is sensitive to southern hemisphere warming.

Chapter 6

6. Conclusion and Future Scope

In this chapter, we have summarized and highlighted the main findings presented in the thesis. Here, we also discuss the future requirement and need for more high-resolution studies for improved understanding of the climatic variability during and before Quaternary from the Eastern Arabian Sea.

6.1 Denitrification and South Asian Monsoon (SAsM) variability in the Arabian Sea on the million-year timescale

The denitrification variability in the Arabian Sea is the result of monsoon-induced productivity and ventilation by oxygen-rich southern water masses. We have reconstructed the ***first*** record of $\delta^{15}N$ variability indicating denitrification intensity from the Arabian Sea for the past 10 Myrs (million years). Many studies suggest that the SAM intensified at 8 Ma (million years ago), but we find that SAsM was persistently weak from ~10.2 to 3.1 Ma. Our study reveals that, during the last 10 Myr, the denitrification first appeared at ~3 Ma during the Mid Pliocene Warm Period (MPWP). We also find SAsM intensification during the MPWP. The denitrification declined after MPWP and attained its modern strength by ~1 Ma. The present study, also, suggests that the SAsM intensified parallel to the East Asian Monsoon and therefore their intensification on such long timescales can be ascribed to the same mechanism.

6.2 Variability of Denitrification and South Asian Monsoon during late Quaternary on the multi-millennial timescale

Our high-resolution study during the late Quaternary (~600 to 40 ka; thousand years ago) shows that the denitrification is affected by monsoon-induced productivity and the intrusion of oxygenated southern water masses in the Arabian Sea. We find that denitrification intensified during interglacial and weakened during the glacial periods during the 560 kyr long study period. The comparative study of denitrification variability from the Eastern and Western Arabian Sea for the past ~70 kyr shows similar variability i.e., stronger denitrification during warmer periods and weaker denitrification during colder periods. The ventilation of the intermediate water has a huge impact on the denitrification variability in the northern and eastern Arabian Sea. During the Holocene, the sea level rise causes the influx of the Red Sea Water (RSW) and the Persian Gulf Water (PGW) that inhibits the intrusion of oxygen-rich water from the Southern Ocean resulting in weakening of ventilation of the Northern and eastern Arabian Sea causing increasing denitrification in contrast to the Western Arabian Sea.

6.3 Quantification of Climate Change of Eastern Arabian Sea during Mid Pleistocene Transition (MPT)

We have also carried out the ***first quantification*** of climate change in terms of exact oceanic mixed layer temperature and salinity variability during the MPT from the Arabian Sea. We also looked at the variability of productivity and denitrification during the MPT. The productivity and denitrification was higher during the warmer periods of the MPT accompanied by weaker ventilation. We also compared our record to the productivity and denitrification variability from the Western Arabian

Sea. We found a synchronous variability between the two regions during MPT. For quantifying the hydrography during MPT, we carried out the paired measurement of Mg/Ca and $\delta^{18}O$ of *G. sacculifer*. Our record shows that the MLT varied from 28 °C to as low as ~19 °C with a mean value of ~23 °C. The $\delta^{18}O_{sw}$ and salinity range from ~39 to ~32 units with a mean value of ~36 units. At the study site, low MLT and high salinity occur during the monsoon as shown by the present day climatology. We find high salinity during the warmer periods (MIS 27, 25, 21 and 19) implying intense monsoon. This is supported by the provenance of organic matter from the present study and complemented by the earlier chemical weathering record from the site U1456 (Cai et al., 2019). We carried out the wavelet transform and redfit analysis to find the influence of external and internal forcing. We also find that there is an influence of precession and insolation at 15˚S (I15˚S) on the SAsM. Our newly generated record provides evidence that SAsM variability is driven by precession. We saw a good match of I15˚S with $\delta^{18}O_{sac}$, which corroborates earlier study of upper-ocean stratification from the Southern Indian Ocean. It supports a robust sensitivity to warming in the Southern Hemisphere. The continuous wavelet transform reveals that the ~24 kyr periodicity dominates from 0.97 Ma to 0.85 Ma. The same periodicity is observed during ~0.79 Ma to ~0.77 Ma. The significance of internal forcing might get reflected by small scale periodicities of ~ 7 kyr and ~15 kyr.

Future work

- The span of the present study extends up to 10 Ma and represents the first record of SAsM, denitrification and oceanic productivity variability. However, the resolution of study is ~140 kyr which is quite coarse. To understand the processes associated with SAsM in the Eastern Arabian Sea, the resolution of study should be increased. Higher resolution studies are required for the proper understanding of the climatic history of the Eastern Arabian Sea for long periods spanning the past several million years.

- The climate transitions like MPT (the period where the climatic cyclicity changed from 40 kyr to ~100 kyr) and MPWP (the period where the atmospheric CO_2 content was similar to present) represents very important periods of earth's history and should be addressed with multiproxy studies.

- Studies of late Quaternary climate variability should be complemented by oceanic temperature and salinity changes on a high resolution.

- Many gaps in the record were observed due to mass transport deposit and the drilling disturbances during the operation also caused a considerable gap in the record. IODP drilled some holes/sites without coring which again caused a gap in the record. Thus more studies based on new deep drilling programs should be done to generate continuous record during the Quaternary period.

- The future work shall also include the development of calibration equations for Mg/Ca based paleothermometry in the Arabian Sea for various species of foraminifera. Specific calibration equations for various species dwelling in different depths are required to accurately reconstruct the SST at those depths.

Reference

1. Acharya, S.S and Panigrahi M.K., (2016). Eastward shift and maintenance of Arabian Sea oxygen minimum zone: Understanding the paradox. Deep Sea Research Part I, 115, 240–252.

2. Agnihotri, et al., (2002). Evidence for solar forcing on the Indian monsoon during the last millennium. Earth Planet. Sci. Lett., 198, 521–527.

3. Agnihotri, et al., (2003). Changes in surface productivity, sub-surface denitrification and SW monsoon during the Holocene: A multi proxy record from the eastern Arabian Sea. The Holocene, 13, 701–713.

4. Agnihotri, et al., (2003). Late-Quaternary biogenic productivity and organic carbon deposition in the eastern Arabian Sea. Paleo3, 197, 43–60.

5. Algeo, et al., (2008). Changes in ocean denitrification during Late Carboniferous glacial–interglacial cycles. Nat. Geosci., 1 (10), 709.

6. Altabet, et al, (2002). The effect of millennial-scale changes in Arabian Sea denitrification on Atmospheric CO2. Nature, 415, 159–162.

7. Altabet, et al., (1994a). Sedimentary nitrogen isotopic ratio as a recorder for surface ocean nitrate utilization. Global Biogeochemical Cycles, 8, 103–116.

8. Altabet, et al., (1994b).The use of nitrogen isotopic ratio for reconstruction of past changes in surface ocean nutrient utilization. In: Zahn R, Kaminski M, Labeyrie L, Pedersen TF, editors. Carbon cycling in the Glacial Ocean: Constraints on the Ocean's Role in Global Change. Heidelberg, New York: Springer. pp. 281–306.

9. Altabet, et al., (1995). Climate related variations in denitrification in the Arabian Sea from 15N/14N ratios. Nature, 373: 506–509.

10. Altabet, et al., (1999a).Climatically linked oscillations in Arabian Sea denitrification over the past l m.y.: Implications for the marine N cycle. Paleoceanogr 14 (6): 732–743.

11. Altabet, et al., (1999b). The nitrogen isotope biogeochemistry of sinking particles from the margin of the eastern North Pacific. Deep-Sea Research Part I 46, 655–679.

12. An, et al., (2001). Evolution of Asian monsoons and phased uplift of the Himalaya-Tibetan plateau since Late Miocene times. Nature, 411, 62–66.

13. Anand, et al., (2003). Calibration of Mg/Ca thermometry in planktonic foraminifera from a sediment trap time series. Paleoceanogr, 18.

14. Anderson, D. M. and Prell, W. L., (1993). A 300 kyr record of upwelling off Oman during the late Quaternary: evidence of the Asian southwest monsoon. Paleoceanogr. Paleoclimatol, 8(2), 193-208.

15. Ao, et al., (2016). Late Miocene–Pliocene Asian monsoon intensification linked to Antarctic ice-sheet growth. Earth Planet. Sci. Lett. 444, 75–87.

16. Bange, et al., (2001). Nitrous oxide cycling in the Arabian Sea. J. Geophys. Res, 106, 1053-1066.

17. Bange, et al., (2001). Nitrous oxide emissions from the Arabian Sea: A synthesis. Atmos. Chem. Phys. 1, 61–71.

18. Barker, et al., (2003). A study of cleaning procedures used for foraminiferal Mg/Ca paleothermometry, Geochem Geophy Geosy, 4 (9), 8407.

19. Bé, A.W.H. and Tolderlund, D.S., (1971). Distribution and ecology of living planktonic foraminifera in surface waters of the Atlantic and Indian oceans, in Micropaleontology of Oceans, edited by B. M. Funnell and W. R. Riedel, 105– 149, Cambridge Univ. Press, London.

20. Berger, et al., (1994). Mid-Pleistocene climate shift: the Nansen connection In: Johannessen, et al. (Eds.), The Polar Oceans and Their Role in Shaping the Global Environment, AGU Geophysical Monograph 85, 295-311.

21. Betzler, et al., (2016). The abrupt onset of the modern South Asian Monsoon winds. Sci. Rep, 6, 29838.

22. Billups, K and Schrag, D.P., (2002). Paleotemperatures and ice volume of the past 27 Myr revisited with paired Mg/Ca and 18O/16O measurements on benthic foraminifera. Paleoceanog 17(1): 1003.

23. Bolton, et al. (2013). A 500, 000 year record of Indian summer monsoon dynamics recorded by eastern equatorial Indian Ocean upper water-column structure. Quat. Sci. Rev. 77, 167–180.

24. Böning, P and Bard, E., (2009). Millennial/centennial-scale thermocline ventilation changes in the Indian Ocean as reflected by aragonite preservation and geochemical variations in Arabian Sea sediments. Geochimica et Cosmochimica Acta 73, 6771–6788.

25. Bouvier-Soumagnac et al., (1986). Isotopic composition of a laboratory cultured planktonic foraminifer Implications for paleoclimatic reconstructions Oceanol. Acta, 9. 519-522.

26. Bower, et al., (2000). Character and dynamics of the Red Sea and Persian Gulf outflows. J. Geophys. Res. 105, 6387–6414.

27. Boyer, et al., (2009). World Ocean Database 2009. In: Levitus S (eds) NOAA Atlas NESDIS 66. Washington DC: U.S. Government Printing Office, 216.

28. Boyle, E.A., and Keigwin, L.D., (1982). Deep circulation of the North Atlantic over the last 200,000 years: geochemical evidence. Science, 218 (4574).

29. Brandes, et al., (1998). Isotopic composition of nitrate in the central Arabian Sea and eastern tropical North Pacific: A tracer for mixing and nitrogen cycles, Limnol. Oceanogr., 43, 1680-1689.

30. Brandes, et al., (2007). New developments in the marine nitrogen cycle. Chemical Reviews 107: 577–589.

31. Brock, et al., (1994). A model study of seasonal mixed-layer primary production in the Arabian Sea. In: Lal, D. (Ed.), Biogeochemistry of the Arabian Sea. Indian Academy of Sciences, Bangalore, 65–78.

32. Brodie, et al., (2011a). Evidence for bias in C/N, δ13C and δ15N values of bulk organic matter, and on environmental interpretation, from a lake sedimentary sequence by pre-analysis acid treatment methods. Quat. Sci. Rev. 30, 3076–3087.

33. Brodie, et al., (2011b). Evidence for the biasing by pre-analysis acid preparation methods on δ15N composition of terrestrial and aquatic organic materials. Rapid Commun. Mass Spectrom. 25, 1089–1099.

34. Broecker, W. S., (1982). Glacial to interglacial changes in ocean chemistry. Prog. Oceanogr, 11, 151–197.

35. Broecker, W. S., (1998). Paleocean circulation during the last deglaciation: A bipolar seasaw? Paleoceanog, 13, 119–121.

36. Cabarcos, et al., (2014). Monsoonal dynamics and evolution of the primary productivity in the eastern Arabian Sea over the past 30 ka. Palaeo3. 411, 249–256.

37. Cai, et al., (2019). Depositional history and Indian summer monsoon controls on the silicate weathering of sediment transported to the eastern Arabian Sea: Geochemical records from IODP Site U1456 since 3.8 Ma. Geochemistry, Geophysics, Geosystems, 20.

38. Cai, et al., (2020). Long-term history of sediment inputs to the eastern Arabian Sea and its implications for the evolution of the Indian summer monsoon since 3.7 Ma. *Geological Magazine.* 157, 908-919.

39. Calvert, et al., (1993), Geochemistry of oxic and anoxic sediments: Implications for the geological record, Mar. Geol., 113, 67–88.

40. Calvert, et al., (1995). On the organic carbon maximum on the continental slope of the eastern Arabian Sea. Journal of Marine Research 53, 269–296.

41. Calvert, S. E., and Pedersen, T. F., (1993). Geochemistry of oxic and anoxic sediments: Implications for the geological record, Mar. Geol., 113, 67–88.

42. Canfield, et al., (1994). Factors influencing organic carbon preservation in marine sediments, Chem. Geol., 114, 315–329.

43. Canfield, et al., (2010). A cryptic sulphur cycle in oxygen-minimum-zone waters off the Chilean coast. Science, 330, 1375–1378.

44. Centurioni, et al., (2017). Northern Arabian Sea Circulation-Autonomous Research (NASCar): A research initiative based on autonomous sensors. Oceanography 30 (2), 74–87.

45. Chalk, et al., (2017).Causes of ice age intensification across the MPT.PNAS, 114 (50) 13114-13119.

46. Charles, et al., (1993). Thermodynamic influences on the marine carbon isotope record. Paleoceanog, 8, 691-697.

47. Chen, et al., (2020). Geochemical records of the provenance and silicate weathering/erosion from the eastern Arabian Sea and their responses to the Indian summer monsoon since the Mid-Pleistocene. Paleoceanography and Paleoclimatology, 35, 2019 PA 003732.

48. Chowdary, et al., (2007). Water mass property and transports in the Arabian Sea form Argo Observations. Journal of Atmospheric & Ocean Science, 10, 235–260.

49. Christensen, et al., (1994). Carbon export from continental shelves, denitrification and atmospheric carbon-dioxide. Cont. Shelf Res., 14, 547– 576.

50. Clark, et al., (2006). The middle Pleistocene transition: characteristics, mechanisms, and implications for long-term changes in atmospheric pCO2. Quat. Sci. Rev. 25, 3150-3184.

51. Clark, P.U., and Mix, A.C., (2002). Ice sheets and sea level of the last glacial maximum. Quat. Sci. Rev., 21, 1-7.

52. Clark, P.U., Pollard, D., (1998). Origin of the middle Pleistocene transition by ice sheet erosion of regolith. Paleoceanography 13, 1–9.

53. Clemens, et al., (1996). Non-stationary phase of the Plio-Pleistocene Asian monsoon. Science, 274 (5289), 943-948.

54. Clemens, S., Prell, W., (2003). A 350,000 year summer-monsoon multiproxy stack from the Owen Ridge, Northern Arabian Sea. Mar. Geol. 201, 35-51.

55. Clift, et al., (2008). Correlation of Himalayan exhumation rates and Asian monsoon intensity. Nature geoscience, 1, 875–880.

56. CLIMAP Project Members, The Ice Age Ocean, Science 191 (1976) 1131.

57. Cocco, et al., (2013) Oxygen and indicators of stress for marine life in multi-model global warming projections. Biogeosciences, 10, 1849–1868.

58. Codispoti, et al., (1976). An analysis of the horizontal regime of denitrification in the eastern tropical North Pacific. Limnol. Oceanogr., 21, 379-388.

59. Coplen, T.B., (2011), Guidelines and recommended terms for expression of stable-isotope-ratio and gas-ratio measurement results: Rapid Communications in Mass Spectrometry, 25, 2538-2560.

60. Cowie et al., (2014). Aqueous geochemistry and stable isotope ratios as a predictive risk management tool for assessing vertical hydraulic connectivity during oil sands resource development in the Athabasca region. Geoconvention 2014: Focus, Calgary, AB. May 12−16.

61. Craig, H., (1961). Isotopic variations in meteoric waters. Science, 133, 1702–1703.

62. Curry, W.B., Lohmann, G.P., (1982). Carbon isotopic changes in benthic foraminifera from the Western South Atlantic: Reconstruction of glacial abyssal circulation patterns. Quaternary Research, 18 (2), 218-235.

63. Deer, et al., (1992). An Introduction to the Rock Forming Minerals, 2 ed., Addison-Wesley-Longman, Reading, Mass., 1992.

64. Dekens, et al., (2002). Core top calibration of Mg/Ca in tropical foraminifera: Refining paleotemperature estimation, Geochem. Geophys. Geosyst., 3(4), 1022.

65. Delaney, et al., (1985). Li, Sr, Mg, and Na in foraminiferal calcite shells from laboratory culture, sediment traps, and sediment cores, Geochim. Cosmochima Acta, 49(6), 1327–1341.

66. Derry, et al., (1996). Neogene Himalayan weathering history and river 87Sr/86Sr: impact on the marine Sr record. Earth Planet. Sci. Lett. 142, 59–74.

67. Deuser, et al., (1978). Evidence for rate of denitrification in the Arabian Sea. Deep-Sea Research 25, 431–445.

68. Deutsch, et al., (2004). Isotopic constraints on glacial/interglacial changes in the oceanic nitrogen budget, Global Biogeochem. Cycles, 18, GB4012.

69. Deutsch, et al., (2007). Spatial coupling of nitrogen inputs and losses in the ocean, Nature, 445, 163– 167.

70. Duplessy, et al., (1991). Surface Salinity Reconstruction of the North-Atlantic Ocean during the Last Glacial Maximum. Oceanol Acta, 14, 311-324.

71. Dwyer, et al., (1995). North Atlantic deep water temperature change during Late Pliocene and Late Quaternary climatic cycles. Science 270: 1347–1351.

72. Eggins, et al., (2003). 'Mg/Ca variation in planktonic foraminifera tests: implications for reconstructing paleo-seawater temperature and habitat migration', Earth and Planetary Science Letters. 212. 291-306.

73. Elderfield, et al., (2000). Sr/Ca in multiple species of planktonic foraminifera: Implications for reconstructions of seawater Sr/Ca. Geochemistry, Geophysics, Geosystems 1(11): 1017.

74. Elderfield, et al., (2006). Calibrations for benthic foraminiferal Mg/Ca paleothermometry and the carbonate ion hypothesis. Earth and Planetary Science Letters 250, 633–649

75. Elderfield, et al., (2012). Evolution of ocean temperature and ice volume through the mid-Pleistocene climate transition. Science, 337 (6095), 704–709.

76. Elderfield, H., and Ganssen, G., (2000). Past temperature and □18O of surface ocean waters inferred from foraminiferal Mg/Ca ratios. Nature 405, 442–445.

77. Emerson, et al., (1988). Processes controlling the organic carbon content of open ocean sediments. Paleoceanog, 3,621–634.

78. Emery, W.J, and Meincke, J., (1986). Global water masses: summary and review. Oceanologica Acta 9: 383–391.

79. Emiliani, C., (1971). Depth habitats and growth stages of pelagic formanifera. Science, 173, 1122–1124.

80. Emrich, et al., (1970). Carbon isotope fractionation during the precipitation of calcium carbonate. Earth Planet. Sci. Lett., 8, 363– 371.

81. Erez, J., (2003). The source of ions for biomineralization in foraminifera and their implications for paleoceanographic proxies. Rev. Mineral. Geochem.54, 115–149.

82. Erez, J., and Luz, B., (1983). Experimental paleotemperature equation for planktonic foraminifera. Geochimica et Cosmochimica Acta, 47, 1025–1031.

83. Fairbanks, et al., (1989). A 17,000-year glacio-eustatic sea level record: influence of glacial melting rates on the Younger Dryas event and deep-ocean circulation. Nature 342, 637–642.

84. Farmer, et al., (2007). Corroborating ecological depth preferences of planktonic foraminifera in the tropical Atlantic with the stable oxygen isotope ratios of core top specimens, Paleoceanog, 22, PA3205.

85. Farquhar, et al., (1989). Carbon isotope discrimination and photosynthesis. Ann. Rev. Plant Physiol. Plant Molecul. Biol. 40, 503–537.

86. Field, et al., (1998), Primary production of the biosphere: Integrating terrestrial and oceanic components, Science, 281, 237–240

87. Fontugne, et al., (1992). Late Pleistocene variability of the carbon isotopic composition of organic matter in the eastern Mediterranean: monitor of changes in carbon sources and atmospheric CO2 levels. Paleoceanog, 7, 1–20.

88. Fralick, P. W., and Kronberg, B. I., (1997). Geochemical discrimination of clastic sedimentary rock sources. Sedimentary Geology, 113(1-2), 111–124.

89. Francois, R., (1988). A study on the regulation of the concentrations of some trace metals (Rb, Sr, Zn, Pb, Cu, V, Cr, Ni, Mn, and Mo) in Saanich Inlet sediments, British Columbia, Canada. Marine Geo. 83, 285–308.

90. Fry, B, and Sherr, E. B., 1984. □13C measurements as indicators of carbon flow in marine and freshwater ecosystems. Contributions in Marine Science 27, 13-47.

91. Gaillardet, et al., (1999). Global silicate weathering and CO2 consumption rates deduced from the chemistry of large rivers. Chemical Geology, 159(1-4), 3–30.

92. Ganeshram, et al., (1995). Large changes in oceanic nutrient inventories from glacial to interglacial periods. Nature, 376, 755–758.

93. Ganeshram, et al., (2000). Glacial– interglacial variability in denitrification in the world's oceans: Causes and consequences. Paleoceanography, 15,361–376.

94. Garzanti, et al., (2014). Provenance versus weathering control on the composition of tropical river mud (southern Africa). Chemical Geology, 366, 61–74.

95. Gauns, et al., (2005). Comparative accounts of biological productivity characteristics and estimates of carbon fluxes in the Arabian Sea and the Bay of Bengal. Deep Sea Research. Part II, Topical Studies in Oceanography, 52(14-15), 2003–2017.

96. Gaye, et al., (2018). Glacial–interglacial changes and Holocene variations in Arabian Sea denitrification. Biogeosciences, 2018, 15(2), 507-527.

97. Gaye-Haake, et al., (2005). Stable nitrogen isotopic ratios of sinking particles and sediments from the northern Indian Ocean. Mar. Chem. 96, 243–255.

98. Gebregiorgis, et al., (2018). Southern Hemisphere forcing of South Asian monsoon precipitation over the past ~1 million years. Nature Communications, 9 (1), 4702.

99. Gonfiantini, R., (1981). The-notation and the mass-spectrometric measurement techniques. Stable Isotope Hydrology, Deuterium and Oxygen-18 in the Water Cycle (J.R. Gat, R. Gonfiantini, Eds) Technical Reports Series No. 210, IAEA, Vienna, Chapter 4, 35–84.

100. Groeneveld, et al., (2011). Mg/Ca of Globorotalia inflata as a recorder of permanent thermocline temperatures in the South Atlantic, Paleoceanog, 26, PA2203.

101. Grootes, P. M., and Stuiver, M., (1997). Oxygen 18/16 variability in Greenland snow and ice with 103 to 105-year time resolution. J. Geophy. Res. - Oceans, 102 (C12), 26455-26470.

102. Grossman, E.L., (1984). Carbon isotopic fractionation in live benthic foraminifera - comparison with inorganic precipitate studies. Geochim. Cosmochim. Acta, 48, 1505–1512.

103. Gupta, et al., (2011). East–West similarities and differences in the surface and deep northern Arabian Sea records during the past 21 kyr. Palaeo3, 301: 75–85.

104. Gupta, et al., (2015). A. Evolution of the South Asian monsoon wind system since the late Middle Miocene. Palaeog3, 438, 160–167.

105. Haass, et al., (2018). Productivity changes across the mid-Pleistocene climate transition. Earth-Science Reviews, 179, 372–391.

106. Haley, B.A, and Klinkhammer, G.P., (2002). Development of a flow-through system for cleaning and dissolving foraminiferal tests. Chem Geo, 185, 51–69.

107. Hastings et al., (1998). Foraminiferal magnesium in G. sacculifer as a paleotemperature proxy. Paleoceanog, 13, 161–169.

108. Haug, et al., (1998). Glacial/interglacial variations in production and nitrogen fixation in the Cariaco Basin during the last 580 kyr, Paleoceanog, 13, 427– 432.

109. Hays, et al., (1976). Variations in the earth's orbit: Pacemakers of the ice ages. Science, 194, 1121–1132.

110. Haywood, et al., (2016). Integrating geological archives and climate models for the mid-Pliocene warm period. Nat. Commun. 7, 1–14.

111. Head, et al., (2008). The Early Middle Pleistocene Transition: characterization and proposed guide for the defining boundary. Episodes, 31 (2), 255-259.

112. Hemleben, et al., (1989). Modern Planktonic Foraminifera, Springer Verlag, Berlin.

113. Henrichs, S.M., (1993). Early diagenesis of organic matter: the dynamics (rates) of cycling of organic compounds. In: Engel MH, Macko SA (eds) Organic geochemistry: principles and applications. Plenum, New York, p 101.

114. Herbert, et al., (2010). Tropical ocean temperatures over the past 3.5 million years. Science 328 (5985), 1530–1534.

115. Hong, et al., (2003). Correlation between Indian Ocean summer monsoon and North Atlantic climate during the Holocene. Earth Planet Sci. Lett. , 211(3-4), 371-380.

116. Huang, et al., (2007). Large-scale hydrological change drove the late Miocene C4 plant expansion in the Himalayan foreland and Arabian Peninsula. Geology 35, 531–534.

117. Hönisch, et al., (2009). Atmospheric carbon dioxide concentration across the mid-Pleistocene transition. Science 324, 1551–1554.

118. Imbrie, et al., (1993). On the structure and origin of major glacial cycles. Part 2. The 100,000-year cycle. Paleoceanog, 8, 699–736.

119. Ishiwatari, R., and Uzaki, M., (1987). Diagenetic changes of lignin compounds in more than 0.6 million-year-old lacustrine sediment (Lake Biwa, Japan). Geochimica et Cosmochimica Acta, 51, 321–328

120. Ivanochko, et al., (2005). Variations in tropical convection as an amplifier of global climate change at the millennial scale. Earth Planet Sci. Lett. , 235 (1-2), 302-314.

121. Izuka, S.K., (1988). Relationships of magnesium and other minor elements in tests of Cassidulina subglobosa and C. Oriangulata to physical oceanic properties. Journal of Foraminiferal Research 18, 151–157.

122. Jenkyns, et al., (2001). Nitrogen isotope evidence for water mass denitrification during the early Toarcian (Jurassic) oceanic anoxic event. Paleoceanogr, 16(6), 593–603.

123. Jensen, et al., (2011). Intensive nitrogen loss over the Omani Shelf due to anammox coupled with dissimilatory nitrite reduction to ammonium. ISME J 5, 1660–1670.

124. Johannessen, et al., (1994). The relationship between surface water masses, oceanographic fronts and paleoclimatic proxies in surface sediments of the Greenland, Iceland, Norwegian Seas Zahn R., Pedersen T.F., Kaminski M.A., Labeyrie L. (Eds.), Carbon Cycling in the Glacial Ocean: Constraints on the Oceans's Role in Global Change, Springer, Berlin (1994), pp. 61-85

125. Johns, et al., (2000). Arabian marginal seas and gulfs: report of a workshop held at Stennis Space Center, Mississippi, 11–13 May, 1999. Technical Report, 60.

126. Jung, et al., (2009). Enhanced Arabian Sea intermediate water flow during glacial North Atlantic cold phases. Earth Planet Sci. Lett., 280 (1-4), 220-228.

127. Karl, et al., (2002). Dinitrogen fixation in the world's oceans. Biogeochemistry, 57/58, 47–98.

128. Keeling, et al., (2010). Ocean deoxygenation in a warming world. Annual Review of Marine Science 2: 199–229.

129. Kemle-von, M.S., and Hemleben, C., (1999). Foraminifera. In: South Atlantic Zooplankton. Boltovskoy D (ed.) Backhuys Publishers, Leiden, 43–73.

130. Kessarkar, et al., (2010). Fluctuations in productivity and denitrification in the southeastern Arabian Sea during the Late Quaternary, Curr. Sci., 99, 485–491.

131.Khim, et al., (2019). Variations in δ13C values of sedimentary organic matter since late Miocene time in the Indus Fan (IODP Site 1457) of the eastern Arabian Sea. Geological Magazine.

132.Kiel et al., (1994). Sorptive preservation of labile organic matter in marine sediments. Nature., 370, 549–552.

133. Kiel et al., (1997). Loss of organic matter from riverine particles in deltas Geochimica et Cosmochimica Acta. 61, 1507-1511.

134. Kiel et al., (1999). Organic matter preservation through the oxygen-deficient zone of the NE Arabian Sea as discerned by organic carbon: mineral surface area ratios. Marine Geo, 161, 13-22.

135.Kim, et al., (2018). Orbital-scale denitrification changes in the Eastern Arabian Sea during the last 800kyrs. Sci Reports, 8 7027.

136.Koutavas, et al., (2002) El Nin˜o-like pattern in Ice Age tropical Pacific sea surface temperature. Science 297: 226–230.

137.Kroon, et al., (1991). Onset of monsoonal related upwelling in the western Arabian Sea. In: Prell, W. L. et al. (eds) Proceedings of the ODP Sci. Results. 117, 257–264.

138.Kroopnick, P., (1980). The distribution of 13C in the Atlantic Ocean, Earth Planet. Sci. Lett., 49(2), 469–484.

139. Kustka, et al., (2003). Iron requirements for dinitrogen- and ammonium- supported growth in cultures of Trichodesmium (IMS 101): Comparison with nitrogen fixation rates and iron: Carbon ratios of field populations, Limnol. Oceanogr., 48, 1869–1884.

140. Kutzbach, (1981). Monsoon climate of the early Holocene: climate experiment with Earth's orbital parameters for 9000 years ago. Science, 214, 59–61.

141. Labeyrie, et al., (1987). Variations in mode of formation and temperature of oceanic deep waters over the past 125,000 years. Nature, 327, 477-482.

142. Labeyrie, et al., (1987). Variations in mode of formation and temperature of oceanic deep waters over the past 125 000 years. Nature, 327, 477–482.

143. Lane and Dole, (1956). Fractionation of oxygen isotopes during respiration, Science, 123 (3197), 574-576.

144. Lane, G. A., and Doyle, M., (1956) Fractionation of oxygen isotopes during respiration; Science, 123, 574.

145. Langen, et al., (2005). Effects of temperature on Mg/Ca in Neogloboquadrina shells determined by living culture. Geochemistry, Geophysics, Geosystems 6, Q10P03.

146. Larsen, et al., (1994). Seven Million Years of Glaciation in Greenland. Science, 264, 952-955.

147. Lea, et al., (1999). Controls on magnesium and strontium uptake in planktonic foraminifera determined by live culturing. Geochimica et Cosmochimica Acta 63, 2369–2379.

148.Lea, et al., (2000). Climate impact of late quaternary equatorial Pacific sea surface temperature variations. Science 289, 1719–1724.

149.Lear, et al., (2002). Benthic foraminiferal Mg/Ca paleothermometry: a revised core-top calibration. Geochim. Cosmochim. Acta 66, 3375-3387.

150.Lear, et al., (2016). Breathing more deeply: deep ocean carbon storage during the mid-Pleistocene climate transition. Geology 44, 12.

151.Levin, et al., (2003). Oxygen minimum zone benthos: Adaptation and community response to hypoxia. Oceanography and Marine Biology: An Annual Review 41, 1–45.

152.Limmer, et al., (2012). Geochemical record of Holocene to recent sedimentation on the western Indus continental shelf, Arabian Sea. Geochemistry, Geophysics, Geosystems, 13, Q01008.

153.Lisiecki, L. E., and M. E. Raymo (2005). A Pliocene-Pleistocene stack of 57 globally distributed benthic □18O records, Paleoceanog, 20, PA1003.

154.Liu, et al., (1989). The eastern tropical Pacific as a source of 15N-enriched nitrate in seawater off southern California. Limnol. Oceanogr. 34, 820–830.

155.Liu, X., and Shi, Z., (2009). Effect of precession on the Asian summer monsoon evolution: a systematic review. Chin. Sci. Bull. 54, 3720-3730.

156.Luthi, et al., (2008). High-resolution carbon dioxide concentration record 650,000–800,000 years before present. Nature 453, 379–382.

157. Mackensen, et al., (1993). The δ13C in benthic foraminiferal tests of Fontbotia wuellerstorfi (Schwager) relative to the δ13C of dissolved inorganic carbon in Southern Ocean deep water: Implications for glacial ocean circulation models, Paleoceanog, 8, 587– 610.

158. Mackenzie, et al., (1980). Molecular parameters of maturation in the Toarcian shales, Paris Basin, France: I. Changes in configuration of acyclic isoprenoid alkanes, steranes and triterpanes. Geochimica et Cosmochimica Acta 44, 1709–1721.

159. Madhupratap, et al., (1996). Mechanism of the biological response to winter cooling in the north eastern Arabian Sea. Nature 384, 549–552.

160. Mahesh, et al., (2014). Change in the intensity of low-salinity water inflow from the Bay of Bengal into the Eastern Arabian Sea from the Last Glacial Maximum to the Holocene: Implications for monsoon variations. Palaeo3. 397, 31–37.

161. Manheim, et al., (1974). Composition and origin of interstitial waters of marine sediments, based on deep sea drill cores: In The Sea, Ideas and Observations (Edited by Goldberg, E. D.), 5, pp. 527-568. (Sillen Memorial). Wiley-Interscience, New York.

162. Marchitto, et al., (2007) Mg/Ca temperature calibration for the benthic foraminifer Cibicidoides pachyderma. Paleoceanog 22, PA1203.

163. Martin, et al., (2002). Quaternary deep sea temperature histories derived from benthic foraminiferal Mg/Ca. Earth and Planetary Science Letters 198, 193–209.

164. Martin, P.A, and Lea, D.W., (2002). A simple evaluation of cleaning procedures on fossil benthic foraminiferal Mg/Ca. Geochemistry, Geophysics, Geosystems 3, 8401.

165. Martinez-Garcia, et al., (2009). Links between iron supply, marine productivity, sea surface temperature, and CO2 over the last 1.1 Ma. Paleoceanog 24, PA1207.

166. Mashiotta, et al., (1999). Glacial-interglacial changes in Subantarctic sea surface temperature and □18O-water using foraminiferal Mg. Earth and Planetary Science Letters 170: 417–432.

167. Mashiotta, et al., (1999). Glacial-interglacial changes in Subantarctic sea surface temperature and d18O-water using foraminiferal Mg. Earth and Planetary Science Letters 170: 417–432.

168. Maslin, et al., (1998). The contribution of orbital forcing to the progressive intensification of Northern Hemisphere Glaciation. Quaternary Science Reviews 17, 411-426.

169. Maslin, et al., (2005). Mid-Pleistocene Revolution and the Eccentricity Myth. In: Special Publication of the Geological Society of London, 247, pp. 19-34.

170. McClain et al., (2004). Subtropical gyre variability observed by ocean-colour satellites, Deep Sea Res., Part II, 51(1–3), 281–301.

171. McConnaughey, (1989b). 13C and 18O isotopic disequilibrium in biological carbonates: II. In vitro simulation of kinetic isotope effects Geochim. Cosmochim. Acta, 53, pp. 163-171.

172. McConnaughey, (1989a). 13C and 18O isotopic disequilibrium in biological carbonates: I. Patterns Geochim. Cosmochim. Acta, 53, pp. 151-162.

173. McConnell MC and Thunell RC (2005) Calibration of the planktonic foraminiferal Mg/Ca paleothermometry: Sediment trap results from the Guaymas Basin, Gulf of California. Paleoceanography 20: PA2016.

174. McCorkle, et al., (1990). The influence of microhabitats on the carbon isotopic composition of deep-sea benthic foraminifera, Paleoceanography, 5, 161– 185.

175. McCreary et al., (2013). Dynamics of the Indian-Ocean oxygen minimum zones. Progress in Oceanography, 112-113, 15–37.

176. Mehta, V. and Lau, K. M., (1997). Influence of solar irradiance on the Indian monsoon-ENSO: Relationship at decadal-multidecadal timescales. Geophys. Res. Lett., 24, 159–162.

177. Meyers, et al., (1996). Organic matter in Pleistocene to Quaternary turbidites from Site 897, 898, 899, and 900, Iberia Abyssal Plain. In Whitmarsh, R.B., Sawyer, D.S., Klaus, A., and Masson, D.G. (Eds.), Proc. ODP, Sci. Results, 149: College Station, TX (Ocean Drilling Program), 305–313.

178. Meyers, P. A. (1994). Preservation of elemental and isotopic source identification of sedimentary organic matter. Chem Geol. 114, 289–302.

179. Miller, et al., (2012). High tide of the warm Pliocene: Implications of global sea level for Antarctic deglaciation. Geology, 40 (5), 407-410.

180. Mills, et al., (2004). Iron and phosphorus co-limit nitrogen fixation in the eastern tropical North Atlantic, Nature, 429, 292– 294.

181. Mitsuguchi, et al., (1996). Mg/Ca thermometry in coral skeletons. Science, 274, 961–963.

182. Mix, A. C., (1989), Influence of productivity variations on long-term atmospheric CO2, Nature, 337, 541–544.

183. Molnar, et al., (2010). Orographic Controls on Climate and Paleoclimate of Asia: Thermal and Mechanical Roles for the Tibetan Plateau. Annu. Rev.Earth Planet. Sci. 38, 77–102.

184. Mucci, A., (1980). The solubility of calcite and aragonite in seawater at various salinities, temperatures and atmosphere total pressure. American Journal of Science, 283, 780-799.

185. Mudelsee, et al., (1997). The Mid-Pleistocene climate transition: onset of 100 ka cycle lags ice volume build up by 280 ka. Earth and Planetary Sci Lett, 151, 117-123.

186. Mudelsee, M., and Schulz, M., (1997). The Mid-Pleistocene climate transition: onset of 100 ka cycle lags ice volume build-up by 280 ka. Earth Planet. Sci. Lett. 151 (1–2), 117–123.

187. Müller, P.J, and Suess, E., (1979). Productivity, sedimentation rate, and sedimentary organic matter in the oceans. I. Organic carbon preservation. Deep Sea Res. 26,1347–1362.

188. Müller, P.J., (1977). C/N ratios in Pacific deep sea sediments: effect of inorganic ammonium and organic nitrogen compounds sorbed by clays. Geochim. Cosmochim. Acta, 41:765–776.

189.Munk, W., (1950) .On the wind-driven Ocean circulation J. Meteorol., 7 (2).

190.Nagoji, et al., (2017). Organic carbon preservation in Southeastern Arabian Sea sediments since mid-Holocene: Implications to South Asian Summer Monsoon variability. Geochem. Geophys , 18(9), 3438-3451.

191.Naidu, P.D., (1993). Distribution patterns of Recent planktonic foraminifera in surface sediments of the western continental margin of India. Marine Geology,Vol 110, 3–4, Pages 403-418

192.Naidu, P.D., and Malmgren A.B., (1995). Do benthic foraminifer records represent a productivity index in oxygen minimum zone areas? An evaluation from the Oman Margin, Arabian Sea. Marine Micropaleontology. 26, 49–55.

193.Nair, et al., (1989). Increased particle flux to the deep ocean related to monsoons. Nature 338, 749–751.

194.Naqvi S.W.A., (1987). Some aspects of the oxygen deficient conditions and denitrification in the Arabian Sea. Marine Res., 29, 459–469.

195.Naqvi, et al., (2006). Coastal biogeochemical processes in the North Indian Ocean. In: A. Robinson and K. Brink, editors, The Sea, Vol. 14, Harvard University Press, pp. 723-780.

196.Naqvi, et al., (2010). Marine hypoxia/anoxia as a source of CH4 and N2O. Biogeosciences 7, 2159–2190.

197.Naqvi, S. W. A., (1991). Geographical extent of denitrification in the Arabian Sea in relation to some physical processes. Oceanol. Acta 14, 281–290.

198.Niitsuma et al., (1991). Oxygen and carbon isotope stratigraphy at site 723, Oman margin. Proc. Ocean Drilling Prog., Sci. Results, 117, 321-341.

199.Nürnberg, et al., (1996). Assessing the reliability of magnesium in foraminiferal calcite as a proxy for water mass temperatures, Geochimica et Cosmochimica Acta, 60(5), 803-814.

200.O'Leary, et al., (1980). Diffusional contribution to carbon isotope fractionation during dark CO2 fixation in CAM plants. Plant Physiol. 66, 931-934.

201.O'Leary, M. H. (1981). Carbon isotope fractionation in plants. Phytochemistry 20, 553- 567.

202.Olson et al., (1993). Maintenance of the low-oxygen layer in the central Arabian Sea. Deep Sea Res.-II, 40 (3), 673-585.

203.Oppo D.W, and Fairbanks R.G, (1989). Carbon isotope composition of tropical surface water during the past 22,000 years. Paleoceanog, 333-351.

204.Ostrom, et al., (1998), Temporal trends in nitrogen isotope values of nitrate leaching from an agricultural soils, Chem. Geol. Isotope Geosci., 146, 219– 227.

205.Pagani, et al., (2012) High Earth-system climate sensitivity determined from Pliocene carbon dioxide concentrations. Nat. Geosci., 3 (1), 27.

206.Pahnke, et al., (2003) 340,000-year centennial-scale marine record of Southern Hemisphere climatic oscillation. Science 301, 948–952.

207.Pandey, et al., (2016). Site 1456. In The Proceedings of the International Ocean Discovery Program 355, 1–61.

208. Parkes, et al., (1994). Deep bacterial biosphere in Pacific Ocean sediments. Nature 371, 410–413.

209. Parkes, J. R. et al. Deep bacterial biosphere in Pacific Ocean sediments. Nature 371, 410–413 (1994).

210. Pattan, et al., (2003). Productivity fluctuations in the southeastern Arabian Sea during the last 140 ka. Palaeo3, 3052, 1–16.

211. Pattan, et al., (2005). Variations in terrigenous sediment discharge in a sediment core from southeastern Arabian Sea during the last 140 ka. Current Science 89, 1421–1425.

212. Paulmier, A., and Ruiz-Pino, D., (2009). Oxygen minimum zones (OMZs) in the modern ocean. Progress in Oceanography, 80(3-4), 113–128.

213. Paulmier, et al., (2011). CO2 maximum in the Oxygen Minimum Zone (OMZ). Biogeosci 8, 239–252.

214. Peltier, W.R, and Fairbanks, R.G., (2006). Global glacial ice volume and last glacial maximum duration from an extended Barbados Sea level record Quat. Sci. Rev., 25 (23–24) 3322-333.

215. Pena, L.D., and Goldstein, S.L., (2014). Thermohaline circulation crisis and impacts during the mid-Pleistocene transition. Science 345, 318–322.

216. Petit, et al., (1999). Climate and atmospheric history of the past 420,000 years from the Vostok ice Core, Antarctica. Nature, 399 (6735), 429-436.

217. Pichevin, et al., (2007). Evidence of ventilation changes in the Arabian Sea during the late Quaternary: Implication for denitrification and nitrous oxide emission, Global Biogeochem. Cycles, 21, GB4008.

218. Pierre, et al., (1991). Oxygen and carbon stable isotope tracers of the water masses in the Central Brazil Basin. Deep Sea Res. Part A, 38(5), 597-606.

219. Pisias, et al., (1981). The evolution of Pleistocene climate: a time series approach. Earth Planet. Sci. Lett. 52, 450-458.

220. Poli, et al., (2012), Glacial-interglacial variations in sediment organic carbon accumulation and benthic foraminiferal assemblages on the Bermuda Rise (ODP Site 1063) during MIS 13 to 10, Paleoceanog, 27, PA3216.

221. Popp et al., (1997). Organic carbon variation in sedimentary rocks as chemostratigraphic and paleoenvironmetal tools. Palaeo3. 132, 119–132.

222. Popp, et al., (1997). Organic carbon variation in sedimentary rocks as chemostratigraphic and paleoenvironmetal tools. Palaeo3. 132, 119–132.

223. Pous, et al., (2004). Hydrology and circulation in the Strait of Hormuz and the Gulf of Oman results from the GOG P99 experiment: 1.Strait of Hormuz. J. Geophys. Res. 109, C12037.

224. Prahl, et al., (1980). The early diagenesis of aliphatic hydrocarbons and organic matter in sedimentary particulates from Dabob Bay, Washington. Geochim. Cosmochim. Acta 44, 1967-1976.

225.Prahl, et al., (1994). An assessment of terrestrial organic carbon contributions to Washington coastal sediments. Geochim. Cosmochim. Acta 58, 3035-3048.

226.Prasad, et al., 2001. Seasonal spreading of the Persian Gulf water mass in the Arabian Sea. J. Geophys. Res. 106, 17059–17073.

227.Prasanna, K. S. & Prasad, T. G. Formation and spreading of Arabian Sea high-salinity water mass. J. Geophys Res. 104, 1455–1464 (1999).

228.Prell, et al., (1986). Graphic correlation of oxygen isotope stratigraphy: Application to the Late Quaternary, Paleoceanog, 1, 137–162.

229.Prell, W.L., (1984). Monsoonal climate of the Arabian Sea during the late Quaternary: a response to changing solar radiation. In: Berger, A.L., et al. (Eds.), Milankovitch and Climate, Part I. D. Reidel Publishing Company, London, 349–366.

230.Premchand, et al., (1986). Water mass structure in the Western Indian Ocean- Part 2: The spreading and transformation of the Persian Gulf Water. Mausam, 37, 179–186.

231.Premuzic, et al., (1982). The nature and distribution of organic matter in the surface sediments of world oceans and seas. Org. Geochem. 4,63-77.

232.Qasim S. Z., (1982). Oceanography of the northern Arabian Sea. Deep Sea Res, 29, 1041–1068.

233.Qasim, S.Z., (1977). Biological productivity of the Indian Ocean. Indian Journal of Marine Sciences 6, 122–137.

234.Quade, et al., (1989). Development of Asian monsoon revealed by marked ecological shift during the latest Miocene in northern Pakistan. Nature 342, 163–165.

235. Rathburn, A.E., and De Deckker, P., (1997). Magnesium and strontium compositions of recent benthic foraminifera from the Coral Sea, Australia and Prydz Bay, Antarctica. Marine Micropaleontology 32, 231–248.

236. Redfield, et al., (1963). The influence of organisms on the composition of seawater, in The Sea, edited by M. N. Hill, 26-77, Wiley Inter sci., Hoboken, N. J.

237. Reichart, et al., (1997). A 225 kyr record of dust supply, paleoproductivity and the Oxygen Minimum Zone from the Murray Ridge (Northern Arabian Sea). Palaeo3 134, 149–169.

238. Reichart, et al., (1998). Temporal variability in the northern Arabian Sea Oxygen Minimum Zone (OMZ) during the last 225,000 years. Paleoceanog 13(6), 607–621.

239. Resplandy, et al., (2012). Controlling factors of the oxygen balance in the Arabian Sea's OMZ. Biogeosciences, 9 (12), 5095–5109.

240. Revsbech, et al., (2009). Determination of ultra-low oxygen concentrations in oxygen minimum zones by the STOX sensor. Limnol Oceanogr Methods 7, 371–381.

241. Reynolds, R.M., (1993).Physical oceanography of the Gulf, Strait of Hormuz, and the Gulf of Oman-results from the Mt Mitchell expedition. Mar.Pollut.Bull. 27, 35-59.

242. Robinson, et al., (2012). A review of nitrogen isotopic alteration in marine sediments. Paleoceanog 27.

243. Rochford, D. J. Salinity maximum in the upper 100 meters of the north Indian Ocean. Aust. J. Mar. Freshwater. Res. 15, 1–24 (1964).

244. Rosenthal et al., (2000) Incorporation and preservation of Mg in G. sacculifer implications for reconstructing the temperature and 18O/16O of seawater. Paleoceanog 15, 135–145.

245. Rosenthal, et al., (1997). Temperature control on the incorporation of Mg, Sr, F and Cd into benthic foraminiferal shells from Little Bahama Bank: Prospects for thermocline paleoceanography. Geochimica et Cosmochimica Acta 61, 3633-3643.

246. Rosenthal, et al., (1999), Precise determination of element/calcium ratios in calcareous samples using sector field inductively coupled plasma mass spectrometry, Analytical Chemistry, 71(15), 3248-3253.

247. Rosenthal, et al., (2000). Incorporation and preservation of Mg in Globigerinoides sacculifer: Implications for reconstructing the temperature and O-18/O-16 of seawater, Paleoceanog, 15, 135-145.

248. Rosenthal, et al., (2002). Accurate estimation of sea surface temperatures using dissolution corrected calibrations for Mg/Ca paleothermometry. Paleoceanog 17, 1044.

249. Rosenthal, et al., (2004). Interlaboratory comparison study of Mg/Ca and Sr/Ca measurements in planktonic foraminifera for paleoceanographic research, Geochem Geophy Geosy, 5.

250. Rosenthal, et al., (2006). Temperature and carbonate ion effects on Mg/Ca and Sr/Ca ratios in benthic foraminifera: Aragonitic species Hoeglundina elegans. Paleoceanog 21, PA1007.

251. Rostek, et al., (1997). Sea surface temperature and productivity records for the past 240 kyr in the Arabian Sea. Deep-Sea Res II 44 (6–7), 1461–1480.

252. Ruddiman, W., (2006). What is the timing of orbital-scale monsoon changes? Quat. Sci. Rev. 25, 657-658.

253. Rullkötter. J. (2006) Organic matter: driving force for early diagenesis. In (ed. Schulz, H. D., Zabel, M.) Marine geochemistry, Springer, Berlin, 125–206.

254. Russell, et al., (2004). Effects of seawater carbonate ion concentration and temperature on shell U, Mg, and Sr in cultured planktonic foraminifera. Geochimica et Cosmochimica Acta 68, 4347–4361.

255. Saher et al., (2009). Western Arabian Sea SST estimation. PANGAEA.

256. Saino, T and Hattori, A., (1987), Geographical variation of the water column distribution of suspended particulate organic nitrogen and its 15N natural abundance in the Pacific and its marginal seas. Deep sea research A, 34, 807-827.

257. Sanudo, et al., (2001). Phosphorus limitation of nitrogen fixation by Trichodesmium in the central Atlantic Ocean. Nature, 411, 66– 69.

258. Saraswat, et al., (2005). A first look at past sea surface temperatures in the equatorial Indian Ocean from Mg/Ca in foraminifera, Geophys. Res. Lett., 32, L24605.

259. Saraswat, et al., (2012). Linkage between seasonal insolation gradient in the tropical northern hemisphere and the sea surface salinity of the equatorial Indian Ocean during the last glacial period, Acta Geol. Sin., 86, 1265–1275.

260. Sarkar, et al., (2000), High-resolution Holocene monsoon record from the eastern Arabian Sea, Earth Planet. Sci. Lett., 177, 209–218.

261. Sarma, et al., (2002). An evaluation of physical and biogeochemical processes regulating perennial suboxic conditions in the water column of the Arabian Sea. Global Biogeochemical Cycles, 16 (4), 1082.

262. Sarmiento, et al., (1990). Oxygen and nitrate new production and remineralization in the North Atlantic Subtropical Gyre, J. Geophys. Res., 95 (10), 18, 303–18, 315.

263. Satpathy, et al., (2019). Monsoon-induced changes in surface hydrography of the eastern Arabian Sea during the early Pleistocene. Geological Magazine. 157 (6), 1-11.

264. Schäfer, P. and Ittekkot, V., Seasonal variability of δ15N in settling particles in the Arabian Sea and its palaeogeochemical significance. Naturwissenschaften., 1993, 80, 511–513.

265. Schepper, et al., (2014). A global synthesis of the marine and terrestrial evidence for glaciation during the Pliocene Epoch. Earth-Science Reviews 135, 83–102.

266. Schlacher, et al., (2014). Effects of acid treatment on carbon and nitrogen stable isotope ratios in ecological samples: a review and synthesis. Methods in Ecology and Evolution 5, 541-550.

267. Schmidt, J., (1925). On the contents of oxygen in the ocean on both sides of Panama. Science, 61, 592–593.

268. Schmittner, (2005). Decline of the marine ecosystem caused by a reduction in the Atlantic overturning circulation, Nature, 434, 628–633.

269. Schmittner, A., and Galbraith, E.D., (2008). Glacial greenhouse-gas fluctuations controlled by ocean circulation changes. Nature, 456 (7220), 373-376.

270. Schrag, (1999). Effects of diagenesis on the isotopic record of late paleogene tropical sea surface temperatures. Chemical Geology, 161, 215–224.

271. Schulte, et al., (1999). Variations of oxygen-minimum and primary productivity recorded in sediments of the Arabian Sea. Earth and Planetary Sci Lett 173: 205–221.

272. Schulz, et al., (1998). Correlation between Arabian Sea and Greenland climate oscillations of the past 110,000 years. Nature 393: 54–57.

273. Shackleton et al., (1983). Carbon isotope data in core V19-30 confirm reduced carbon dioxide concentration in the ice age atmosphere. Nature, 306. 319-322.

274. Shankar, et al., (2005). Hydrography of the eastern Arabian Sea during summer monsoon 2002, J. Earth Syst. Sci., 114 (5), 459–474.

275. Sharma, et al., (1978). Incursion of Pacific Ocean water into Indian-Ocean, Proc. Indian Acad. Sci. Section A., 87 (3), 29– 45.

276. Shetye,et al., (1994). Circulation and water masses of the Arabian Sea. Proc. Indian Acad. Sci. 103, 107–123.

277. Shrag, (1999). Effects of diagenesis on the isotopic record of late paleogene tropical sea surface temperatures. Chemical Geology 161, 215–224.

278. Sigman et al., (1997). Natural abundance-level measurement of the nitrogen isotopic composition of oceanic nitrate: an adaptation of the ammonia diffusion method. Mar. Chem., 57(3), 227–242.

279. Sigman et al., (2009). Ocean process tracers: nitrogen isotopes in the ocean, in Encyclopedia of Ocean Sciences (2nd Ed.), edited by J.H. Steele, K.K. Turekian, and S.A. Thorpe, 2009, Academic Press, London, 40-54.

280. Singh, et al., (2007). Episodic preservation of pteropods in the eastern Arabian sea: Monsoonal change, Oxygen Minimum Zone intensity and aragonite compensation depth. Indian Journal of Marine Sciences 36, 4378–4383.

281. Singh, et al., (2011). Productivity collapses in the Arabian Sea during glacial cold phases. Paleoceanogr. Paleoclimtol, 26 (3).

282. Singh, et al., (2011). Productivity collapses in the Arabian Sea during glacial cold phases, Paleoceanog, 26, PA3210.

283. Sirocko, et al., (1993). Century-scale events in monsoonal climate over the past 24,000 years. Nature, 364 (6435), 322.

284. Skinner, et al., (2003) Millennial-scale variability of deep-water temperature and d18Odw indicating deep-water source variations in the Northeast Atlantic, 0–34 cal. ka BP. Geochemistry, Geophysics, Geosystems 4, 1098.

285. Smith, B.N. and Epstein, S. (1971) Two Categories of 13C/12C Ratios for Higher Plants. Plant Physiology, 47, 380-384.

286. Smith, et al., (1998). The 1994–1996 Arabian Sea Expedition: And integrated, interdisciplinary investigation of the response of the north western Indian Ocean to monsoonal forcing, Deep Sea Res., Part II, 45, 1905–1915.

287. Somes, et al., (2010). Simulating the global distribution of nitrogen isotopes in the ocean. Global Biogeochemical Cycles, 24.

288. Spero, et al., (1997). Effect of seawater carbonates concentration on foraminiferal carbon and oxygen isotopes. Nature, 390, 497-500.

289. Spero, et al., (1997). Effects of seawater carbonate chemistry on planktonic foraminiferal carbon and oxygen isotope values. Nature, 390, 497–500.

290. Spero, H.J, and Lea, D.W., (1993). Intraspecific stable isotope variability in the planktonic foraminifera Globigerinoides sacculifer: Results from laboratory experiments. Marine Micropaleontology 22, 221–234.

291. Spielhagen, R.F., and Erlenkeuser, H., (1994). Stable oxygen and carbon isotopes in planktic foraminifers from Arctic Ocean surface sediments: reflection of the low salinity surface water layer. Marine Geo, 119 (3/4), 227–250.

292. Steinacher, et al., (2010), Projected 21st century decreases in marine productivity: A multi-model analysis, Biogeosciences, 7 (3), 979–1005.

293. Stommel, H., and Arons, A.B., (1959). On the Abyssal circulation of the World Ocean I. stationary planetary flow patterns on a sphere Deep-Sea Res., 140-154.

294. Stott, et al., (2002) Super ENSO and global climate oscillations at millennial time scales. Science 279, 222–226.

295. Stramma, et al., (2008). Expanding Oxygen-Minimum Zones in the tropical oceans. Science 320, 655–658.

296. Stramma, et al., (2010). Ocean oxygen minima expansions and their biological impacts. Deep-Sea Res. I 57, 587–595.

297. Sun, et al., (2006). Grain size of loess, palaeosol and Red Clay deposits on the Chinese Loess Plateau: Significance for understanding pedogenic alteration and palaeomonsoon evolution. Palaeo3. 241, 129–138.

298. Suthhof, et al., (2001). Millennial-scale oscillation of denitrification intensity in the Arabian Sea during the Late Quaternary and its potential influence on atmospheric N2O and global climate. Global Biogeochem Cycles., 15 (3), 637-649.

299. Swallow, J. C., (1984). Some aspects of the physical oceanography of the Indian Ocean. Deep Sea Res Part A, 31 (6-8), 639-650.

300. Swift, S., Bower, A., 2003. Formation and circulation of dense water in the Persian/ Arabian Gulf. J. Geophys. Res. 108, 3004.

301. Tally, L. D., Pickard, G. L., Emery, W. J. & Swift, J. H. (2012). Descriptive physical oceanography: An Introduction. Elsevier, China, 387–399.

302. Thamban, et al., (1997). Controls on organic carbon distribution in sediments from the eastern Arabian Sea. Geo-Marine Letters 17, 220–227.

303. Thamban, M., Rao, V. P., Schneider, R. R. and Grootes, P. M., Glacial to Holocene fluctuations in hydrography and productivity along the southwestern continental margin of India. Palaeo3. 2001, 165 (1-2), 113-127.

304. Thamdrup, et al., (2012). Widespread functional anoxia in the oxygen minimum zone of the eastern South Pacific. Deep Sea Res Part I Oceanogr Res Pap 65, 36–45.

305. Thiede, et al., (2011). Millions of Years of Greenland Ice Sheet History Recorded in Ocean Sediments , Polarforschung, Bremerhaven, Alfred Wegener Institute for Polar and Marine Research & German Society of Polar Research, 80 (3), 141-159.

306. Tiwari, et al., (2015). Multi-centennial scale SST and Indian summer monsoon precipitation variability since the mid-Holocene and its nonlinear response to solar activity. Holocene, 25 (9), 1415-1424.

307. Toggweiler, J.R. and Russell, J., (2008). Ocean circulation in a warming climate Nature, 451 (7176), 286-288.

308. Toyofuku, et al., (2000). Evaluation of Mg/Ca thermometry in foraminifera: Comparison of experimental results and measurements in nature. Paleoceanog 15, 456–464.

309. Tripathi, et al., (2017). First evidence of denitrification vis-à-vis monsoon in the Arabian Sea since Late Miocene. Scientific Reports 7, 43056.

310. Tyrrell, T. (1999). The relative influences of nitrogen and phosphorus on oceanic primary production, Nature, 400, 525– 531.

311. Ujiié, et al., (2001). Upward decrease of organic C/N rations in the Okinawa Trough cores: proxy for tracing the post-glacial retreat of the continental shore line. Palaeo3 165, 129- 140.

312. Van Campo, E., (1986). Monsoon fluctuations in two 20,000 yr B.P. oxygen isotope/pollen records off southwest India. Quaternary Research 26, 376–388.

313. Villiers et al., (2002). An intensity ratio calibration method for the accurate determination of Mg/Ca and Sr/Ca of marine carbonates by ICP-AES. Geochem. Geophys. Geosyst. 3, GC000169.

314. Villiers, et al., (2002). An intensity ratio calibration method for the accurate determination of Mg/Ca and Sr/Ca of marine carbonates by ICP-AES, Geochem. Geophys. Geosyst, 3(1), 1001.

315. Visser, et al., (2003). Magnitude and timing of temperature change in the Indo-Pacific warm pool during deglaciation. Nature 421, 152–155.

316. Waelbroeck, et al., (2002) Sea-level and deep water temperature changes derived from benthic foraminifera isotopic records. Quaternary Science Reviews 21, 295–305.

317. Wan, et al., (2017). Enhanced silicate weathering of tropical shelf sediments exposed during glacial lowstands: A sink for atmospheric CO2. Geochimica et Cosmochimica Acta, 200, 123–144.

318. Wang, et al., (2005). Evolution and variability of the Asian monsoon system: state of the art and outstanding issues. Quaternary Science Reviews. 24, 595–629.

319. Wang, P. et al. Site 1148. Proc. Ocean Drill. Prog. Init. Rep. 184, 121 (2000).

320. Waples, D. W, and Sloan, J. R., (1980). Carbon and nitrogen diagenesis in deep sea sediments. Geochim. Cosmochim. Acta, 44: 1463-1470.

321. Ward, et al., (2009) Denitrification as the dominant nitrogen loss process in the Arabian Sea. Nature, 461, 78–81.

322. Winkler, (1888). Die Bestimmung des im Wasser Gelösten Sauerstoffes. Berichte der Deutschen Chemischen Gesellschaft 21, 2843–2855

323. Wolff, et al., (2010). Millennial scale variability during the last glacial: the ice core record. Quat. Sci. Rev. 29, 2828–2838.

324. Wyrtki, K., (1971). Oceanographic Atlas of the International Indian Ocean Expedition. Washington, DC: National Science Foundation, 531.

325. Wyrtki, K., (1973). Physical oceanography of the Indian Ocean. In The biology of the Indian Ocean, Springer, Berlin, Heidelberg, 18-36.

326. Xu, et al., (2018). Bathyal records of enhanced silicate erosion and weathering on the exposed Luzon shelf during glacial lowstands and their significance for atmospheric CO2 sink. Chemical Geology, 476, 302–315.

327. Yokoyama et al, (2000). Timing of the last glacial maximum from observed Sea-level minima Nature, 406 (6797), 713-716.

328. You, Y., (1998). Intermediate water circulation and ventilation of the Indian Ocean derived from water-mass contributions. Marine Res., 56 (5), 1029-1067.

329. Yu, et al., (2018). Antarctic Intermediate Water penetration into the Northern Indian Ocean during the last deglaciation Earth Planet Sci. Lett., 500, 67-75.

330. Yu, J.M, and Elderfield, H., (2008). Mg/Ca in the benthic foraminifera Cibicidoides wuellerstorfi and Cibicidoides mundulus: Temperature versus carbonate ion saturation. Earth Planet Sci Lett 276, 129–139.

331. Zachos, et al., (2001). Trends, rhythms and aberrations in global climate 65 Ma to present. Science, 292, 686-693.

332. Zhang, Y. G., Ji, J., Balsam, W., Liu, L. & Chen, J. (2009), Mid-Pliocene Asian monsoon intensification and the onset of Northern Hemisphere glaciation. Geology, 37, 599–602.

333. Zhaojie, et al., (2019). Sea level-controlled sediment transport to the eastern Arabian Sea over the past 600 kyr: Clay minerals and Sr Nd isotopic evidence from IODP site U1457. Quaternary Science Reviews 205, 22-34.

334. Zonneveld, et al., (2010). Selective preservation of organic matter in marine environments; processes and impact on the sedimentary record. Biogeosciences 7, 483–511.